Modeling, Discretization, Optimization, and Simulation of Phase-Field Fracture Problems

Denis Khimin[1], **Leon Kolditz**[1], **Viktor Kosin**[2,1], **Katrin Mang**[3,1], **Thomas Wick**[1,2]

[1] *Leibniz University Hannover, Institute of Applied Mathematics, Welfengarten 1, 30167 Hannover, Germany*
[2] *Université Paris-Saclay, CentraleSupélec, ENS Paris-Saclay, CNRS, LMPS – Laboratoire de Mécanique Paris-Saclay, Gif-sur-Yvette, France*
[3] *HDI Global SE, Hannover, Germany*

November 11, 2023
http://dx.doi.org/10.15488/15172

Preface

This course is devoted to phase-field fracture methods. Four different sessions are centered around modeling, discretizations, solvers, adaptivity, optimization, simulations and current developments.

The key focus is on research work and teaching materials concerned with the accurate, efficient and robust numerical modeling. These include relationships of model, discretization, and material parameters and their influence on discretizations and the nonlinear (Newton-type methods) and linear numerical solution. One application of such high-fidelity forward models is in optimal control, where a cost functional is minimized by controlling Neumann boundary conditions. Therein, as a side-project (which is itself novel), space-time phase-field fracture models have been developed and rigorously mathematically proved. Emphasis in the entire course is on a fruitful mixture of theory, algorithmic concepts and exercises. Besides these lecture notes, further materials[1] are available, such as for instance `pfm-cracks` `https://github.com/tjhei/cracks` with an overview given in [76] as well as tutorial steps in DOpElib [67] `http://www.dopelib.net`.

The prerequisites are lectures in continuum mechanics, introduction to numerical methods, finite elements, and numerical methods for ODEs and PDEs. In addition, functional analysis (FA) and theory of PDEs is helpful, but for most parts not necessarily mandatory.

Discussions with many colleagues in our research work and funding from the German Research Foundation within the Priority Program 1962 (DFG SPP 1962) within the subproject *Optimizing Fracture Propagation using a Phase-Field Approach* with the project number 314067056 (D. Khimin, T. Wick), and support of the French-German University (V. Kosin) through the French-German Doctoral college “Sophisticated Numerical and Testing Approaches" (CDFA-DFDK 19-04) is gratefully acknowledged.

Hannover
November 2023

Denis Khimin
Leon Kolditz
Viktor Kosin
Katrin Mang
Thomas Wick

[1] In the online version of these lecture notes, links, references, and URLs are active with hyperlinks, despite that they are not specifically highlighted, which is for better reading purposes.

Contents

Chapter 1

Introduction

1.1 Brief background

Fracture and damage computations are long-standing topics in practical field problems, experimental studies, engineering, and applied mathematics. The seminal work by Francfort and Marigo in 1998 opened the way for a variational formulation in terms of energy minimization of brittle fracture [59], with a subsequent numerical implementation by Bourdin et al. [24]. Since then, the idea has influenced numerous groups for modeling, discretizing and simulations of fracture mechanics. In the year 2010 further thermodynamical arguments were given in [121] and [100] and the name *phase-field* was established. Our own naming is *phase-field fracture*.

Over the years, advancements (not all can be listed here) have been made by different groups and people [23, 27, 21, 35, 120, 5, 6, 4, 118, 177, 73, 64, 65, 99, 151, 103, 101, 102, 147, 48, 96, 47, 56].

Our own main contributions started in the year 2013 with [122] (see also [124]). The motivation was to have a rigorous mathematical model for phase-field modeling in fractured porous media. Afterwards, we concentrated on investigations of the crack irreversibility constraint [123, 74, 166, 113], efficient and robust numerical solutions [166, 167, 74, 34, 52], global-local multiscale formulations [3, 2, 131], adaptivity [74, 165, 131, 110], incompressible and nearly incompressible solids [108, 111, 113, 109, 17], multiphysics phase-field fracture [163, 169, 164, 105, 104], parameter estimation [89, 132, 133, 134], and optimal control [87, 88, 86]. Very recently, we made advancements in space-time phase-field fracture modeling including its rigorous justification of the governing functional framework [88, 86].

Monographs and summaries are for example [25, 174, 57, 26, 72]. Our own summaries and overviews are provided in [163, 49, 169]. Moreover, we contributed to a benchmark collection in solid mechanics published in [145].

These lecture notes shall give a selection in a teaching fashion with a focus on classical numerical topics such as modeling of the basic system, discretization, and numerical solution. Moreover, phase-field fracture optimal control will be discussed. In the last part, outlooks to extensions (either published or currently investigated) are given. Therein, brand-new research results by setting up `pfm-cracks` [76] with the CARPIUC benchmark [37] are included as well.

1.2 Phase-field fracture

Key idea The principal idea is to approximate (lower-dimensional) discontinuities in some material with the help of an additional smoothed field. As shown in Figure 1.1, that is a smoothed indicator variable varying from 0 (fracture/damage) to 1 (intact material) is used to approximate the discontinuities in a displacement field (highlighted in Figure 1.2). The approximation width is represented through a regularization parameter $\varepsilon > 0$.

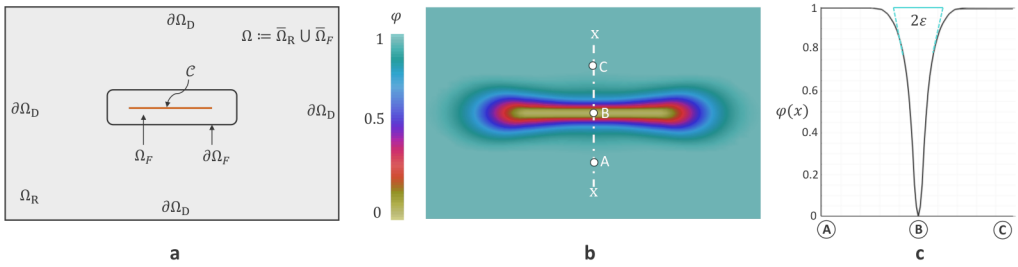

Figure 1.1: Prototype setup: the unbroken domain is denoted by Ω_R and $\mathcal{C}$ is the fracture. The latter is approximated by the domain Ω_F. The half thickness of Ω_F is ε. The fracture boundary is $\partial\Omega_F$ and the outer boundary is $\partial\Omega_D$. The corresponding realization using phase-field is shown in the right sub-figure. Here, the lower-dimensional fracture ($\varphi = 0$) is approximated with the phase-field variable. The transition zone with $0 < \varphi < 1$ has the thickness of ε on each side of the fracture. Consequently, Ω_F can be represented with the help of φ. Figure taken from [135] with permission from Elsevier.

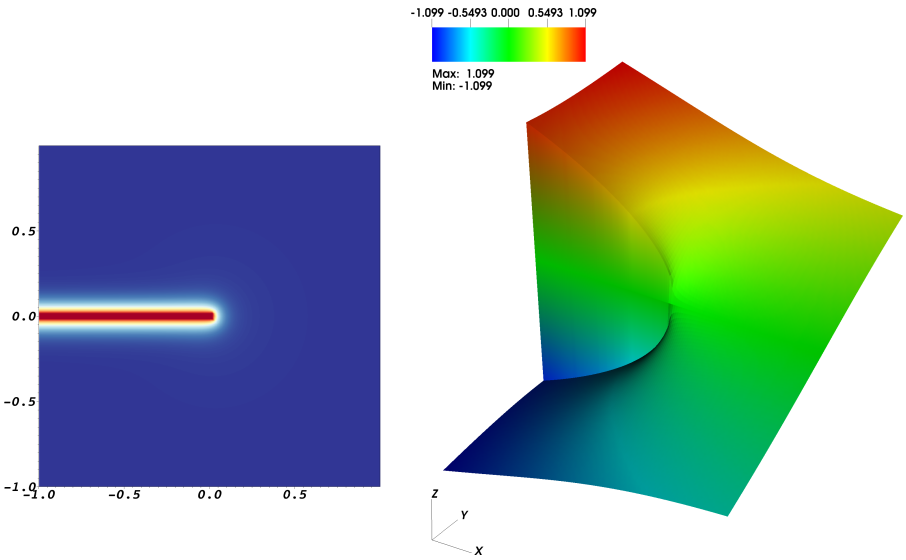

Figure 1.2: The crack is denoted in red color in the left snapshot of the phase-field. On the right side, a 3D plot of the displacement field shows the discontinuity along the line $(x, 0)$ for $-1 \leq x \leq 0$.

Typical goals and questions The most immediate goals of the above idea is to address some of the following questions:

1. Can we compute an (a priori unknown) fracture path?
2. Can we work with multiple fractures and fracture networks?
3. Does this fracture path depend on the numerical discretization method, mesh, input data, boundary conditions?
4. How do boundary conditions influence the fracture path?
5. Under which conditions does φ 'converge' to the lower-dimensional surface? (Hint: Γ-convergence; not covered in these lecture notes!)
6. The role of the regularization parameter ε (length scale) in mathematics and practical applications?
7. What are possible constitutive relations for the governing equations?
8. How do we design 'good' numerical schemes in terms of feasibility, accuracy, efficiency, and robustness?
9. What is the relationship between regularization (i.e., ε and later an elasticity regularization κ), discretization, and material parameters?
10. Is it possible to perform a rigorous numerical analysis of the proposed algorithms?
11. For which settings can we perform a mathematical analysis (well-posedness, a priori error estimations, and so forth)?
12. What are advanced possibilities to further enhance the accuracy while keeping the computational cost at a reasonable level?
13. What are typical functionals of interest, i.e., in what physical quantities (entire solution? Parts of a solution? Stress values? Local deflections and deformations?) is an engineer or practitioner interested in?
14. Is it possible to apply the method from 'simple' academic test cases to practical field problems?
15. Can we determine with sufficient accuracy crack tip mechanics and the fracture speed?
16. Can we compute the fracture width, the fracture volume, and fracture length with sufficient accuracy?
17. Can we apply further physics?
18. Can we estimate unknown parameters?
19. Can we control the crack path in certain directions or suppress it to avoid fracture?
20. Can we use phase-field to make predictions of practical relevance?

Advantages and interest in phase-field fracture Phase-field fracture is a regularized approach that has (as many numerical methods) advantages and shortcomings. A list from the authors' experience is as follows:

- Continuum description based on first physical principles to determine the unknown crack path. Thermodynamical analyses can be carried out;
- Fixed-mesh approach in which no re-meshing or update of basis functions to resolve the crack path is needed;
- Application of classical Galerkin finite elements (FEM) or isogeometric analysis (IGA) in space and time;
- Hard, but beautiful, mathematical and numerical questions arise;
- Computation and representation of nonplanar and complex crack patterns in two and three spatial dimensions;
- The model allows for nucleation (however still mathematical discussions and improvements ongoing), branching and merging; explicit calculation of stress intensity factors not necessary;
- Computation of fracture networks (see Figure 1.3) in possibly highly heterogeneous media.

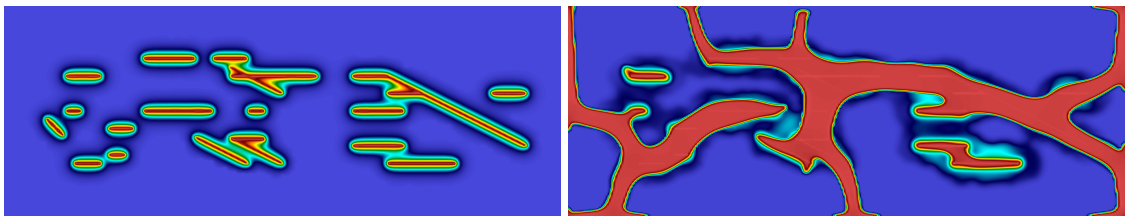

Figure 1.3: Fracture network (initial configuration at left) with growing fractures (at right) using a phase-field model. Red colors indicate the fracture ($\varphi = 0$) and blue colors the unbroken zone ($\varphi = 1$). The transition zone is indicated in yellow/green. This computation has been done with the model presented in [123].

Challenges and shortcomings

- The mesh (e.g., using finite elements) needs to resolve the interface to a certain accuracy, i.e., the relationship between spatial discretization parameter and phase-field regularization parameter, which comes at a computational cost;
- On the energy level, the formulation is non-convex which makes it challenging for both theory and design of numerical algorithms. Specifically, robust monolithic solutions are very challenging. Both partitioned (alternating minimization) and monolithic algorithms may require many nonlinear and linear iterations, and result overall in a high computational cost;
- Accurate crack width computations require care;

- Applying further physics (pressure, temperature) on the fracture interface are limited in their accuracy by the smeared fracture transition zone Here, local mesh adaptivity helps to a great extent in order to achieve sufficient accuracy, but still will not track the crack boundary in an exact fashion as done in interface-tracking.

As demonstrated in numerous studies published in the literature, ideas have been proposed how to cope with these challenges. In view of the enduring increasing popularity, it, however, seems that the advantages outweigh the shortcomings for today's applications.

1.3 Course structure

This one-day course is structured as follows:

- 10:00 - 11:30 Session 1, Exercise 1;
- 11:45 - 13:15 Session 2, Exercise 2;
- 14:30 - 16:00 Session 3, Exercise 3;
- 16:15 - 17:45 Session 4, Discussion.

Each class is around 45 minutes, followed by 45 minutes exercises. We also show numerical simulations, which can be discussed together in more detail, and for which it is useful (while not mandatory) to have `deal.II` `www.dealii.org` with Trilinos [77] and p4est [36] to be installed, and furthermore `pfm-cracks` [76].

1.4 Numerical road map from problem statements to output functionals

In large parts of numerical modeling in these lecture notes, we follow the road map outlined in [171][Section 12.3 and 12.4][1]. We provide a road map from strong form problem statements to postprocessing of quantities of interest measured in terms of goal functionals. Of course, not all steps are always necessary. For instance, sometimes equations are already posed in a space-time weak form. Sometimes, problems are linear and do not need a nonlinear solution.

1. **Problem statement:** Given the strong form including all problem data such as boundary and initial conditions, model and material parameters, right hand sides, and also the geometry.
2. **Weak form:** Design function spaces X and Y. Let $U \in X$ be the trial function and let $\Psi \in Y$ be the test function. Derive a weak form:
$$\text{Find } U \in X: \quad A(U)(\Psi) = F(\Psi) \quad \forall \Psi \in Y.$$
3. **Regularization:** In case of non-smooth problems, e.g., variational inequalities (as phase-field fracture) or vanishing coefficients, one option is to regularize the problem with some regularization parameter $\varepsilon > 0$:
$$\text{Find } U \in X: \quad A_\varepsilon(U)(\Psi) = F(\Psi) \quad \forall \Psi \in Y,$$

[1] `https://thomaswick.org/links/Wi23_st_book_preprint_Aug_8_2023.pdf`

with $U := U_\varepsilon \in X := X_\varepsilon$ and $\Psi := \Psi_\varepsilon \in Y := Y_\varepsilon$.

4. **Temporal discretization:** Design semi-discrete function spaces X_k^r and Y_k^r, where $r \geq 0$ is the polynomial degree. Derive semi-discrete weak form

$$\text{Find } U_k \in X_k^r : \quad A(U_k)(\Psi_k) = F(\Psi_k) \quad \forall \Psi_k \in Y_k^r.$$

5. **Spatial discretization:** Design fully discrete function spaces $X_{k,h}^{r,s}$ and $Y_{k,h}^{r,s}$, where $s \geq 1$ is the polynomial degree. Derive fully discrete weak form

$$\text{Find } U_{kh} \in X_{k,h}^{r,s} : \quad A(U_{kh})(\Psi_{kh}) = F(\Psi_{kh}) \quad \forall \Psi_{kh} \in Y_{k,h}^{r,s}.$$

6. **Nonlinear solution:** Define

$$g(U_{kh})(\Psi_{kh}) := A(U_{kh})(\Psi_{kh}) - F(\Psi_{kh}),$$

and solve $g(U_{kh})(\Psi_{kh}) = 0$ with nonlinear methods such as fixed-point or Newton-type methods.

7. **Linear solution:** Within $g(U_{kh})(\Psi_{kh}) = 0$ linear systems, or in the case of linear problems from the start, solve immediately $A(U_{kh})(\Psi_{kh}) = F(\Psi_{kh})$ with direct, iterative, or multigrid methods.

8. **Postprocessing:** Evaluate goal functionals $J(U_{kh})$, or errors in goal functionals $J(U) - J(U_{kh})$ or errors in global norms $\|U - U_{kh}\|$. Moreover, output the solution in terms of graphical output, e.g., `vtk`.

9. **Further loops, applications, verification, and validation:** According to the postprocessing, increase accuracy and efficiency by adaptivity in discretization errors, model errors, linear and nonlinear solvers. Utilize such high fidelity numerical models $g(U_{kh})(\Psi_{kh})$ within model order reduction, parameter estimation, inverse problems, and optimal control, or for validation in practical applications.

1.5 Verifications and benchmarking

Developing numerical schemes require debugging and testing by various means. Two principle concepts need to be distinguished:

1. **Verification:** Process to determine that a model discretization and implementation result into a sufficiently accurate numerical solution U_{kh};
2. **Validation:** Process to determine whether a certain model describes with sufficient accuracy some specific given real world application within the scope of the intended use of the model.

In the following, we are interested in verification. From the scientific computing perspective two types can be distinguished. First, double-checking the conceptional development of algorithms and descrizations schemes. Second, debugging the programming code. A list of numerical concepts and possible error sources is provided in [170][Chapter 2]. Finally, both can be approved (or disproved) with the obtained numerical solution. Such a computational convergence analysis consists of basically three steps (with increasing level of difficulty). These steps hold true for classical norm-based error-estimation $\|U - U_{kh}\|$ as well as goal-oriented error estimation $J(U) - J(U_{kh})$.

1. Does the solution make sense?
   - If possible test your code with an acknowledged benchmark configuration and/or manufactured solution and verify whether $J(U_{kh})$ matches the benchmark values in a given range and on a sequence of at least three meshes. This first step can be performed with uniform and adaptive mesh refinement. In time-dependent problems, please compute at least with three different time step sizes.
   - If no benchmark configuration is available, study a simple, prototype configuration and observe whether the solution makes sense.
2. Do the true error $J(U) - J(U_{kh})$ and the error estimator η descrease under mesh refinement?
   - Compute $J(U)$ either on a uniformly-refined super-fine mesh or even analytically (i.e., a manufactured solution). Compute the error $J(U) - J(U_{kh})$ and observe whether the error is decreasing.
   - Consider separately η_k (fixing the spatial mesh) and η_h (fixing the temporal mesh) and observe their behavior.
   - If a priori estimates are available, see if the orders of convergence are as expected. But be careful, often goal functionals are nonlinear, for which rigorous a priori error estimates might not be available.
3. Compare η and $J(U) - J(U_{kh})$ in terms of the effectivity index I_{eff}. Do we asymptotically obtain values around $I_{eff} \approx 1$? For nonlinear problems, one easily observes $0.1 \leq I_{eff} \leq 10$, which might be still okay depending on the problem statement.

In particular the last step No. 3 is often difficult when not all theoretical requirements (smoothness of data and boundary conditions, regularity of the goal functional, regularity of the PDE, smoothness of domains and boundaries) are fulfilled.

Chapter 2

Modeling (Session 1)

In this chapter, the objective is to obtain phase-field fracture models in weak formulations. First, a classical quasi-static model is derived in which 'time' arises in an incremental form and no true time derivatives appear. Second, a space-time formulation is derived in which the crack irreversibility constraint is kept in temporal form and an appropriate mathematical functional framework is designed. In order to understand these derivations, a prototype model is discussed first. Mechanical and thermo-dynamical aspects (such as energy splitting into tensile and compressice forces as well as strain history functions [119]) of phase-field fracture will not be discussed in these lecture notes. Overall, we mainly concentrate on typical numerical aspects such as rigorous derivations of the Euler-Lagrange formulation from energy minimization, the mathematical relation to the obstacle problem, and finally, the already mentioned space-time formulation.

2.1 Notation

We introduce the global notation used in these lecture notes. Specific definitions might be added later when necessary.

2.1.1 Spatial domains, boundaries, fracture

Let d be the spatial dimension. In the following, let $B \subset \mathbb{R}^d, d = 2, 3$ the total domain wherein $\mathcal{C} := \mathcal{C}(t) \subset \mathbb{R}^{d-1}$ denotes a (propagating) fracture (or multiple fractures) and $\Omega := \Omega(t) \subset \mathbb{R}^d$ is the intact domain (Figure 2.1). A point in B is denoted by

$$x = (x_1, \dots, x_d).$$

The domain $\Omega_F := \Omega_F(t) \subset \mathbb{R}^d$ is the domain, which arises when $\mathcal{C}$ is approximated with a higher-dimensional object, mainly determined by $\varepsilon > 0$. This introduces the internal boundary (interface) $\partial\mathcal{C} := \partial\mathcal{C}(t) := \overline{\Omega}_F \cap \overline{\Omega}$. For the limit case (no transition zone, phase-field regularization parameter $\varepsilon = 0$), it holds $\Omega_F = \mathcal{C}$. Detailed discussions on how Ω_F is constructed in practice can be found in [163, 169].

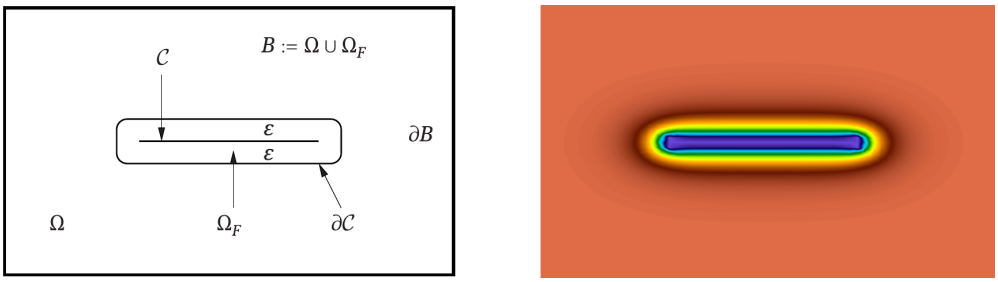

Figure 2.1: Setup of the notation: the unbroken domain is denoted by Ω and $\mathcal{C}$ is the fracture. The latter one is approximated by the domain Ω_F. The half thickness of Ω_F is ε. The fracture boundary is $\partial\mathcal{C}$ and the outer boundary is ∂B. The corresponding realization using phase-field is shown in the right subfigure. Here, the lower-dimensional fracture ($\varphi = 0$) is approximated with the phase-field variable. The transition zone with $0 < \varphi < 1$ has the thickness of ε on each side of the fracture. Consequently, Ω_F can be represented in terms of φ.

The outer boundary may be decomposed into $\partial B = \partial B_{HD} \cup \partial B_{ND} \cup \partial B_{HN} \cup \partial B_{NN}$, where ∂B_{HD} denotes homogeneous Dirichlet conditions, ∂B_{ND} denotes nonhomogeneous Dirichlet conditions, ∂B_{HN} denotes homogeneous Neumann conditions, and ∂B_{NN} denotes nonhomogeneous Neumann conditions. Not always do we deal simultaneously with all four situations, but seperately all of them will appear in Chapter 5.

2.1.2 Time / loading intervals

The loading / time-interval is denoted by $I := (0, T)$ with the end time value $T > 0$.

2.1.3 Model, material and discretization parameters

Regularization and penalization parameters The most important model parameters are the phase-field regularization parameter $\varepsilon > 0$ and the bulk regularization parameter $\kappa > 0$. Both are linked; see e.g., [9, 30]. For some models, we use $\gamma > 0$ for denoting a penalization parameter for treating the crack irreversibility constraint. In Section 3.2.2, the active set constant is denoted by $c > 0$. Finally, in Chapter 4 the Tikhonov regularization parameter in phase-field fracture optimal control is denoted by $\alpha > 0$.

Material parameters The Lamé parameters are denoted with $\mu > 0$ (shear modulus) and $\lambda > -\frac{2}{3}\mu$ with the unit $\mathrm{Pa} = \mathrm{N/m^2} = \mathrm{kg/m\,s^2}$. We denote with σ_s (often simply σ) the Cauchy solid stress tensor with the unit $\mathrm{Pa/m^2}$. The critical energy release rate is denoted with $G_c > 0$ and the unit $\mathrm{J/m^2} = \mathrm{N/m}$. Poisson's ratio is denoted with $-1 \leq \nu_s \leq 0.5$ and is dimensionless. Young's modulus $E_Y > 0$ has the unit $\mathrm{Pa} = \mathrm{N/m^2} = \mathrm{kg/m\,s^2}$.

Spatial and temporal discretization The time (loading) step size is defined as $k_n = t_n - t_{n-1}$ with $k := \max_n(k_n)$, where

$$0 =: t_0 < t_1 < \ldots < t_{n-1} < t_n < \ldots < t_N := T.$$

The time points t_n can have non-uniform distances. The spatial discretization parameter, namely the diagonal of a quadrilateral or hexahedral element, is denoted as usually by h, which is the maximal diameter of all elements of the mesh decomposition.

2.1.4 Solution variables

The unknown solution variables are:

- vector-valued displacements $u := u(x,t) : B \times I \to \mathbb{R}^d$;
- a smoothed scalar-valued indicator phase-field function $\varphi := \varphi(x,t) : B \times I \to [0,1]$. That indeed $0 \leq \varphi \leq 1$ holds true is proven in Theorem [169].

The latter one describes the crack path in a smeared fashion. Specifically:

- $\varphi = 0$ denotes the crack region;
- $\varphi = 1$ characterizes the unbroken material;
- $0 < \varphi < 1$ are intermediate values constituting a smooth transition zone dependent on the regularization parameter ε. In engineering or physics, ε is often a so-called length-scale parameter. We notice that in related fields that use phase-field methods such as phase transitions in materials science, ε is a so-called interaction length. In two-phase flow, ε is known as interfacial thickness. This may be justified since this zone weakens the material and is a physical transition zone from the unbroken material to a fully damaged state.

We often consider several solution variables and then use U as joint variable. For instance, $U = (u, \varphi)$. Moreover, we notice that the solutions are dependent on the regularization parameter ε, i.e.,

$$U := U_\varepsilon.$$

2.1.5 Gradient, divergence, trace, Laplace

It is convenient to work with the nabla operator (see [33] for a concise overview) to define spatial derivative expressions. The gradient of a single-valued function $v : \mathbb{R}^d \to \mathbb{R}$ reads:

$$\nabla v = \begin{pmatrix} \partial_1 v \\ \vdots \\ \partial_d v \end{pmatrix},$$

where $\partial_i v := \frac{\partial v}{\partial x_i}$, where x_i is the ith coordinate direction.

The gradient of a vector-valued function $v : \mathbb{R}^d \to \mathbb{R}^m$ is called Jacobian matrix and reads:

$$\nabla v = \begin{pmatrix} \partial_1 v_1 & \dots & \partial_d v_1 \\ \vdots & & \vdots \\ \partial_1 v_m & \dots & \partial_d v_m \end{pmatrix}.$$

The divergence is defined for vector-valued functions $v : \mathbb{R}^d \to \mathbb{R}^d$:

$$\operatorname{div} v := \nabla \cdot v := \nabla \cdot \begin{pmatrix} v_1 \\ \vdots \\ v_d \end{pmatrix} = \sum_{j=1}^{d} \partial_j v_j.$$

The divergence for a tensor $\sigma \in \mathbb{R}^{d\times d}$ is defined as:

$$\nabla \cdot \sigma = \big(\sum_{j=1}^{d} \frac{\partial \sigma_{ij}}{\partial x_j}\big)_{1\le i\le d}.$$

The trace of a matrix $A \in \mathbb{R}^{d\times d}$ is defined as

$$tr(A) = \sum_{i=1}^{d} a_{ii}.$$

Definition 1 (Laplace operator)**.** *The Laplace operator of a two-times continuously differentiable scalar-valued function $u : \mathbb{R}^d \to \mathbb{R}$ is defined as*

$$\nabla \cdot (\nabla u) = \Delta u = \sum_{j=1}^{d} \partial_{jj} u.$$

Definition 2. *For a vector-valued function $u : \mathbb{R}^d \to \mathbb{R}^m$, we define the Laplace operator componentwise as*

$$\Delta u = \Delta \begin{pmatrix} u_1 \\ \vdots \\ u_m \end{pmatrix} = \begin{pmatrix} \sum_{j=1}^{d} \partial_{jj} u_1 \\ \vdots \\ \sum_{j=1}^{d} \partial_{jj} u_m \end{pmatrix}.$$

2.1.6 Functional frameworks

General notation

We adopt standard notation for the usual Lebesgue and Sobolev spaces [172, 1]. We denote in the following $D := B$ or $D := \Omega$ or $D := \Omega_F$. By $L^p(D), 1 \le p \le \infty$, we indicate the standard Lebesgue space that consists of measurable functions u, which are Lebesgue-integrable to the p-th power. The set $L^p(D)$ forms a Banach space with the norm $\|u\|_{L^p(D)}$:

$$\|u\|_{L^p(D)} := \left(\int_D |u(\boldsymbol{x})|^p \, dx\right)^{\frac{1}{p}}, \quad 1 \le p < \infty,$$
$$\|u\|_{L^\infty(D)} := \text{ess sup } |u(\boldsymbol{x})|.$$

We obtain the Hilbert space $L^2(D)$ for $p = 2$, equipped with the inner product

$$(u, v)_{L^2(D)} := \int_D u(\boldsymbol{x}) v(\boldsymbol{x}) \, dx.$$

The Sobolev space $W^{m,p}(D), m \in \mathbb{N}, 1 \le p \le \infty$ is the space of functions in $L^p(D)$ that have distributional derivatives of order up to m, which belong to $L^p(D)$. This space is equipped with the norm

$$\|u\|_{W^{m,p}(D)} := \left(\sum_{|\alpha|\le m} \|D^\alpha u\|^p_{L^p(D)}\right)^{\frac{1}{p}}, \quad 1 \le p < \infty,$$
$$\|u\|_{W^{m,\infty}(D)} := \max_{|\alpha|\le m} \|D^\alpha u\|_{L^\infty(D)}.$$

Definition 3. *The symbol $\alpha = (\alpha_1, \ldots, \alpha_d) \in \mathbb{N}^d$ denotes a multi-index with the properties*

$$|\alpha| := \sum_{j=1}^{d} \alpha_j, \quad D^\alpha := \frac{\partial^{|\alpha|}}{\partial x_1^{\alpha_1} \cdots \partial x_d^{\alpha_d}}.$$

If $k \in \mathbb{N}_0$, we define the set of all partial derivatives of order k:

$$D^k u(x) := \{D^\alpha u(x) : \ |\alpha| = k\}.$$

For $p = 2, H^m(D) := W^{m,2}(D)$ is a Hilbert space equipped with the inner product

$$(u, v)_{H^m(D)} := \sum_{|\alpha| \le m} (D^\alpha u, D^\alpha v)_{L^2(D)},$$

and the norm $|| \cdot ||_{H^m(D)}$ [172]. Semi-norms are defined by

$$|u|_{W^{m,p}(D)} := \left(\sum_{|\alpha|=m} \|D^\alpha u\|_{L^p(D)}^p \right)^{\frac{1}{p}}, \quad 1 \le p < \infty,$$
$$|u|_{W^{m,\infty}(D)} := \max_{|\alpha|=m} \|D^\alpha u\|_{L^\infty(D)}.$$

Finally, we indicate the subspace $W^{m,p}(D)$ of functions with zero trace on ∂X by $W_0^{m,p}(D)$. Specifically, we define $H_0^1(D) = \{u \in H^1(D) : \ u = 0 \text{ on } \Gamma_D \subset \partial X\}$.

Comments on space-time function spaces / almost all

For time-dependent weak formulations, one can work with space-time Sobolev spaces, so-called Bochner spaces (e.g., [45, 172]). This would be the most elegant notation. We rather use fruitful consequences of Lebuesgue measures, namely that L^2 integrals in $I = (0, T)$ can be approximated almost everywhere in I on the time-continuous level.

Definition 4 (Almost everywhere, a.e.)**.** *Let $\Omega \subset \mathbb{R}^d$ be a Lebesgue-measurable open domain. Measurable functions are defined almost everywhere, in short a.e., in Ω:*

$$f(x) = g(x) \quad \textit{a.e. } \Omega,$$

when there is $Z \subset \Omega$ such that the Lebesgue measure of Z is zero and

$$f(x) = g(x) \quad \textit{for all } x \in \Omega \setminus Z.$$

Short: Almost everywhere means except on a set of Lebesgue measure zero.

Definition 5 (Almost all)**.** *On the time-continuous level $I = (0, T)$, rather than working with L^2 integrals, we use the fact from Lebuesgue theory that such functions can be approximated for almost all $t \in I$.*

Remark 1. *Clearly after time-discretization, we evaluate the semi-discrete problem for all $n = 1, 2, 3, \ldots, N$.*

Notation for phase-field fracture problems

We frequently use the short notation

$$V_B := H^1(B), \quad V_B^0 := H_0^1(B).$$

For vector-valued function spaces (for instance the displacements $u : B \to \mathbb{R}^d$ are vector-valued), we use the same notation:

$$V_B := H^1(B)^d, \quad V_B^0 := H_0^1(B)^d.$$

The context should make clear whether we work in the scalar-valued or vector-valued case. Our fundamental space for phase-field fracture is

Definition 6 (Governing spaces for displacements and phase-field)**.** *Let $V_u := H^1(B)^d$. The trial space for the displacements is defined as:*

$$V_u^D := V_u^D(B) := \{u \in V_u |\ u = u_D \text{ on } \partial\Omega_D,\ u = 0 \text{ on } \partial B \setminus \partial\Omega_D\}.$$

The test space for the displacements is the classical $H_0^1(B)^d$ space and defined in our notation as

$$V_u^0 := V_u^0(B) := \{u \in V_u |\ u = 0 \text{ on } \partial B\}.$$

The trial and test space for the phase-field variable is

$$V_\varphi := V_\varphi(B) = H^1(B).$$

These spaces are sufficient as prototype spaces. Often in applications, homogeneous Neumann conditions ∂B_N will also play a role in the displacements, which is then specifically indicated.

Remark 2. *For general algorithmic concepts in which the boundary conditions do usually not cause specific changes, we simply work with V.*

We then seek

$$u \in V_u^D,$$

and

$$\varphi \in V_\varphi.$$

We introduce the convex set for including the variational inequality constraint in time, i.e., the crack irreversibility constraint, for quasi-brittle fracture

$$K := K(\varphi^{n-1}) := \{\varphi \in V_\varphi :\ 0 \le \varphi^n \le \varphi^{n-1} \le 1 \text{ a.e. in } B\},$$

and in space-time quasi-brittle phase-field fracture, we have

$$K := K(\varphi^{n-1}) := \{\varphi :\ \partial_t \varphi \le 0 \text{ a.e. in } I \times B\}.$$

Here, we write on purpose φ without specifying the Hilbert space since further regularity assumptions are necessary [88] that exceed the intention of these lecture notes.

When useful, we work with the following convention:

Definition 7. *We denote the product space by*

$$X = V_u^D \times V_\varphi,$$

such that we seek $U \in X$, i.e., $(u, \varphi) \in V_u^D \times V_\varphi$. If necessary, we also use the notation $X^D = X = V_u^D \times V_\varphi$ and $X^0 = V_u^0 \times V_\varphi$.

2.1.7 Notation for weak forms and related terminology

We briefly recall our important notation for representing weak variational forms:

1. Let $f, g \in V^d$. Then the scalar product is denoted by:

$$(f, g) = \int_B f \cdot g \, dx, \quad f, g \in V^d.$$

2. Let $F, G \in V^{d \times d}$. Then the scalar product for matrices is denoted by:

$$(F, G) = \int_B F : G \, dx, \quad F, G \in V^{d \times d}.$$

   Here, : stands for the Frobenius scalar product.

3. Often, we use: Find $u \in V$ such that

$$a(u, \varphi) = l(\varphi) \quad \forall \varphi \in V.$$

   Here $a(u, \varphi) : V \times V \to \mathbb{R}$ is a bilinear form and $l(\varphi) \in V^*$ is a linear form (linear functional). Here V^* denotes the dual space $V^* = L(V, \mathbb{R})$.

4. For nonlinear problems, the solution variable $u \in V$ is nonlinear, while the test function is still linear. We use the notation: Find $u \in V$ such that

$$a(u)(\varphi) = l(\varphi) \quad \forall \varphi \in V.$$

   Here, $a(u)(\varphi)$ is a so-called semi-linear form, where the first argument $u \in V$ is nonlinear and the second argument $\varphi \in V$ is linear.

5. For (linear) PDE systems, we define the space X, e.g., $X = V_u^D \times V_\varphi$, and the notation is: Find $U = (u, \varphi) \in X$ such that

$$A(U, \Psi) = F(\Psi) \quad \forall \Psi := (w, \psi) \in X^0 := V_u^0 \times V_\varphi.$$

6. For nonlinear PDE systems, the notation is: Find $U \in X$ such that

$$A(U)(\Psi) = F(\Psi) \quad \forall \Psi \in X^0.$$

Lastly, to notice is that we do not distinguish between scalar-valued, vector-valued, and tensor-valued variables in these lecture notes by using bold letters, arrows, or similar notations. All variables are in non-bold fonts. We expect the reader to distinguish them out of the context.

2.2 Prerequisites in differentiation and integration

Very briefly, we list some fundamental results that are necessary throughout these lecture notes.

2.2.1 Gauss-Green theorem / divergence theorem

The Gauss-Green theorem or often known as divergence theorem. Let $\Omega \subset \mathbb{R}^d$ an bounded, open domain and $\partial\Omega$ of class C^1.

Theorem 1 (Gauss-Green theorem / divergence theorem)**.** *Suppose that $u := u(x) \in C^1(\bar{\Omega})$ with $x = (x_1, \ldots, x_d)$. Then:*

$$\int_\Omega u_{x_i}\, dx = \int_{\partial\Omega} u n_i\, ds, \quad \text{for } i = 1, \ldots, d.$$

Here, n_i is the ith component of the normal vector n. In compact notation, we have

$$\int_\Omega div\, u\, dx = \int_{\partial\Omega} u \cdot n\, ds$$

for each vector field $u \in C^1(\bar{\Omega}; \mathbb{R}^d)$.

Proof. Please see for example [95]. □

2.2.2 Integration by parts and Green's formula

From the divergence theorem, we obtain immediately:

Proposition 1 (Integration by parts)**.** *Let $u, v \in C^1(\bar{\Omega})$. Then:*

$$\int_\Omega u_{x_i} v\, dx = -\int_\Omega u v_{x_i}\, dx + \int_{\partial\Omega} u v n_i\, ds, \quad \text{for } i = 1, \ldots, d.$$

In compact notation:

$$\int_\Omega \nabla u v\, dx = -\int_\Omega u \nabla v\, dx + \int_{\partial\Omega} u v n\, ds.$$

Proof. Follows from the divergence theorem to uv. □

We obtain some further results, which are useful, but are all based directly on integration by parts.

Proposition 2 (Green's formulae)**.** *Let $u, v \in C^2(\bar{\Omega})$. Then it holds:*

$$\int_\Omega \Delta u\, dx = \int_{\partial\Omega} \partial_n u\, ds,$$
$$\int_\Omega \nabla u \cdot \nabla v\, dx = -\int_\Omega \Delta u\, v\, dx + \int_{\partial\Omega} v\, \partial_n u\, ds.$$

Proof. Follows from integration by parts. □

2.2.3 Change of variables in Lebuesgue integrals

Theorem 2 (Integration by substitution / change of variables)**.** *Let $\widehat{B} \subset \mathbb{R}^d$ be open. Let $\widehat{T} : \widehat{B} \to \mathbb{R}^d$ be a diffeomorphism in $\mathbb{R}^d$. Then, the function $f : \widehat{T}(\widehat{B}) \to \mathbb{R}$ is Lebuesgue-integrable on $\widehat{T}(\widehat{B})$ if and only if the function $\hat{\boldsymbol{x}} \in \widehat{B} \to f(\widehat{T}(\hat{\boldsymbol{x}}))|det(\widehat{\boldsymbol{\nabla}}\widehat{T}(\hat{\boldsymbol{x}}))| \in \mathbb{R}$ is Lebuesgue-integrable on $\widehat{B}$. Then, we have*

$$\int_{\widehat{T}(\widehat{B})} f(x)\,dx = \int_{\widehat{B}} f(\widehat{T}(\hat{\boldsymbol{x}}))|det(\widehat{\boldsymbol{\nabla}}\widehat{T}(\hat{\boldsymbol{x}}))|\,d\hat{\boldsymbol{x}}.$$

Theorem 3. *Let $B \subset \mathbb{R}^m$ be measurable and $A \subset \mathbb{R}^d$ be open. Let the function $f : A \times B \to \mathbb{R}$ be Lebuesgue integrable in B for all fixed $x \in A$. Moreover, let f be continuously differentiable for $x \in A$ for almost all $y \in B$. We assume the bound $g : B \to \mathbb{R}$ with $\|\nabla_x f(x,y)\| \leq g(y)$ for all $x \in A$ and almost all $y \in B$. Then:*

1. *$\nabla_x f(x,y)$ is Lebuesgue integrable on B for all fixed $x \in A$;*
2. *The parameter integral $F(x) = \int_B f(x,y)\,dy$ is continuously differentiable with the derivative*

$$\nabla F(x) = \int_B \nabla_x f(x,y)\,dy.$$

2.2.4 Differentiation in Banach spaces

At several places, we need differentation in Banach spaces. From the literature, e.g., [158, 43, 162], we cite some well-known results in this section.

Definition 8 (Directional derivative in a Banach space)**.** *Let V and W be normed vector spaces and let $U \subset V$ be non-empty. Let $f : U \to W$ be a given mapping. If the limit*

$$f'(u)(\phi) := \lim_{h \to 0} \frac{f(u + h\phi) - f(u)}{h}, \quad u \in U, \phi \in V,$$

exists, then $f'(u)(\phi)$ is called the directional derivative of the mapping f at u in direction ϕ. If the directional derivative exists for all $\phi \in V$, then f is called directionally differentiable at u.

Remark 3. *Often, the direction ϕ is denoted by δu in order to highlight that the direction is related with the variable u. This notation is useful, when several solution variables exist and several directional derivatives need to be computed.*

Remark 4. *The definition of the directional derivative in Banach spaces is in agreement with the definition of derivatives in $\mathbb{R}$ at $x \in \mathbb{R}$ (see [94]):*

$$f'(x) := \lim_{h \to 0} \frac{f(x + h) - f(x)}{h},$$

and in $\mathbb{R}^d$ we have (see [95]) into the direction $\phi \in \mathbb{R}^d$:

$$f'(x)(\phi) := \lim_{h \to 0} \frac{f(x + h\phi) - f(x)}{h}.$$

A function is called differentiable when all directional derivatives exist in the point $x \in \mathbb{R}^d$ (similar to the Gâteaux derivative). The derivatives in the directions $e_i, i = 1, \ldots, d$ of the standard basis are the well-known partial derivatives.

Definition 9 (Gâteaux derivative)**.** *Let the assumptions hold as in Definition 8. A directional-differentiable mapping as defined in Definition 8, is called Gâteaux-differentiable at $u \in U$, if there exists a linear continuous mapping $A : U \to W$ such that*

$$f'(u)(\phi) = A(\phi),$$

holds true for all $\phi \in U$. Then, A is the Gâteaux derivative of f at u and we write $A = f'(u)$.

Remark 5. *The Gâteaux derivative is computed with the help of directional deriatives and it holds $f'(u) \in L(U, W)$. If $W = \mathbb{R}$, then $f'(u) \in U^*$.*

Definition 10 (Fréchet derivative)**.** *A mapping $f : U \to W$ is Fréchet-differentiable at $u \in U$ if there exists an operator $A \in L(U, W)$ and a mapping $r(u, \cdot) : U \to W$ such that for each $\phi \in U$ with $u + \phi \in U$, it holds:*

$$f(u + \phi) = f(u) + A(\phi) + r(u, \phi),$$

with

$$\frac{\|r(u, \phi)\|_W}{\|\phi\|_U} \to 0 \quad \text{for } \|\phi\|_U \to 0.$$

The operator $A(\cdot)$ is the Fréchet derivative of f at u and we write $A = f'(u)$.

Definition 11 (Equivalent formulation denoting derivatives)**.** *In the literature and above, we have (at least) three common notations and ways to compute directional derivatives:*

$$\begin{aligned} f'(u)(\phi) &= \lim_{h \to 0} \frac{f(u + h\phi) - f(u)}{h} \\ &= \frac{d}{dh} f(u + h\phi)|_{h=0} \\ &= f(u + \phi) - f(u) - r(u, \phi). \end{aligned}$$

Example 1. *The bilinear form $a(u, \varphi) = (\nabla u, \nabla \varphi)$ is Fréchet-differentiable in the first argument u (of course also in the second argument! But u is the variable we are interested in):*

$$a(u + \phi, \varphi) = (\nabla(u + \phi), \nabla \varphi) = \underbrace{(\nabla u, \nabla \varphi)}_{= a(u, \varphi)} + \underbrace{(\nabla \phi, \nabla \varphi)}_{= a'_u(u, \varphi)(\phi)}.$$

Here the remainder term is zero, i.e., $r(u, \phi) = 0$, because the bilinear form is linear in u. Thus, the Fréchet derivative of $a(u, \varphi) = (\nabla u, \nabla \varphi)$ is $a'_u(u, \varphi)(\phi) = (\nabla \phi, \nabla \varphi)$.

2.2.5 Chain rules

The chain rule in $\mathbb{R}^{d+1}$ is as follows:

Definition 12. *Let the functions $g : (a, b) \to \mathbb{R}^{d+1}$ and $f : \mathbb{R}^{d+1} \to \mathbb{R}$ and its composition*

$h = f \circ g \in \mathbb{R}$ be given and specifically $g(t,x) := (t,x) := (t, x_1, x_2, \ldots, x_d)$:

$$\begin{aligned}
\frac{d}{dt}h(t,x) &= \frac{d}{dt}f(g(t,x)) = \frac{d}{dt}f(t,x) \\
&= \sum_{j=0}^{d} \partial_j f(g(x)) \cdot \partial_t g_j \\
&= \sum_{j=0}^{d} \partial_j f(t, x_1, \ldots, x_d) \cdot \partial_t x_j, \quad \text{where } x_0 := t \\
&= \partial_t f \cdot \partial_t t + \sum_{j=1}^{d} \partial_j f(t, x_1, \ldots, x_d) \cdot \partial_t x_k \\
&= \partial_t f + \nabla f \cdot (\partial_t x_1, \cdots, \partial_t x_d)^T \\
&= \partial_t f + \nabla f \cdot v.
\end{aligned}$$

For instance $d = 3$ and time t, this means that we deal with a four-dimensional setting (t, x, y, z).

Remark 6. *See also [95][page 54 and page 93] for definitions of the chain rule.*

The chain rule in Banach spaces is [158, 43, 162]:

Definition 13. *Let U, V, W be Banach spaces. Let U and V be open sets. We have the mappings $F : U \to V$ and $G : V \to W$. Let F be differentiable at $u \in U$ and G be differentiable at $F(u) \in V$. Then, the composition $H = G \circ F$ defined by $H(u) = G(F(u))$ with $H : U \to W$ is Fréchet differentiable at $u \in U$ and it holds*

$$H'(u) = G'(F(u))F'(u).$$

More specifically, in a direction $\delta u \in U$, it holds

$$H'(u)(\delta u) = G'(F(u))F'(u)(\delta u).$$

Example 2. *We apply the chain rule to an operator $T : U \to W$:*

$$T(u) = u^3$$

then

$$T(u + \phi) = (u + \phi)^3 = u^3 + 3u^2\phi + 3u\phi^2 + \phi^3.$$

Here, we now have four terms to describe $T(u), A(\phi)$ and $r(u, \phi)$.

- *The identification of $T(u) = u^3$ is obvious.*
- *According to the theory $A(\phi)$ is a linear operator in ϕ. Therefore: $A(\phi) = 3u^2\phi$.*
- *The rest goes into $r(u, \phi) = 3u\phi^2 + \phi^3$.*

To check that we deal with a Fréchet derivative, we need to verify

$$\frac{\|r(u,\phi)\|_W}{\|\phi\|_U} \to 0 \quad \text{for } \|\phi\|_U \to 0.$$

Here, it is important to remark that u is fixed and we only vary in ϕ. Since we have ϕ^2 and ϕ^3 in the nominator, but only ϕ in the denominator, one can indeed check that $T(u) = u^3$ is Fréchet-differentiable.

Example 3. *Let $v \in V_1$ and $u \in V_2$ be solution variables. For brevity, we neglect the governing equation for v. Let u be determined by the semi-linear form*

$$A(v,u)(\varphi) := (v\nabla u, \nabla\varphi) + (u^3, \varphi).$$

Then, the directional derivative in direction $(\delta v, \delta u) \in V_1 \times V_2$ is given by:

$$A'(v,u)((\delta v, \delta u), \varphi) = (\delta v \nabla u + v\nabla\delta u, \nabla\varphi) + (3u^2\delta u, \varphi),$$

using the product and chain rules, respectively. If $v \in V_1$ would be given and not an unknown, then

$$A'(v,u)((\delta v, \delta u), \varphi) = (v\nabla\delta u, \nabla\varphi) + (3u^2\delta u, \varphi).$$

2.3 A prototype model problem

The materials of this section are taken from [169][Section 2.3]. The main idea is to extract the key components from established phase-field fracture models and to break them down to student level pieces. To get started, we recall that we are interested in two solution variables, namely one describing the displacements u and one indicating fracture φ. To determine both solution variables u and φ we need two equations. Later, displacements are computed with the help of elasticity. For the moment, however, we work with the Laplacian to make it as simple as possible. Let B a domain with boundary ∂B with classical assumptions on their smoothness (e.g., [29]). Find $u : B \to \mathbb{R}$ such that

$$-\nabla \cdot (a\nabla u) = f \quad \text{in } B, \quad \text{plus bc on } \partial B, \tag{2.1}$$

where 'bc' = 'boundary conditions' and with a material coefficient $a > 0$. Soon, we shall see that in phase-field fracture, the parameter a depends on $x \in B$ as well as on a second solution variable.

The phase-field function φ describes the crack path ($\varphi = 1$ for unbroken solid and $\varphi = 0$ for a fully damaged material) and is in the limit a lower-dimensional manifold. Here, [24] proposed to employ an Ambrosio-Tortorelli elliptic functional (1990/1992) [8, 9]. Further details will follow later. For now, we are satisfied to know that we work with an elliptic functional, whose corresponding PDE is very familiar to us (again a Laplacian with a reaction term and a parameter $\varepsilon > 0$): Find $\varphi : B \to \mathbb{R}$ such that

$$-\varepsilon\Delta\varphi - \frac{1}{\varepsilon}(1-\varphi) = g \quad \text{in } B, \quad \text{plus bc on } \partial B, \tag{2.2}$$

where $g : B \to \mathbb{R}$ is a right hand side force. One can establish that (2.2) is bounded in the H^1 norm (see [169][Theorem 5]), which is the natural norm for this equation. Moreover, it can be shown that $0 \le \varphi \le 1$; see again [169][Theorem 5] (and also the literature [128, 58]). Together with (2.2), this yields:

Proposition 3. *Given equation* (2.2) *and assuming the later result from [169][Theorem 5] that φ is indeed well defined in the H^1 setting and $0 \le \varphi \le 1$, it holds:*

1. *The variable φ is indeed an indicator function with values between* 0 *and* 1.
2. *The gradient $\nabla\varphi$ smoothes the transition from $\varphi = 0$ to $\varphi = 1$. For large ε, we have a smoother (larger) transition zone. For small ε the transition zone becomes smaller and the gradients $\nabla\varphi$ steeper, i.e., values $\varphi = 0$ and $\varphi = 1$ are accented and we loose smoothness in the limit for $\varepsilon \to 0$.*

Proof. We refer to [169][Theorem 5] for the mathematical statements. The descriptive illustration follows trivially. See also Figure 2.2. □

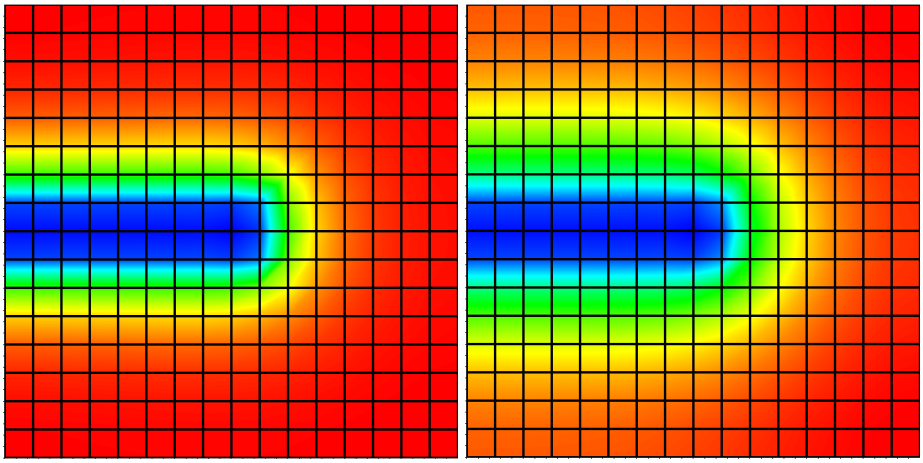

Figure 2.2: Approximation of a fracture with phase-field. At left, the regularization parameter is chosen as $\varepsilon = h$. At right, the regularization parameter is chosen as $\varepsilon = 2h$.

However, an additional constraint is the crack irreversibility (the crack cannot heal in time), which is imposed as:

$$\partial_t \varphi \leq 0. \tag{2.3}$$

Consequently, the equation determining φ becomes an inequality and is linked to the constraint (2.3) via a complementarity condition. Therefore, the system is very close to the well-known and well-studied obstacle problem, see e.g., the classical books [51, 90, 91, 156, 155]. However, the two main PDEs do not have any time derivatives, but only the constraint does. This constitutes a difference to the standard obstacle problem.

With the help of these definitions, a simplified phase-field fracture problem can be formulated. This allows us to identify important characteristic aspects of the full problem. To this end, we study first:

Problem 1 (A simplified strong problem formulation)**.** *Let B be a domain with the boundary $\partial B := \partial\Omega_{HD} \cup \partial\Omega_{ND} \cup \partial\Omega_{HN}$. Find a displacement function $u : B \times I \to \mathbb{R}$ and a phase-field indicator function $\varphi : B \times I \to [0, 1]$, such that*

$$-\nabla \cdot (\varphi^2 \nabla u) = f \quad \text{in } B \times I, \quad (u\text{-equation}) \tag{2.4}$$

$$\varphi |\nabla u|^2 - \varepsilon \Delta \varphi - \frac{1}{\varepsilon}(1 - \varphi) \leq 0 \quad \text{in } B \times I, \quad (\varphi\text{-equation}) \tag{2.5}$$

$$\partial_t \varphi \leq 0 \quad \text{in } B \times I, \quad (\text{crack irreversibility}) \tag{2.6}$$

$$\Big[\varphi |\nabla u|^2 - \varepsilon \Delta \varphi - \frac{1}{\varepsilon}(1 - \varphi)\Big] \cdot \partial_t \varphi = 0 \quad \text{in } B \times I, \quad (\text{complementarity condition}). \tag{2.7}$$

These equations are complemented with the following boundary and initial conditions:

$$\begin{aligned} u(x,t) &= u_D(x,t) && \text{on } \partial\Omega_{ND} \times I, \\ u(x,t) &= 0 && \text{on } \partial\Omega_{HD} \times I, \\ \varphi^2 \nabla u \cdot n &= 0 && \text{on } \partial\Omega_{HN} \times I, \\ \varepsilon \partial_n \varphi &= 0 && \text{on } \partial B \times I, \\ \varphi(x,0) &= \varphi_0 && \text{on } B \times \{0\}, \end{aligned}$$

with an initial fracture φ_0 and with $\varepsilon > 0$ as the so-called phase-field regularization parameter.

Remark 7 (Coupling terms)**.** *Observing* (2.1) *and* (2.2)*, we obtain Formulation 1 by setting $a = \varphi^2$ and $g = -\varphi|\nabla u|^2$.*

Remark 8 (Brief comments on the classification)**.** *The fully coupled system (2.4) to (2.7) is nonlinear (to be specific: quasi-linear). If we decouple the system, the single expressions* (2.4) *and* (2.5) *become linear. However,* (2.5) - (2.7) *forms an inequality and therefore, we nevertheless deal with a nonlinear problem since the underlying space is only a convex set and not anymore a linear function space.*

Remark 9. *The PDE* (2.4) *and* (2.5) *are not time-dependent, but the constraint* (2.6) *depends on time. This constraint can be discretized using a backward difference quotient:*

$$\partial_t \varphi \approx \frac{\varphi^n - \varphi^{n-1}}{k} \leq 0 \quad \Leftrightarrow \quad \varphi^n \leq \varphi^{n-1}$$

where $\varphi^n := \varphi(t_n)$ and the time step size $k = t_n - t_{n-1}$. In these lecture notes, this constraint shall be treated with a primal-dual active set method in Section 3.2.2, a summary (and literature references) of alternatives is provided in [169][Chapter 5].

2.4 Excursus I: the obstacle problem

There are several striking similarities between the obstacle problem [51, 155, 90, 91, 70, 156] and the previously introduced model. For this reason, we recapitulate known models and results for an illustrative understanding.

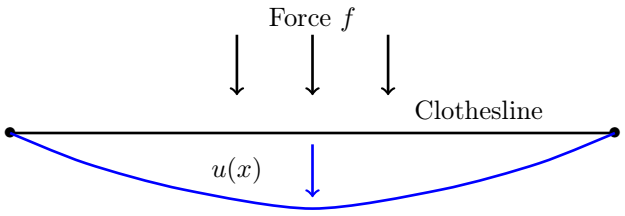

Figure 2.3: Clothesline problem (Poisson problem in one dimension). Displacement $u(x)$ induced by a force f.

The classical Poisson problems reads: Find $u : \Omega \to \mathbb{R}$ such that

$$\begin{aligned} -\Delta u &= f \quad \text{in } \Omega \\ u &= 0 \quad \text{on } \partial\Omega. \end{aligned}$$

The obstacle problem is defined as

$$\begin{aligned} -\Delta u &\geq f \quad \text{in } \Omega, \quad \text{(PDE)},\\ u &\geq g \quad \text{in } \Omega, \quad \text{(Inequality constraint)},\\ (f+\Delta u)(u-g) &= 0 \quad \text{in } \Omega, \quad \text{(Complementarity condition)},\\ u &= 0 \quad \text{on } \partial\Omega, \quad \text{(Boundary condition)}. \end{aligned}$$

The obstacle problem is a free boundary problem that splits the domain Ω into two parts $\mathcal{I}$ (inactive set) and $\mathcal{A}$ (active set):

- If $f + \Delta u = 0$, then we solve the PDE and the constraint is fulfilled (inactive), i.e., $u > g$ in the so-called inactive set $\mathcal{I}$. In other words, the obstacle condition is not active.
- If $f + \Delta u < 0$, we are 'sitting' on the obstacle, i.e., $u = g$, and we are in the active set $\mathcal{A}$.

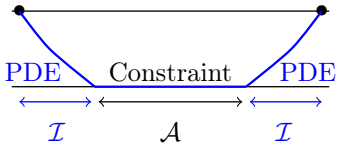

Figure 2.4: Obstacle problem: a clothesline touches the ground in the active set $\mathcal{A}$ in which the obstacle condition is active. In the inactive set $\mathcal{I}$, the PDE is solved.

In the contact problem of a membrane, we have an active set $\mathcal{A} = \Omega \backslash \mathcal{I}$, where the membrane touches the table with $\mathcal{A} = \{x \in \Omega : \ u = g\}$. The active set is also called contact zone. The inactive set is called $\mathcal{I}$ and the free boundary is defined as $\Gamma := \partial\mathcal{A} \cap \partial\mathcal{I}$. We define the sub-regions as

- $\mathcal{A} = \Omega \setminus \mathcal{I}$: active set or contact zone (we sit on the obstacle), defined by

$$\mathcal{A} = \{x \in \Omega : \ u = g\},$$

- $\mathcal{I}$ is the inactive set (we solve the PDE),
- $\Gamma = \partial\mathcal{A} \cap \partial\mathcal{I}$ is the free boundary.

2.4.1 Energy formulation

The potential energy $E(u)$ can be defined as

$$E(u) = \int_\Omega [\mu(\sqrt{1+|\nabla u|^2} - 1) - fu] \, dx \overset{Taylor}{\approx} \int_\Omega [\frac{\mu}{2}|\nabla u|^2 - fu] \, dx,$$

with a material parameter $\mu > 0$.

Problem 2 (Physical state)**.** *Physically, the state without any constraint can be formulated as*

$$\min_{u \in V} E(u) \ \textit{with} \ V := \{v \in H^1(\Omega) |\ v = u_0 \ \textit{on} \ \partial\Omega\}.$$

Problem 3. *The minimization problem with a constraint can be written as*

$$\min_{u\in V, u\geq g} E(u), \quad \text{with } g \in L^2.$$

The admissible function space can be defined as follows:

$$K := \{v \in H^1(\Omega) |\ v = u_0 \text{ on } \partial\Omega, v \geq g \text{ in } \Omega\},$$

such that we can write:

$$\min_{u\in K} E(u).$$

Definition 14 (Convex set)**.** *We say K is a convex set if*

$$u, v \in K: \quad \theta u + (1-\theta)v \in K,$$

for $0 \leq \theta \leq 1$.

Definition 15 (Convex functional)**.** *A functional $E : K \to \mathbb{R}$ is convex if and only if*

$$E(\theta u + (1-\theta)v) \leq \theta E(u) + (1-\theta)E(v)$$

for all $u, v \in K$ and $0 \leq \theta \leq 1$.

Using these definitions, we obtain:

Problem 4.

$$E(u) = \min_{v\in K} E(v),$$

where $u \in K$ is the minimum of the energy functional.

2.4.2 Weak formulation

We derive a variational formulation in this section. Let $\theta v + (1-\theta)u = u + \theta(v-u) \in K$ with $\theta \in [0,1]$. Then, we can follow by using the previously defined convex set properties:

$$\begin{aligned}
& E(u+\theta(v-u)) \geq E(u) \\
\Rightarrow \quad & \frac{d}{d\theta} E(u+\theta(v-u))|_{\theta=0} \geq \frac{d}{d\theta} E(u), \\
\Leftrightarrow \quad & \frac{d}{d\theta} E(u+\theta(v-u))|_{\theta=0} \geq 0 \\
\Rightarrow \quad & \frac{d}{d\theta} \int_\Omega (\mu \frac{1}{2} |\nabla(u+\theta(v-u))|^2 - f(v-u))\, dx|_{\theta=0} \geq 0 \\
\Rightarrow & \int_\Omega (\mu \nabla(u+\theta(v-u)) \cdot \nabla(v-u) - f(v-u))\, dx|_{\theta=0} \geq 0 \\
\Rightarrow \quad & \int_\Omega (\mu \nabla u \cdot \nabla(v-u) - f(v-u))\, dx \geq 0 \\
\Leftrightarrow \quad & \int_\Omega \mu \nabla u \cdot \nabla(v-u)\ dx - \int_\Omega f(v-u)\ dx \geq 0 \\
\Leftrightarrow \quad & \int_\Omega \mu \nabla u \cdot \nabla(v-u)\ dx - \int_\Omega f(v-u)\ dx \geq 0 \quad \forall v \in K.
\end{aligned}$$

In short hand notation, the last line is usually written as:

$$(\mu\nabla u, \nabla(v-u)) \geq (f, v-u).$$

With these calculations, we obtain the following variational form:

Problem 5 (Variational formulation of the obstacle problem)**.** *The obstacle problem in a VI (variational inequality) formulation is given by: Find $u \in K$ such that*

$$(\mu\nabla u, \nabla(v-u)) \geq (f, v-u),$$

for $K = \{v \in H^1 | v = u_0 \text{ on } \partial\Omega,\ v \geq g \text{ in } \Omega\}$.

2.4.3 Strong formulation

Using the fundamental lemma of calculus of variations (e.g., [43]), we derive the strong form:

Problem 6 (Strong form)**.** *Find $u : \Omega \to \mathbb{R}$, such that*

$$\begin{aligned}
-\nabla\cdot(\mu\nabla u) &\geq f && \text{in } \Omega,\\
u &\geq g && \text{in } \Omega,\\
(\nabla\cdot(\mu\nabla u) + f)(u-g) &= 0 && \text{in } \Omega,\\
u &= g && \text{on } \partial\Omega,\\
u &= g && \text{on } \Gamma,\\
\mu\nabla u\cdot n &= \mu\nabla g\cdot n && \text{on } \Gamma.
\end{aligned}$$

Remark 10 (Complementarity condition)**.** *The complementarity condition*

$$(\nabla\cdot(\mu\nabla u) + f)(u-g) = 0,$$

is a necessary condition since otherwise the first two inequalities have no direct relationship. In the variational form this is ensured by the function space K.

2.4.4 Lagrange multiplier formulations

In optimization it is well-known to treat Lagrange multipliers directly as solution variables. They serve as starting point for augmented Lagrangian formulations and the primal-dual active set method. For phase-field fracture, the latter has been worked out in [93] and part of these lecture notes in Chapter 3.

To begin and as background, it is of interest to work directly with the linear function space V rather than with the closed convex set K. The prize to pay is a second solution variable (which is more expensive in the solution approach though). To this end, a Lagrange multiplier $p \in L^2$ as an additional solution variable is introduced:

$$p = \begin{cases} 0 & \text{if } x \in \mathcal{I} \\ -\nabla\cdot(\mu\nabla u) - f & \text{if } x \in \mathcal{A} \end{cases}$$

With this definition it also becomes clear that the physical meaning of the Lagrange multiplier is a force in this problem. This force acts against the PDE in order to fulfill the constraint $u \geq g$.

Using the Lagrange multiplier, the strong form reads:

Problem 7 (Lagrange multiplier strong form)**.** *Find $u : \Omega \to \mathbb{R}$ and $p : \Omega \to \mathbb{R}$, such that*

$$\begin{aligned} -\nabla \cdot (\mu \nabla u) - p &= f && \text{in } \Omega, \\ u &\geq g && \text{in } \Omega, \\ p &\geq 0 && \text{in } \Omega, \\ p(u-g) &= 0 && \text{in } \Omega, \\ u &= u_0 && \text{on } \partial\Omega, \\ u &= g && \text{on } \Gamma, \\ \mu \nabla u \cdot n &= \mu \nabla g \cdot n && \text{on } \Gamma. \end{aligned}$$

Remark 11. *This formulation is clearly more expensive since the Lagrange multiplier is considered to be a solution variable. Nonetheless, a recent implementation for phase-field fracture was done in [113].*

We now turn to the weak setting:

Problem 8 (Lagrange multiplier weak form)**.** *The weak form reads formally: Find $\{u, p\} \in V \times N$:*

$$\begin{aligned} (\mu \nabla u, \nabla \phi) - (p, \phi) &= (f, \phi) \quad \forall \phi \in V \\ (u - g, q - p) &\geq 0 \quad \forall q \in N \end{aligned}$$

where $N := \{q \in Q^* | q \geq 0\}$ with Q^* being the dual space of a Hilbert space Q. For details see [90][p. 38ff].

2.4.5 Penalization for numerical treatment of the obstacle constraint

In practice, we face the question, how to realize the obstacle constraint. One possibility (in its basic form not the best!) is penalization, which is a well-known technique in nonlinear programming, e.g., [155, 156]. The idea is to asymptotically fulfill the constraint by including an additional term that acts against the optimization goal if the constraints are violated.

We introduce the penalty parameter $\gamma > 0$ (and have $\gamma \to \infty$ in mind for later). As before: Find $u \in K$:

$$(\mu \nabla u, \nabla (v - u)) \geq (f, v - u) \quad \forall v \in K.$$

A penalized version reads: Find $u_\gamma \in H_0^1$:

$$(\mu \nabla u_\gamma, \nabla v) - \gamma \int_\Omega [g - u]_+ v \, dx = (f, v) \quad \forall v \in H_0^1.$$

Here, $[x]_+ = \max(x, 0)$. Indeed we have

- $u_\gamma \geq g$ yields $0 \geq g - u$. Thus $[g - u]_+ = 0$
- $u_\gamma < g$ yields $0 < g - u$. Thus $[g - u]_+ > 0$

Remark 12 (Ill-conditioning)**.** *For large γ (which are necessary to enforce the constraint), the system matrix becomes ill-conditioned, i.e., the condition number is large since some entries are zero and others have their regular values. Therefore, the stability of the discrete system is heavily affected resulting in a significant error propagation (e.g., round-off errors due to machine precision) in the linear and nonlinear solution. Consequently, one has to find a trade-off between sufficiently small and large γ. An extension is an augmented Lagrangian method or active set method. A detailed discussion can be found for instance in [130].*

2.5 Kinematics and stress

In this section, we introduce basic ingredients of continuum mechanics such as displacements, strain, stress and constitutive laws.

Definition 16 (Displacements)**.** *Let $B \subset \mathbb{R}^d$ and $I \subset \mathbb{R}$. The displacement variable is denoted by $u := u(x,t) : B \times I \to \mathbb{R}^d$. In detail:*

$$u := u(x,t) = (u_1(x,t), \dots, u_d(x,t)) : B \times I \to \mathbb{R}^d.$$

Definition 17. *The linearized strain tensor is denoted by*

$$e = e(u) = \frac{1}{2}(\nabla u + \nabla u^T).$$

Example 4 (Gradient of displacements in $\mathbb{R}^3$)**.** *In $\mathbb{R}^3$ the gradient of displacements is a $\mathbb{R}^{3\times 3}$ matrix:*

$$\nabla u = \begin{pmatrix} \partial_x u_x & \partial_y u_x & \partial_z u_x \\ \partial_x u_y & \partial_y u_y & \partial_z u_y \\ \partial_x u_z & \partial_y u_z & \partial_z u_z \end{pmatrix}.$$

Definition 18 (Linear-stress relationship)**.** *A well-known linear stress-strain relationship is given by, e.g., [41, 140]:*

$$\sigma := \sigma(u) = Ce(u).$$

The tensor $C = (C_{ijkl})_{i,j,k,l=1}^3$ is a fourth-order material tensor that is positive definite, i.e., there exists a positive constant $\alpha > 0$ such that for any symmetric matrix ξ with the entries ξ_{ij} and any point $x \in B$,

$$\alpha|\xi|^2 \le C(x)\xi : \xi = \sum_{i,j,k,l=1}^{d} C_{ijkl}\xi_{ij}\xi_{kl}.$$

This reduces under the assumption of isotropy, homogeneity, and symmetry (see e.g. [140][p. 51]) to the following well-known law:

$$\sigma = Ce(u) = 2\mu e(u) + \lambda tr(e(u))I, \tag{2.8}$$

where I is the identity tensor and $tr(\cdot)$ the trace operator.

Definition 19. *We denote by $W(e(u))$ the elastic (strain) energy density.*

Example 5. *Two examples of energy density functions are provided.*

1. *In the case of the Laplacian or Poisson equation, the energy density function is*

$$W(e(u)) = \frac{\mu}{2}|\nabla u|^2,$$

where $\mu > 0$ is a material parameter. The energy is defined as

$$E_b(u) = \frac{1}{2}\int_B \mu|\nabla u|^2\,dx - \int_B fu\,dx. \tag{2.9}$$

The PDEs which we have to solve, are the Euler-Lagrange equations:

$$E_b'(u)(\psi) = \frac{1}{2}\int_B \mu\nabla u \cdot \nabla\psi\,dx - \int_B f\psi\,dx. \tag{2.10}$$

2. For a general elastic model, we have

$$W(e(u)) = Ce(u) : e(u),$$

which is the energy density using the Frobenius scalar product. Further details on $W(e(u))$ can be found in the literature, e.g., [80].

Remark 13. *Often, and in these lecture notes as well, C reduces to a few independent components as in (2.8). As an example that sometimes several components of C are of interest, we point to our own work [159] in which we computed 36 components (out of 81).*

Definition 20. *In engineering, material properties are often defined in terms of Young's modulus E_Y and the Poisson ratio ν_s. The relationship to the Lamé parameters μ_s and λ_s is as follows:*

$$\nu_s = \frac{\lambda_s}{2(\lambda_s+\mu_s)}, \quad E_Y = \frac{\mu_s(\lambda_s+2\mu_s)}{\lambda_s+\mu_s},$$
$$\mu_s = \frac{E_Y}{2(1+\nu_s)}, \quad \lambda_s = \frac{\nu_s E_Y}{(1+\nu_s)(1-2\nu_s)}.$$

Remark 14 (Signs of the solid material parameters)**.** *It can be shown that*

$$E_Y, \mu_s, \lambda_s > 0 \quad \textit{and} \quad -1 \leq \nu_s \leq 0.5.$$

Further calculations (e.g., [139]), yield the refined choice:

$$-1 \leq \nu_s \leq 0.5, \quad E_Y, \mu_s > 0, \quad \lambda_s > -\frac{2}{3}\mu_s. \tag{2.11}$$

As background we notice that Poisson's ratio describes the ratio that a compressed material expands into the two directions orthogonal to the compression direction. For $\nu_s \to 0.5$, an elastic material becomes incompressible. For most materials, it holds $0.5 \geq \nu_s > 0$. Some polymers have negative ν_s, which means that they become thicker when they are stretched. Moreover, the bulk modulus is often used, which is defined by $k = \lambda_s + \frac{2}{3}\mu_s$.

Definition 21. *For a given small parameter $\kappa > 0$, let us define the degradation function in terms of the phase-field function $\varphi : B \times I \to [0,1]$ as*

$$g(\varphi) := (1-\kappa)\varphi^2 + \kappa.$$

2.6 Modeling brittle fracture in a nutshell

We summarize the necessary notation to understand the following sections. A fundamental quantity is the critical surface energy density G_c (e.g., [176]), which can be related to the so-called fracture toughness.

Definition 22 (Critical energy release rate)**.** *The toughness (in this context better: critical energy release rate) G_c is a fundamental quantity that describes the resistance of a material to break. In other words, G_c is the energy required to create an infinitesimal crack at a point $x \in \bar{B}$, where B is the domain occupied by the material under consideration [176][Chapter 4].*

Definition 23 (Current energy release rate)**.** *The current energy release rate is denoted by G and defined as*

$$G := G(x) = -\frac{\partial(U - V)}{\partial A}, \quad x \in B, \tag{2.12}$$

where U is the potential energy available in the specimen $B \subset \mathbb{R}^d$ to create new fractures, V is the work associated to external forces and A is the fractured area. The current energy release rate has the unit $[G] = \mathrm{J/m^2}$.

The propagation of a fracture can be divided into three cases, e.g., [176, 25]:

- $G < G_c$: current surface energy density smaller than critical;
- $G = G_c$: propagation, (stable) growth;
- $G > G_c$: unstable growth.

2.7 Griffith's model

According to Griffith [69], a fracture propagates if the rate of elastic energy G decrease per unit surface area of the incremental step is equal to the quasi-static critical energy release rate G_c. The surface energy is a macroscopic description of the lattice debonding observed on the microscopic level.

Prescription of crack growth is based on a competition between bulk (elastic) and crack energy as modeled for brittle fracture:

Proposition 4. *Griffith's theory postulates:*

- *Surface energy is associated with surfaces where the deformation is discontinuous;*
- *A propagation criterion for these surfaces;*
- *An irreversibility condition for the fracture process.*

Remark 15. *Only recently, strong minimizers of Griffith's model was rigorously established in [44] for a 2D configuration.*

In Griffith's postulates, the fracture process is quasi-static and the laws hold true for brittle fractures, e.g. glass, concrete (in contrast to ductile fracture, e.g. steel), with a preexisting and well-defined crack path.

Definition 24 (Crack)**.** *A crack or fracture is defined as follows:*

$$\mathcal{C}(l) = \mathcal{C}_0 \cup \{x(s); 0 \leq s \leq l\}.$$

An illustration is provided in Figure 2.5. The length of a sufficiently smooth curve can be computed via the line integral $L_0 = \int_{x_0}^{x_l} ds$.

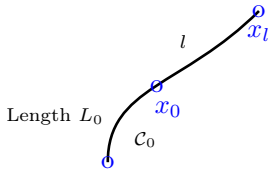

Figure 2.5: Old $\mathcal{C}_0$ and new part $\{x(s)\}$ of a crack resulting in $\mathcal{C}(l)$. The new crack contains the old crack.

Definition 25 (Bulk and surface energies)**.** *We define the potential and surface energies, respectively:*

$$\begin{aligned} \textit{Potential energy: } P(t,l) &:= E_b(\mathcal{C}(l), u_0) && \rightarrow \textit{monotonically decreasing} \\ \textit{Surface energy: } Q(t,l) &:= E_s(\mathcal{C}(l)) - E_s(\mathcal{C}_0) && \rightarrow \textit{monotonically increasing} \end{aligned}$$

Here, u_0 is a given initial displacement field. We shall investigate the trajectory of a crack along its path:

$$t \mapsto l(t),$$

where t is the time or loading step. The (current) energy release rate is defined as

$$G := -\frac{\partial P}{\partial l}.$$

Proposition 5 (Griffith's laws)**.** *Let $l(t)$ be absolutely continuous in t, then Griffith's law of crack evolution is satisfied:*

a) $l(0) = 0$ *(initial crack);*

b) $\partial_t l(t) \geq 0$ *(crack can only grow; irreversibility);*

c) $G \leq G_c$ *(energy release rate is bounded by the critical energy release rate);*

d) $(-G + G_c)\partial_t l = 0$ *(complementarity condition; crack can only grow when energy release rate is critical).*

The proof can be found in Proposition 4.8 in [59].

2.8 Francfort and Marigo's variational model for brittle fracture

In the year 1998, Francfort and Marigo [59] generalized Griffith's idea within a variational framework and for which we briefly recapitulate the main ideas.

2.8.1 Surface and bulk energies

In the following, we introduce the (crack) surface energy E_s, which connects G_c with the energy of current fracture.

Definition 26 (Surface energy)**.** *The surface energy of the crack $\mathcal{C} \subset \bar{B}$ is defined as:*

$$E_s(\mathcal{C}) = \int_{\mathcal{C}} G_c(s)\, ds = G_c \mathcal{H}^{d-1}(\mathcal{C}),$$

where $\mathcal{H}$ is the Hausdorff measure [71]. For smooth surfaces, the Hausdorff measure corresponds to the length of a crack $\mathcal{C}$ (1D) in a 2D setting and the crack area (2D) in a 3D setting.

Remark 16. *The interpretation of the previous definition is as follows. The higher $E_s(\mathcal{C})$, the more material is fractured. Moreover, the larger $G_c > 0$, the more energy is required to create new fractures. For $G_c = \infty$ the material cannot break.*

Next, we define a second energy, the bulk energy. The interplay of surface and bulk energies are key for a variational formulation of fracture.

Definition 27 (Bulk energy)**.** *The bulk energy is defined as*

$$E_b(\mathcal{C}, u) = \int_{\Omega} W(e(u))\, dx - \int_{\Omega} f u\, dx.$$

In fracture settings, volume forces are often of minor importance and therefore $f \equiv 0$. Then:

$$E_b(\mathcal{C}, u) = \int_{\Omega} W(e(u))\, dx.$$

In the following, elementary properties of the energy integrals are listed.

Proposition 6. *The bulk and surface energies shall satisfy the following elementary properties:*

a) E_s is strictly monotonically increasing in $\mathcal{C}$;

b) E_b is monotonically decreasing in $\mathcal{C}$ for any fixed $u \in V_u^D$.

Proposition 7 (Total energy in B)**.** *Let $\mathcal{C}$ be a given crack and u_D a given loading on $\partial\Omega_D$. Then the total energy $E_T(\mathcal{C}, u)$ is defined as*

$$E_T(\mathcal{C}, u) = E_b(\mathcal{C}, u) + E_s(\mathcal{C}).$$

Formally we obtain $u \in V_u^D$ by solving

$$\min_{u \in V_u^D} E_T(\mathcal{C}, u). \tag{2.13}$$

The functional $E_T(\mathcal{C}, u)$ is nonlinear. Discussions, technical details and further information can be found in [25].

2.8.2 Evolution laws

Proposition 8 (Law 2.9 from Francfort and Marigo [59])**.** *Let $u(x,t)$ be a monotonically increasing load on $\partial\Omega_D$ with $u(x,t) = t\bar{u}(x)$, given $\bar{u}$, for $t \geq 0$. Then $\mathcal{C}(t)$ for $t \in I$ should satisfy:*

1. *Irreversibility (entropy inequality principle): $\mathcal{C}(t)$ is an increasing function in t, where $\mathcal{C}(t) = \mathcal{C}_0$ is the initial fracture for $t = 0$.*

2. *Energy minimization: For $t \in I$ and $\tau \in I$ it holds*

$$E_T(\mathcal{C}(t), u(t)) \leq E_T(\mathcal{C}, u(t)) \quad \forall \cup_{\tau<t} \mathcal{C}(\tau) \subset \mathcal{C}.$$

3. *Constraint on the set of the solution:*

$$E_T(\mathcal{C}(t), u(t)) \leq E_T(\mathcal{C}(\tau), u(t)) \quad \forall \tau < t.$$

   This last law avoids admissibility of too many fracture solutions. For all details, we refer the reader to [59].

With these laws, irreversible quasi-static fracture propagation with minimal energy can be defined as a mapping $t \mapsto (u(t), \mathcal{C}(t))$ satisfying three conditions:

1. global stability: for every time $t \in I$, the solution $(u(t), \mathcal{C}(t))$ yields minimal energy at time t;

2. irreversibility: $\mathcal{C}(\tau) \subset \mathcal{C}(t)$ for $0 \leq \tau < t \leq T$;

3. energy balance: increment in stored energy plus crack energy increase equals the work performed by external forces (first law of thermodynamics).

Remark 17. *For $t \to \infty$ with a monotonically increasing load, a mechanical failure (thus total cracking) of the specimen arises. Thermodynamic interpretations of the previous laws $t \to \infty$ are discussed in detail in [119].*

Remark 18 (Entropy)**.** *Entropy characterizes the direction of energy transfer. In general, mechanical energy can be dissipated into other forms of energy. For instance, in fracture processes as in these lecture notes, we consider dissipation of mechanical energy into crack energy. The contrary is in general not true: once cracks (at least these cracks that we have in mind) are created, they will not heal. Physically speaking, when entropy holds in the strict sense, crack energy cannot be transformed back into mechanical energy. These considerations can be illustrated with a daily life example: take your scissors and cut a sheet of paper. The cut in the paper will always remain and the paper (if not cheating with adhesive tape) cannot be repaired.*

2.8.3 Specific forms of the total energy

Employing Proposition 7, we provide two specific examples:

1. Given the displacement $u : \Omega \to \mathbb{R}$ as a scalar-valued function, we deal with

$$E_T(\mathcal{C}, u) = \frac{1}{2}\int_\Omega |\nabla u|^2 \, dx + \int_{\mathcal{C}} G_c(x) \, ds.$$

2. Given $u : \Omega \to \mathbb{R}^d$ as the vector-valued elasticity, the energy functional is given as

$$E_T(\mathcal{C}, u) = \frac{1}{2}\int_\Omega \sigma(u) : e(u)\, dx + \int_{\mathcal{C}} G_c(x)\, ds.$$

In the following, we discuss some properties and their consequences and treatments.

Methods for evaluating the crack surface integral

In principle, we could now compute fracture problems that are covered by the previous physical laws. However E_b is defined on $\Omega \subset \mathbb{R}^d$ and E_s is defined in $\mathcal{C} \subset \mathbb{R}^{d-1}$. This causes numerical and mathematical problems in terms of discretization and well-posedness, respectively. Because the fracture $\mathcal{C}$ is an interface itself. In fact, extended/generalized finite elements [126, 60, 117, 15] or boundary element methods [40, 136, 141, 115] represent the interface as a sharp line or area. In phase-field, the main idea is to approximate E_s via domain integrals that live on the entire domain B.

Treatment of the surface energy: interface-capturing with elliptic functionals

Our problem belongs to the class of free discontinuity problems. Here, we seek an unknown pair: (u, Γ), where Γ is varying in a class of closed subsets of a fixed open set $B \subset \mathbb{R}^d$. Then, we seek $u : B\backslash\Gamma \to \mathbb{R}^d$ by minimizing $E_T(\mathcal{C}, u)$. That the limit case for $\varepsilon = 0$ is well-posed requires the space of special functions of bounded variation, going back to [66] based mainly on ideas of di Giorgi.

The idea of using elliptic functionals for approximation goes back to Modica and Mortola [125] who approximated the perimeter functional with such a procedure. Ambrosio and Tortorelli [8, 9] introduced an approximation procedure with an auxiliary variable φ. Beside fracture, other applications of this approximation procedure is image segmentation in which contours from input images shall be reconstructed [127, 38, 39, 31] or in materials sciences [138]. A concise overview is provided in [7][Introduction, Part I, page 3]. Further chapters in that book provide more information, for instance from Alberti (in particular p. 99 - 101) and Braides, pages 171 - 180.

Proposition 9 (Elliptic approximation functional)**.** *To approximate the surface energy on the interface $\mathcal{C}$, in [8, 9], the following elliptic functional is proposed:*

$$\frac{1}{2}\int_B G_c\Big(\frac{1}{\varepsilon}(1-\varphi)^2 + \varepsilon|\nabla\varphi|^2\Big)\, dx \quad \to \quad \int_{\mathcal{C}} G_c\, ds \quad \text{for } \varepsilon \to 0.$$

Remark 19 (AT1 vs. AT2)**.** *The term $(1-\varphi)^\alpha$ with $\alpha = 2$ is also known as part of a so-called AT2 model*[1]*. In some works, the AT1 model with $\alpha = 1$ is of interest, e.g., [28, 55].*

Let us give some qualitative explanations of the choice of

$$\frac{1}{2}\int_B \left(\frac{1}{\varepsilon}(1-\varphi)^2 + \varepsilon|\nabla\varphi|^2\right) dx.$$

The first term is actually the term we are interested in, namely determining values that are 0 (crack) or 1 (unbroken solid). In fact for $\varepsilon \to 0$ we enforce the behavior of sharp changes between

[1] AT = Ambrosio-Tortorelli

0 and 1 since the first term dominates. For regularity purposes, we add the gradient penalty term smoothing the transition from 0 to 1. The larger ε, the smoother the transition zone. Proofs are provided in [128, 58] and [169][Section 5.5].

We now apply the previous proposition to $E_T(u, C)$:

Proposition 10 (Regularized phase-field for Laplacian)**.** *The non-regularized energy functional reads:*

$$E_T(u, \mathcal{C}) = \frac{1}{2} \int_\Omega |\nabla u|^2 \, dx + G_c H^{d-1}(\mathcal{C}).$$

Using Ambrosio-Tortorelli elliptic functionals, we replace the sharp lower-dimensional crack $\mathcal{C}$ by a smoothed indicator function φ and we obtain with the help of Definition 21 the following regularized version:

$$E_{T,\varepsilon}(u, \varphi) = \frac{1}{2} \int_B g(\varphi) |\nabla u|^2 \, dx + \frac{1}{2} \int_B G_c \left(\frac{1}{\varepsilon}(1-\varphi)^2 + \varepsilon |\nabla \varphi|^2 \right) dx$$

with $u \in H^1(B)$, $u\varphi \in H^1(B)$, and $0 \leq \varphi \leq 1$.

Remark 20 (Regularization parameter κ)**.** *While using the elliptic surface approximation, we also modified the bulk energy term by inserting the so-called degradation function $g(\varphi)$ with the regularization parameter κ in order to extend the bulk energy from Ω to B. This parameter is numerically useful when $\varphi \to 0$ such that the discrete system matrix remains regular:*

$$[(1-\kappa)\varphi^2 + \kappa] |\nabla u|^2 \quad \to \quad \kappa |\nabla u|^2 \quad \text{for } \varphi = 0.$$

Mathematically, $\varphi^2 |\nabla u|^2$ (thus $\kappa = 0$) works as well; see Braides 1998 [30] or [9]. In the latter reference on page 107, there is however a discussion what might happen in the theory when $\kappa = 0$; see further in [10]. For dynamic fracture, Borden et al. [21] also worked with $\kappa = 0$ because here, the acceleration term $\partial_t^2 u$ is not weighted with $g(\varphi)$ and thus provides non-zero matrix entries in the discrete system.

Remark 21 (κ and ε)**.** *The investigation of κ and ε has been an important part of our numerical work over the last years. A summary of our current findings and thoughts can be found in [169][Section 5.5].*

Proposition 11. *Using Γ-convergence (e.g., again [30]) for $\varepsilon \to 0$:*

$$E_{T,\varepsilon}(u, \varphi) = \begin{cases} E_T(u, \mathcal{C}) & \text{if } \varphi = 1 \text{ a.e. in } B, \\ +\infty, & \text{otherwise.} \end{cases}$$

Proof. See [24][Section 2.1]. □

In a similar way, we obtain for linearized elasticity:

Proposition 12 (Regularized phase-field for linearized elasticity)**.** *The total energy functional reads:*

$$E_{T,\varepsilon}(u, \varphi) = \frac{1}{2} \int_B g(\varphi) \sigma(u) : e(u) \, dx + \frac{1}{2} \int_B G_c \Big(\frac{1}{\varepsilon}(1-\varphi)^2 + \varepsilon |\nabla \varphi|^2 \Big) \, dx$$

with $u \in H^1(B)^d$, $\varphi u \in H^1(B)^d$, and $0 \leq \varphi \leq 1$.

2.9 Euler-Lagrange equations: derivation of weak forms

2.9.1 Euler-Lagrange equations without inequality constraint

For solving $\min E_{T,\varepsilon}(u,\varphi)$, we derive the first variation, resulting in the Euler-Lagrange equations. Of course, we only obtain stationary points rather than local minima. Starting with energy minimization

$$\min_{u\in V_u^D,\varphi\in K} E_{T,\varepsilon}(u,\varphi),$$

we obtain from differentiation the first variation:

$$E'_{T,\varepsilon}(u,\varphi)(w,\psi-\varphi)\geq 0.$$

We deal with a VI in φ because of the irreversibility constraint $0\leq\varphi^n\leq\varphi^{n-1}\leq 1$. Let us assume for the moment that we are interested in

$$E'_{T,\varepsilon}(u,\varphi)(w,\psi)=0.$$

Then, we have

Lemma 1. *The first variations for $(u,\varphi)\in V_u^D\times H^1(B)$ are given by:*

$$\begin{aligned}
E'_{T,\varepsilon,u}(u,\varphi)(w) &= \int_B g(\varphi)\nabla u\cdot\nabla w\,dx,\\
E'_{T,\varepsilon,\varphi}(u,\varphi)(\psi) &= \int_B(1-\kappa)\varphi|\nabla u|^2\psi\,dx+\int_B G_c\left(\frac{1}{\varepsilon}(1-\varphi)(-\psi)+\varepsilon\nabla\varphi\cdot\nabla\psi\right)dx.
\end{aligned}$$

Proof. First, we notice that the directional derivative of $f(u):=|\nabla u|^2$ into the direction w is formally obtained with the help of the chain rule (e.g., [43]) and given by

$$\begin{aligned}
f'(u)(w) &= \lim_{s\to 0}\frac{f(u+sw)-f(u)}{s}\\
&= [|\nabla u|^2]'(w)=\left(\sum_{i=1}^d(\partial_i u)^2\right)'(w)=2\sum_{i=1}^d(\partial_i u)(\partial_i w)\\
&= 2\nabla u\cdot\nabla w.
\end{aligned}$$

For the energy functional itself, we simply evaluate for u

$$E'_{T,\varepsilon,u}(u,\varphi)(w)=\lim_{s\to 0}\frac{E_{T,\varepsilon}(u+sw,\varphi)-E_{T,\varepsilon}(u,\varphi)}{s}.$$

To this end, we obtain for variations in u, while fixing φ:

$$\begin{aligned}
&\lim_{s\to 0} \frac{E_{T,\varepsilon}(u+sw,\varphi) - E_{T,\varepsilon}(u,\varphi)}{s} \\
&= \lim_{s\to 0} \left(\frac{1}{2}\int_B g(\varphi)|\nabla(u+sw)|^2\,dx - \frac{1}{2}\int_B g(\varphi)|\nabla u|^2\,dx \right) s^{-1} \\
&= \lim_{s\to 0} \left(\frac{1}{2}\int_B g(\varphi)(|\nabla u|^2 + 2s\nabla u\cdot\nabla w + s^2|\nabla w|^2)\,dx - \frac{1}{2}\int_B g(\varphi)|\nabla u|^2\,dx \right) s^{-1} \\
&= \lim_{s\to 0} \left(\frac{1}{2}\int_B g(\varphi)(2s\nabla u\cdot\nabla w + s^2|\nabla w|^2)\,dx \right) s^{-1} \\
&= \int_B g(\varphi)\nabla u\cdot\nabla w\,dx.
\end{aligned}$$

In the last step, we utilized

$$\lim_{s\to 0} \frac{1}{2}\int_B g(\varphi)s|\nabla w|^2)\,dx = 0.$$

For the directional derivative into φ, while fixing u, we notice first

$$g'(\varphi)(\psi) = 2(1-\kappa)\varphi\psi.$$

Thus

$$E'_{T,\varepsilon,\varphi}(u,\varphi)(\psi) = \lim_{s\to 0} \frac{E_{T,\varepsilon}(u,\varphi+s\psi) - E_{T,\varepsilon}(u,\varphi)}{s}.$$

Then, we obtain with the same differentiation rules as before

$$\begin{aligned}
E'_{T,\varepsilon,\varphi}(u,\varphi)(\psi) &= \frac{1}{2}\int_B g'(\varphi)(\psi)|\nabla u|^2\,dx \\
&\quad + \frac{1}{2}\int_B G_c\Big(2\frac{1}{\varepsilon}(1-\varphi)(-\psi) + 2\varepsilon\nabla\varphi\cdot\nabla\psi\Big)\,dx \\
&= \int_B (1-\kappa)\varphi\psi|\nabla u|^2\,dx + \int_B G_c\Big(-\frac{1}{\varepsilon}(1-\varphi)\psi + \varepsilon\nabla\varphi\cdot\nabla\psi\Big)\,dx.
\end{aligned}$$

□

Writing the same contents in the usual notation, we obtain:

Problem 9. *Introducing a semi-linear form $A(\cdot)(\cdot)$ in which the first argument may be nonlinear and the second argument is linear, we write the previous statements in the following notation:*

$$\begin{aligned}
A_1(U)(\Psi) &= E'_{T,\varepsilon,u}(u,\varphi)(w) = (g(\varphi)\nabla u, \nabla w) \\
A_2(U)(\Psi) &= E'_{T,\varepsilon,\varphi}(u,\varphi)(\psi) = \big((1-\kappa)\varphi|\nabla u|^2, \psi\big) - \frac{1}{\varepsilon}(G_c(1-\varphi),\psi) + \varepsilon(G_c\nabla\varphi,\nabla\psi).
\end{aligned}$$

These formulations are similar in their structure as earlier discussed in (2.4) and (2.5).

2.9.2 Euler-Lagrange system for elasticity with crack irreversibility

In this section, we extend from the scalar-valued case from the Laplacian to elasticity, and second, we consider the irreversibility constraint. The starting point now is Proposition 12 and the energy minimization problem

$$\min_{u\in V_u^D,\varphi\in K} E_{T,\varepsilon}(u,\varphi),$$

and the first variation:

$$E'_{T,\varepsilon}(u,\varphi)(w,\psi-\varphi)\geq 0.$$

Then, we obtain

Proposition 13. *We consider now vector-valued displacements $u : B\times I\to\mathbb{R}^d$, namely elasticity. The first variations for $(u,\varphi)\in V_u^D\times K$ are given by:*

$$\begin{aligned}
E'_{T,\varepsilon,u}(u,\varphi)(w) &= \int_B g(\varphi)\sigma(u):\nabla w\,dx,\\
E'_{T,\varepsilon,\varphi}(u,\varphi)(\psi-\varphi) &= \int_B (1-\kappa)\varphi\sigma(u):e(u)(\psi-\varphi)\,dx\\
&\quad+\int_B G_c\left(-\frac{1}{\varepsilon}(1-\varphi)(\psi-\varphi)+\varepsilon\nabla\varphi\cdot\nabla(\psi-\varphi)\right)dx.
\end{aligned}$$

Proof. The proof follows from Lemma 1 by considering the convex set K and the steps from Section 2.4.2. Next, for the first integral, we notice that

$$\sigma(u):e(u)=\sum_{i,j=1}^{d}\sigma_{ij}(u)e_{ij}(u).$$

The directional derivative into the direction $w=(w_1,\dots,w_d)$ (now vector-valued) is obtained from applying the product rule to $\sigma(u):e(u)$:

$$(\sigma(u):e(u))'(w)=\sigma'(u)(w):e(u)+\sigma(u):e(u)'(w).$$

The component-wise representation will yield the result. As example, we obtain for $d=3$, for instance

$$e(u)'(w)=\frac{1}{2}(\nabla w+\nabla w^T),$$

with

$$\nabla w=\begin{pmatrix}\partial_x w_x & \partial_y w_x & \partial_z w_x\\ \partial_x w_y & \partial_y w_y & \partial_z w_y\\ \partial_x w_z & \partial_y w_z & \partial_z w_z\end{pmatrix}.$$

□

2.10 A weak formulation of quasi-static brittle phase-field fracture

With the previous derivations, we formulate the following problem statement for quasi-static brittle phase-field fracture. To this end, we apply Proposition 13 to a loading sequence in time and we obtain as coupled variational inequality system (CVIS)

Proposition 14 (CVIS for quasi-static brittle phase-field fracture)**.** *For the loading steps $n = 1, 2, 3, \dots, N$, given φ^{n-1}, set up $K := K(\varphi^{n-1})$, find $U = (u, \varphi) := U^n = (u^n, \varphi^n) \in V_u^D \times K$ with $\varphi(0) = \varphi_0$ such that*

$$A(U)(\Psi - \Phi) \geq 0 \quad \forall \Psi = (w, \psi) \in V_u^0 \times K,$$

with $\Phi = (0, \psi)$ and the decomposition into single semi-linear forms

$$A(U)(\Psi - \Phi) = A_1(U)(\Psi) + A_2(U)(\Psi - \Phi),$$

and

$$\begin{aligned} A_1(U)(\Psi) &= \int_B g(\varphi)\sigma(u) : \nabla w \, dx, \\ A_2(U)(\Psi - \Phi) &= \int_B (1-\kappa)\varphi\sigma(u) : e(u) \cdot (\psi - \varphi) \, dx \\ &\quad - \int_B \frac{G_c}{\varepsilon}(1-\varphi) \cdot (\psi - \varphi) \, dx + \int_B G_c \varepsilon \nabla\varphi \cdot \nabla(\psi - \varphi) \, dx. \end{aligned}$$

Or alternatively using parentheses to represent integrals:

$$\begin{aligned} A_1(U)(\Psi) &= \left(g(\varphi)\sigma(u), \nabla w\right), \\ A_2(U)(\Psi - \Phi) &= \left((1-\kappa)\varphi\sigma(u) : e(u), \psi - \varphi\right) \\ &\quad + \left(-\frac{G_c}{\varepsilon}(1-\varphi), \psi - \varphi\right) + \left(G_c \varepsilon \nabla\varphi, \nabla(\psi - \varphi)\right). \end{aligned}$$

The corresponding energy formulation is provided in Proposition 12.

Proof. We employ Proposition 13 for the loading sequence $n = 1, 2, 3, \dots, N$ while defininining the convex set $K := K(\varphi^{n-1})$, and then obtain for each step t_n the corresponding formulation. □

2.11 A space-time phase-field fracture model

The main idea is to treat the irreversibility $\partial_t \varphi \leq 0$ in a time-continuous fashion. However, we continue with the previous quasi-brittle fracture model. The extension to dynamic fracture with time derivatives in the displacement PDE, e.g., [27], is possible to be designed in a space-time fashion as well and partially addressed in these lecture notes. To formulate the space-time forward problem, we first introduce some basic notation and then proceed with the construction of function spaces and a space-time weak formulation. Afterwards, a space-time Galerkin discretization is derived with discontinuous (dG) functions in time and a classical continuous Galerkin (cG) method in space.

2.11.1 Notation

Let[2] $\Omega \subset \mathbb{R}^2$ be a bounded domain with the partitioned boundary $\partial\Omega = \Gamma_N \dot\cup \Gamma_D$. Here, the Hausdorff measure for the Neumann boundary Γ_N and the Dirichlet boundary Γ_D is nonzero. Further, we introduce $V \coloneqq H^1_D(\Omega;\mathbb{R}^2) \times H^1(\Omega)$ for the displacement field u and the phase-field φ, where

$$H^1(\Omega;\mathbb{R}^2) \coloneqq \{v \in L^2(\Omega;\mathbb{R}^2)\colon D^\alpha v \in L^2(\Omega;\mathbb{R}^2)\ \forall \alpha \in \mathbb{N}_0^2,\ |\alpha| \le 1\},$$
$$H^1_D(\Omega;\mathbb{R}^2) \coloneqq \{v \in H^1(\Omega;\mathbb{R}^2)\colon v|_{\Gamma_D} = 0\}.$$

For a bounded time interval $I = [0,T]$ we define the following temporal space:

$$X \coloneqq \{U = (u,\varphi)\colon U \in L^2(I,V),\ \partial_t\varphi \in L^2(I, H^1(\Omega)^*)\}$$

where $H^1(\Omega)^*$ denotes the topological dual space to $H^1(\Omega)$. On V and X we define the usual L^2 scalar products

$$(U,V) \coloneqq \int_\Omega U \cdot V \,\mathrm{d}x \quad \forall U,V \in V,$$
$$(U,V)_I \coloneqq \int_I \int_\Omega U \cdot V \,\mathrm{d}x\,\mathrm{d}t = \int_I (U(t),V(t))\,\mathrm{d}t \quad \forall U,V \in X,$$

with the corresponding norms $\|\cdot\|$ and $\|\cdot\|_I$, and in addition the restricted inner products

$$(U(t),V(t))_{\{\partial_t\varphi(t)>0\}} \coloneqq \begin{cases} (U(t),V(t)), & \partial_t\varphi(t) > 0, \\ 0, & \text{else}, \end{cases}$$
$$(U,V)_{\{\partial_t\varphi>0,I\}} \coloneqq \int_I (U(t),V(t))_{\{\partial_t\varphi(t)>0\}}\,\mathrm{d}t \quad \forall U,V \in X.$$

Later we will use $(\cdot,\cdot)_{\{\varphi(t_i)>\varphi(t_j)\}}$, defined similar to $(\cdot,\cdot)_{\{\partial_t\varphi(t)>0\}}$.

2.11.2 Bochner spaces - space-time functions

For the correct function spaces for formulating time-dependent variational forms, we define the Bochner integral. Let $I \coloneqq [0,T]$ with $0 < T < \infty$ be a bounded time interval with end time value T. For any Banach space X and $1 \le p \le \infty$, the space

$$L^p(I,X)$$

denotes the space of L^p integrable functions f from the time interval I into X. This is a Banach space, the so-called Bochner space, with the norm, see [172],

$$\|v\|_{L^p(I,X)} \coloneqq \Big(\int_I \|v(t)\|_X^p\,dt\Big)^{1/p}$$
$$\|v\|_{L^\infty(I,X)} \coloneqq \operatorname*{ess\,sup}_{t\in I} \|v(t)\|_X.$$

[2]It is important to notice that the dimension is restricted to 2 due to Sobolev embedding theorems. More details in [87, 88, 86]. This does not mean that three-dimensional problems cannot be addressed. Computationally, one can simply try, but mathematically it is not rigorously justified, and certainly requires adjustments in the functional framework.

Example 6. *For instance, we can define a H^1-space in time:*

$$H^1(I,X) = \left\{ v \in L^2(I,X) |\, \partial_t v \in L^2(I,X) \right\}.$$

Functions that are even continuous in time, i.e., $u : I \to X$, are contained in spaces like $C(I;X)$ with

$$\|u\|_{C(I;X)} := \max_{0\le t\le T} \|u(t)\| < \infty.$$

Definition 28 (Weak derivative of space-time functions)**.** *Let $u \in L^1(I;X)$. A function $v \in L^1(I;X)$ is the weak derivative of v, denoted as*

$$\partial_t u = v,$$

if

$$\int_0^T \partial_t \varphi(t) u(t)\, dt = -\int_0^T \varphi(t) v(t)\, dt,$$

for all test functions $\varphi \in C_c^\infty(I)$.

In particular, the following result holds:

Theorem 4 ([54])**.** *Assume $v \in L^2(I, H_0^1)$ and $\partial_t v \in L^2(I, H^{-1})$. Then, v is continuous in time, i.e.,*

$$v \in C(I, L^2),$$

(possibly redefined on a set of measure zero). Furthermore, the mapping

$$t \mapsto \|v(t)\|^2_{L^2(X)}$$

is absolutely continuous with

$$\frac{d}{dt}\|v(t)\|^2_{L^2(X)} = 2\langle \frac{d}{dt} v(t), v(t)\rangle,$$

for a.e. $0 \le t \le T$.

Proof. See Evans [54], Theorem 3 in Section 5.9.2. □

Remark 22. *The importance of this theorem lies in the fact that now the point-wise prescription of initial conditions makes sense in weak formulations.*

Remark 23. *More details of these spaces by means of the Bochner integral can be found in [45, 172] and also [54].*

2.11.3 Weak formulation

We introduce the space-time weak formulation in the following way:

Proposition 15. *Given initial values $U_0 = (u_0, \varphi_0) \in V$ we seek $U \in X$ that solves*

$$\begin{aligned} (g(\varphi)\mathbb{C}e(u), e(\Phi_u))_I &= 0, \\ G_c\varepsilon(\nabla\varphi, \nabla\Phi_\varphi)_I - \frac{G_c}{\varepsilon}(1-\varphi, \Phi_\varphi)_I + (1-\kappa)(\varphi\mathbb{C}e(u) : e(u), \Phi_\varphi)_I & \\ + \gamma(\partial_t\varphi, \Phi_\varphi)_{\{\partial_t\varphi>0, I\}} + \eta(\partial_t\varphi, \Phi_\varphi)_I &= 0, \end{aligned} \tag{2.14}$$

for every test function $\Phi = (\Phi_u, \Phi_\varphi) \in X$. By $\Phi_{u:\perp}$ we denote the component of Φ_u that is orthogonal to Γ_N. In order to extend the displacements to the entire domain Ω (including the broken area), as before, we employ the degradation function $g(\varphi) \coloneqq (1-\kappa)\varphi^2 + \kappa$. Further $\mathbb{C}$ represents the elasticity tensor as before.

Remark 24. *The crack irreversibility constraint $\partial_t \varphi \leq 0$ is preserved on the time-continuous level in the weak formulation (2.14) in order to implement a Galerkin discretization in time. This is a minor deviation from the physics modeling point of view from many other phase-field fracture formulations found in the literature. But it is major change in terms of mathematical modeling and numerical modeling.*

Remark 25 (Convexification)**.** *We observe that the numerical solution procsess of (2.14) is enhanced by strict positivity $\eta > 0$. In fact, it was shown for the quasi-static case (in phase-field fracture optimal control) that the control-to-state mapping is single valued for sufficiently large values of η [129]. This is due to the resulting strict convexity of the energy corresponding to the equation. Unfortunately crack growth is also penalized by the convexification term $\eta(\partial_t \varphi, \Phi_\varphi)_I$. Therefore we must select $\gamma \gg \eta$ to guarantee the dominance of the physically motivated term $\gamma(\partial_t \varphi, \Phi_\varphi)_{\{\partial_t \varphi > 0, I\}}$.*

2.12 A phase-field model for dynamic fracture (extensive exercise)

In this section, we concentrate on an extensive exercise that focuses on dynamic fracture. As previously mentioned, space-time formulations are the most natural settings for dynamic fracture.

Remark 26. *For a better adaptation to our lecture, the model is modified. Note, that the version presented below is commonly not used in the literature in this specific form.*

2.12.1 The model (partially incomplete - to be augmented in the exercises)

Let $\Omega \subset \mathbb{R}^d$, $d = 2$ be open and let $I := [0, T]$ with $T > 0$ being the end time value. Find $u : \Omega \times I \to \mathbb{R}$ and $\varphi : \Omega \times I \to \mathbb{R}$ such that

$$
\begin{aligned}
\rho_s \partial_t^2 u - \nabla \cdot (\varphi^2 \nabla u) &= f \quad \text{in } \Omega \times I, \\
\partial_t^2 \varphi + \varphi |\nabla u|^2 - \varepsilon \Delta \varphi + \frac{1}{\varepsilon}(1-\varphi) &\leq 0 \quad \text{in } \Omega \times I, \\
\partial_t \varphi &\leq 0 \quad \text{in } \Omega \times I, \\
u &= 0 \quad \text{on } \partial\Omega \times I, \\
\varepsilon \partial_n \varphi &= 0 \quad \text{on } \partial\Omega \times I, \\
u &= u_0 \quad \text{in } \Omega \times \{0\}, \\
\partial_t u &= v_0 \quad \text{in } \Omega \times \{0\}, \\
\varphi &= \varphi_0 \quad \text{in } \Omega \times \{0\}, \\
\partial_t \varphi &= \chi_0 \quad \text{in } \Omega \times \{0\}.
\end{aligned}
$$

2.12.2 Space-time formulation of the elastic wave equation

The above model consists of two wave equations, which are both space- and time-dependent. One of the most elegant ways for a variational formulation (neglecting the inequality constraints for a moment) is a space-time formulation. We briefly introduce the concept in this section.

Let us consider a second-order hyperbolic PDE as follows:

Problem 10. *Let $\Omega \subset \mathbb{R}^d$ be open and let $I := [0,T]$ with $T > 0$. Find $u : \Omega \times I \to \mathbb{R}$ and $\partial_t u : \Omega \times I \to \mathbb{R}$ such that*

$$\begin{aligned} \rho \partial_t^2 u - \nabla \cdot (a \nabla u) &= f \quad \text{in } \Omega \times I, \\ u &= 0 \quad \text{on } \partial\Omega_D \times I, \\ a \partial_n u &= 0 \quad \text{on } \partial\Omega_N \times I, \\ u &= u_0 \quad \text{in } \Omega \times \{0\}, \\ v &= v_0 \quad \text{in } \Omega \times \{0\}. \end{aligned}$$

We need proper functions spaces required for the weak formulation. Let us denote L^2 and H^1 as the usual Hilbert spaces and H^{-1} as the dual space to H^1. For the initial functions u_0 and v_0 we assume:

- $u_0 \in H_0^1(\Omega)^d$;
- $v_0 \in L^2(\Omega)^d$.

For the right hand side (source term) we assume

- $f \in L^2(I, H^{-1}(\Omega))$, where $L^2(\cdot,\cdot)$ is a Bochner space; see Section 2.11.2.

We introduce the following short-hand notation:

- $H := L^2(\Omega)^d$;
- $V := H_0^1(\Omega)^d$;
- V^* is the dual space to V;
- $\bar{H} := L^2(I, H)$;
- $\bar{V} := \{v \in L^2(I,V) |\ \partial_t v \in \bar{H}\}$.

Remark 27. *We note that the initial values are well-defined due to Theorem 4.*

Theorem 5. *If the operator $A := -\nabla \cdot (a \nabla u)$ satisfies the coercivity estimate:*

$$(Au, u) \geq \beta \|u\|_1^2, \quad u \in V, \quad \beta > 0,$$

then there exists a unique weak solution with the following properties:

- $u \in \bar{V} \cap C(\bar{I}, V)$;
- $\partial_t u \in \bar{H} \cap C(\bar{I}, H)$;
- $\partial_t^2 u \in L^2(I, V^*)$.

Proof. See Lions and Magenes [107] or Wloka [172]. □

Definition 29. *The previous derivations allow us to define a compact space-time function space for the wave equation:*

$$\bar{X} := \{v \in \bar{V} \,|\, v \in C(\bar{I}, V), \partial_t v \in C(\bar{I}, H), \partial_t^2 v \in L^2(I, V^*)\}.$$

To design a Galerkin time discretization, we need to get rid of the second-order time derivatives and therefore usually the wave equation is re-written in terms of a mixed first-order system:

Problem 11. *Let $\Omega \subset \mathbb{R}^d$ be open and let $I := [0, T]$ with $T > 0$. Find $u : \Omega \times I \to \mathbb{R}$ and $\partial_t u = v : \Omega \times I \to \mathbb{R}$ such that*

$$\begin{aligned}
\rho \partial_t v - \nabla \cdot (a \nabla u) &= f \quad \text{in } \Omega \times I, \\
\rho \partial_t u - \rho v &= 0 \quad \text{in } \Omega \times I, \\
u &= 0 \quad \text{on } \partial\Omega_D \times I, \\
a \partial_n u &= 0 \quad \text{on } \partial\Omega_N \times I, \\
u &= u_0 \quad \text{in } \Omega \times \{0\}, \\
v &= v_0 \quad \text{in } \Omega \times \{0\}.
\end{aligned}$$

To derive a space-time formulation, we first integrate formally in space. Below we explain why we choose the notation for the test function in this way:

$$\begin{aligned}
A_v(U)(\psi^u) &= (\rho \partial_t v, \psi^u) + (a \nabla u, \nabla \psi^u) - (f, \psi^u), \\
A_u(U)(\psi^v) &= (\rho \partial_t u, \psi^v) - (\rho v, \psi^v).
\end{aligned}$$

And then in time:

$$\begin{aligned}
\bar{A}_v(U)(\psi^u) &= \int_I \left((\rho \partial_t v, \psi^u) + (a \nabla u, \nabla \psi^u) - (f, \psi^u) \right) dt + (v(0) - v_0, \psi^u(0)), \\
\bar{A}_u(U)(\psi^v) &= \int_I \left((\rho \partial_t u, \psi^v) - (\rho v, \psi^v) \right) dt + (u(0) - u_0, \psi^v(0)).
\end{aligned}$$

The total problem reads:

Problem 12. *Find $U = (u, v) \in X_u \times X_v$ with $X_u = X$ and $X_v := \{w \in \bar{H} | w \in C(\bar{I}, H), \partial_t w \in L^2(I, V^*)\}$ such that*

$$\bar{A}(U)(\Psi) = 0 \quad \forall \Psi = (\psi^u, \psi^v) \in X_u \times X_v,$$

where

$$\bar{A}(U)(\Psi) := \bar{A}_v(U)(\psi^u) + \bar{A}_u(U)(\psi^v).$$

Such a formulation is the starting point for the discretization: either in space-time or using a sequential time-stepping scheme and for instance FEM in space.

Remark 28. *Be careful that the trial and test functions are switched in the wave equation. What does this mean? Formally, we compute in the first equation v using as test function ψ^u which belongs to the trial space of u. Vice versa for the second equation. That this choice can be justified can be seen in the following: the variable u needs higher-order regularity in space, therefore we work with the space X_u. Once differentiating in time, yields less regularity for v. In order to apply the correct boundary conditions and partial integration in the first equation $\bar{A}_v$ (to determine v), we need an object from the stronger space, namely X_u as test function.*

2.13 Exercises

Exercise 1. *Given the energy functional in Proposition 12, derive the Euler-Lagrange equations.*

Exercise 2. *Describe the number and type of nonlinearities in Proposition 14. Can further nonlinearities arise? If yes, which ones?*

Exercise 3.

1. *Write $\varphi^2 \nabla u$ component-wise.*
2. *Write $\varphi |\nabla u|^2$ component-wise.*

Exercise 4. *Concerning he dynamic fracture model in Section 2.12.1, please select three exercises you want to work on.*

1. *The dynamic fracture model in Section 2.12.1 is incomplete because the compatibility condition is missing. Please write down this condition.*
2. *Which coupling: volume or surface (interface)?*
3. *Is the model linear or nonlinear?*
4. *Is it a variational equation or variational inequality?*
5. *Is the model stationary or time-dependent?*
6. *Derive the weak formulation.*
7. *Formulate a compact semi-linear form to describe the weak form.*
8. *Using the compact semi-linear form, write down the compact abstract problem as a root-finding problem.*
9. *Derive the energy formulation corresponding to the weak form?*
10. *Double-check that the energy derivative of the energy formulation yields the PDE in a weak form (actually this is also known as Euler-Lagrange equations).*
11. *What does it mean that the energy formulation exists?*
12. *Manipulate the PDE such that no energy formulation exists.*
13. *Derive a quasi-static version by manipulating the above model.*
14. *How can we linearize the problem?*
15. *Use penalization, see Section 2.4.5 and rewrite the variational inequality as variational equation.*
16. *Space-time: In order to derive a Galerkin formulation for the discretization in space and time, we need to get rid of the second-order derivatives in time. Write down a model with first-order derivatives in time. How many solution variables do we have now?*
    Hint: For space-time formulations of second-order hyperbolic PDEs, we also refer to Section 2.12.2.

Chapter 3

Regularization, discretization and numerical solution (Session 2)

In the previous chapter, we arrived at a coupled variational inequality system (CVIS), namely Proposition 14. Therein, we deal with three nonlinearities: nonlinear coupling between displacement and the phase-field systems, possible nonlinear constitutive laws, and the variational inequality constraint. The later needs to be regularized for which in the literature various methods have been proposed; see [169][Chapter 5]. We pursue an approach to which a primal-dual active set method can be applied [74, 93]. Afterwards, the resulting system is discretized with a adaptive Galerkin finite element method, which is nowadays standard and for details we refer to classical textbooks [32, 29, 42]. Adaptivity is based on a predictor-corrector approach by choosing a given small regularization parameter ε while guaranteeing $h < \varepsilon$, where h is the local mesh size. The resulting discrete systems are still nonlinear, for which we introduce a combined Newton primal-dual active set method in which all nonlinearities are treated simultaneously. Inside, the linear systems are solved with GMRES [142] and block-preconditioning using an algebraic multigrid method; Trilinos [77]. The entire algorithms are fully parallel (MPI parallelization with scalability tested on 1024 cores [75]) and to this end, we have a modern, efficient numerical solution at hand. The resulting implementation is open-source in the `pfm-cracks` library [76] based on the finite element library `deal.II` [14, 13]. For the space-time model that is discussed towards the end of this chapter, we mention that this implementation is done in `DOpElib` [67] in which specifically the predictor-corrector scheme and the parallel linear iterative solution have not yet been implemented. Therein, we currently rely on the sparse direct solver Umfpack [46].

3.1 Regularization and first linearizations

3.1.1 Quasi-monolithic form: linearizing the degradation function

Proposition 14 has several nonlinearities, namely nonlinear coupling of variables in the displacement PDE (partial differential equation) and the phase-field part, while the inequality constraint introduces its own nonlinear behavior. A brief analysis of the coupling terms reveals that the nonlinear behavior in the displacement equation is more severe (being of quasi-linear type; for the definition of quasi-linear, we refer the reader to [54]) in comparison to the phase-field part,

which is semi-linear only. Therefore, if linearizations are of interest, it is reasonble to address the quasi-linear part first. Indeed, the fully monolithic system is a big challenge to be solved [63, 168, 166, 96, 97, 103, 161, 68, 173]. We follow our prior work [74][1] and formulate a quasi-monolithic system in which we linearize $(\varphi^n)^2$ by using known information about older incremental steps. In the first approach, we use an extrapolation for φ^n such that

$$\tilde{\varphi}^n \coloneqq \tilde{\varphi}^n(\varphi^{n-1}, \varphi^{n-2}) = \varphi^{n-2}\frac{t_n - t_{n-1}}{t_{n-2} - t_{n-1}} + \varphi^{n-1}\frac{t_n - t_{n-2}}{t_{n-1} - t_{n-2}}.$$

In a second approach, we simply use the solution from the previous timestep such that

$$\tilde{\varphi}^n \coloneqq \tilde{\varphi}^n(\varphi^{n-1}) = \varphi^{n-1}.$$

Furthermore, the stress σ can be split into a compressive σ^- and a tensile part σ^+ (e.g., [121]) such that the energy degradation only acts on the tensile stress, which introduces a third nonlinearity in the system. With these modifications, we obtain the following modified form of Proposition 14.

Problem 13. *(Linearized Euler-Lagrange equations with stress-splitting) For a given φ^0 and for every incremental step t_n with $n = 1, ..., N$, find $U^n \coloneqq \{u^n, \varphi^n\} \in V_u^0 \times K$ such that it holds for $\Phi \coloneqq \{0, \varphi^n\} \in V_u^0 \times K$*

$$A(U^n)(\Psi - \Phi) \geq 0 \quad \forall \Psi \coloneqq \{\psi^u, \psi^\varphi\} \in V_u^0 \times K \cap L^\infty,$$

where $A(U^n)(\Psi - \Phi)$ is defined as

$$\begin{aligned} A(U^n)(\Psi - \Phi) \coloneqq & \left(g(\tilde{\varphi}^n)\sigma^+(u^n), e(\psi^u)\right) + \left(\sigma^-(u^n), e(\psi^u)\right) \\ & + (1-\kappa)(\varphi^n \sigma^+(u^n) : e(u^n), \psi^\varphi - \varphi^n) \\ & + G_C \left(\frac{1}{\varepsilon}(1 - \varphi^n, \psi^\varphi - \varphi^n) + \varepsilon(\nabla\varphi^n, \nabla(\psi^\varphi - \varphi^n))\right). \end{aligned}$$

3.1.2 Complementarity system due to inequality constraint

To treat the inequality in Problem 13, we employ a Lagrange multiplier λ^n by following [90]. Initially, this Lagrange parameter exists in the dual space of $H^1(\Omega)$, but in [157], the author states that $\lambda^n \in L^2(\Omega)$ for single constraint variational inequality problems with solution variables in $L^2(\Omega)$. We assume that the argumentation can be transferred to Problem 13 and a rigorous proof is a goal for future work. With this, we can define

$$L^2_-(\Omega) \coloneqq \left\{v \in L^2(\Omega) \,|\, v \leq 0 \quad \text{a.e. in } \Omega\right\},$$

and

$$N_+ \coloneqq \left\{\mu \in L^2(\Omega) \,|\, (\mu, v)_{L^2(\Omega)} \leq 0 \quad \forall v \in L^2_-(\Omega)\right\},$$

such that we can formulate a variational inequality system the classical L^2 inner products and N_+ as solution set for the Lagrange multiplier λ^n.

[1] Several parts of this chapter are close or copied from [93] for which permission from Elsevier is acknowledged. We notice that some notation has been adjusted in order to have a self-contained notation of these lecture notes.

Problem 14. *For a given φ^0 and for the incremental steps t_n with $n = 1, ..., N$, find $U^n \in V_u^0 \times V_\varphi$ and $\lambda^n \in N_+$ such that*

$$\begin{aligned} A(U^n)(\Psi) + (\lambda^n, \psi^\varphi) = 0 \quad & \forall \Psi \in V_u^0 \times V_\varphi \cap L^\infty, \\ (\lambda^n - \xi, \varphi^n - \varphi^{n-1}) \geq 0 \quad & \forall \xi \in N_+, \end{aligned}$$

where $A(\cdot)(\cdot)$ is defined as before in Problem 13.

The numerical method, which is introduced in Section 3.2 to solve the inequality system, is designed to treat the variational inequality

$$(\lambda^n - \xi, \varphi^n - \varphi^{n-1}) \geq 0 \quad \forall \xi \in N_+,$$

in a complementarity formulation. The following result states the equivalence of the previous variational inequality and a complementarity condition.

Lemma 2. *The variational inequality*

$$(\lambda^n - \xi, \varphi^n - \varphi^{n-1}) \geq 0 \quad \forall \xi \in N_+, \tag{3.1}$$

can equivalently be formulated as a complementarity condition of the form

$$C(\varphi^n, \lambda^n) \coloneqq \lambda^n - \max\{0,\, \lambda^n + c(\varphi^n - \varphi^{n-1})\} = 0, \tag{3.2}$$

for every $c > 0$ and the max *operation defined as*

$$\max\{0,\, \lambda^n + c(\varphi^n - \varphi^{n-1})\} = \begin{cases} 0 & \text{in } \mathcal{I}, \\ \lambda + c(\varphi^n - \varphi^{n-1}) & \text{in } \mathcal{A}, \end{cases}$$

where the inactive set $\mathcal{I} \subset \Omega$ and, the active set $\mathcal{A} \subset \Omega$ are defined such that

$$\begin{aligned} \lambda^n + c(\varphi^n - \varphi^{n-1}) \leq 0 \ \text{a.e. in } \mathcal{I}, \\ \lambda^n + c(\varphi^n - \varphi^{n-1}) > 0 \ \text{a.e. in } \mathcal{A}. \end{aligned}$$

These two situations can be explained as follows. For $\lambda^n = 0$ we are in the so-called inactive set, namely we solve the PDE part of phase-field. In $\mathcal{A}$ the constraint is active, 'we sit on the obstacle', and we deal with $\lambda^n > 0$. Note, that $\mathcal{A}$ and $\mathcal{I}$ do not need to be connected, but note that $\Omega \setminus \mathcal{I} \cup \mathcal{A}$ is a null set. The sets can be understood as unions of all nonempty subsets of Ω with positive Lebesgue measure, on which the relations $>$ or $\leq$ are fulfilled almost everywhere.

Proof. The proof contains two major steps. Firstly, we prove the equivalence of (3.1) and a strong formulation of the form

$$\varphi^n - \varphi^{n-1} \leq 0 \quad \text{a.e. in } \Omega, \tag{3.3}$$

$$\lambda^n \geq 0 \quad \text{a.e. in } \Omega, \tag{3.4}$$

$$(\lambda^n, \varphi^n - \varphi^{n-1}) = 0. \tag{3.5}$$

Secondly, we show that (3.3)-(3.5) can be equivalently formulated as (3.2).

Step 1: ($\Rightarrow$) Assume that (3.1) is satisfied. For (3.3), we assume the existence of a subset $\mathcal{T} \subset \Omega$ with a positive Lebesgue measure such that it holds $\varphi^n - \varphi^{n-1} > 0$ a.e. in $\mathcal{T}$. We define

$$\chi \coloneqq \begin{cases} 2\lambda^n + 1 & \text{in } \mathcal{T}, \\ \lambda^n & \text{in } \Omega \setminus \mathcal{T}. \end{cases} \tag{3.6}$$

We have $\chi \in N_+$ and obtain that the variational inequality must hold for $\mu = \chi$. But it holds

$$\begin{aligned} (\lambda^n - \chi, \varphi^n - \varphi^{n-1}) &= (\lambda^n - \chi, \varphi^n - \varphi^{n-1})_{L^2(\mathcal{T})} \\ &\quad + (\lambda^n - \chi, \varphi^n - \varphi^{n-1})_{L^2(\Omega\setminus\mathcal{T})} \\ &= (\lambda^n - 2\lambda^n - 1, \varphi^n - \varphi^{n-1})_{L^2(\mathcal{T})} \\ &\quad + (\lambda^n - \lambda^n, \varphi^n - \varphi^{n-1})_{L^2(\Omega\setminus\mathcal{T})} \\ &= (-\lambda^n - 1, \varphi^n - \varphi^{n-1})_{L^2(\mathcal{T})} \\ &= (\lambda^n + 1, \varphi^{n-1} - \varphi^n)_{L^2(\mathcal{T})} < 0, \end{aligned}$$

since $\varphi^{n-1} - \varphi^n < 0$ a.e. in $\mathcal{T}$, $\lambda^n \in N_+$ and $\lambda^n + 1 > 0$ a.e. in Ω. Summarizing, we obtain

$$(\lambda^n - \chi, \varphi^n - \varphi^{n-1}) < 0,$$

which is a contradiction to the assumption that (3.1) is fulfilled. Thus, it must hold $\varphi^n - \varphi^{n-1} \leq 0$ a.e. in Ω. For (3.4), we assume $\lambda^n < 0$ a.e. in a subset $\mathcal{O} \subset \Omega$ with a positive Lebesgue measure. Then, we define

$$v \coloneqq \begin{cases} \lambda^n & \text{in } \mathcal{O}, \\ 0 & \text{in } \Omega \setminus \mathcal{O}. \end{cases}$$

Then, it holds $v \leq 0$ a.e. in Ω. Thus, per definition of N_+ and since $\lambda^n \in N_+$, it must hold that $(\lambda^n, v) \leq 0$. But we find

$$\begin{aligned} (\lambda^n, v) &= \int_\Omega \lambda^n v \,\mathrm{d}x \\ &= \int_\mathcal{O} \lambda^n v \,\mathrm{d}x + \int_{\Omega\setminus\mathcal{O}} \lambda^n v \,\mathrm{d}x \\ &= \int_\mathcal{O} \lambda^n \lambda^n \,\mathrm{d}x + \int_{\Omega\setminus\mathcal{O}} \lambda^n \cdot 0 \,\mathrm{d}x \\ &= \int_\mathcal{O} (\lambda^n)^2 \,\mathrm{d}x > 0, \end{aligned}$$

which is a contradiction. Thus, it must hold $\lambda^n \geq 0$ a.e. in Ω.
Lastly, we derive (3.5). We choose $\xi = 0$. Then, we have $\xi \in N_+$ We obtain

$$(\lambda^n - 0, \varphi^n - \varphi^{n-1}) = (\lambda^n, \varphi^n - \varphi^{n-1}) \geq 0.$$

In a similar way, we can set $\xi = 2\lambda^n$ to obtain

$$(\lambda^n - 2\lambda^n, \varphi^n - \varphi^{n-1}) = (-\lambda^n, \varphi^n - \varphi^{n-1}) = -(\lambda^n, \varphi^n - \varphi^{n-1}) \geq 0,$$

which yields $(\lambda^n, \varphi^n - \varphi^{n-1}) \leq 0$. Combining both inequalities finally leads to $(\lambda^n, \varphi^n - \varphi^{n-1}) = 0$.
($\Leftarrow$) Now, we assume that (3.3)-(3.5) hold true. Firstly, (3.4) validates the choice of N_+ as

solution space for λ^n. Let $v \in L^2_-$ be arbitrary. Then, we obtain $(\lambda^n, v) \leq 0$, and consequently $\lambda^n \in N_+$. Now, let $\mu \in N_-$ be arbitrary. Due to (3.3), we have $(\mu, \varphi^n - \varphi^{n-1}) \leq 0$, and thus $(-\mu, \varphi^n - \varphi^{n-1}) \geq 0$. In combination with (3.5) we find

$$(\lambda^n - \mu, \varphi^n - \varphi^{n-1}) \geq 0.$$

Since μ was chosen arbitrarily, we obtain (3.1).

Step 2: ($\Rightarrow$) Let (3.3)-(3.5) be fulfilled. We define A, $B \subset \Omega$ such that $\varphi^n - \varphi^{n-1} < 0$ a.e. in A and $\lambda^n > 0$ a.e. in B. As before, the sets A and B can be understood unions of all subsets on Ω with positive Lebesgue measure, on which the relations $>$ or $\leq$ are fulfilled almost everywhere. We start by proving that $A \cap B$ is a null set. For this, we assume that $A \cap B$ has a positive Lebesgue measure. We find $\lambda^n > 0$ a.e. in $A \cap B$, and $\varphi^n - \varphi^{n-1} < 0$ a.e. in $A \cap B$. This yields

$$\begin{aligned}(\lambda^n, \varphi^n - \varphi^{n-1})_\Omega &= (\lambda^n, \varphi^n - \varphi^{n-1})_{A\cap B} + (\lambda^n, \varphi^n - \varphi^{n-1})_{\Omega\setminus A\cap B} \\ &= (\lambda^n, \varphi^n - \varphi^{n-1})_{A\cap B} < 0,\end{aligned}$$

which is a contradiction to (3.5). Thus, $A \cap B$ is a null set. In a next step, we prove that $C(\varphi^n, \lambda^n) = 0$ a.e. in Ω. It suffices to show that

$$\begin{aligned}C(\varphi^n, \lambda^n)\big|_{\mathcal{A}} &= 0 \quad \text{a.e. in } \mathcal{A}, \\ C(\varphi^n, \lambda^n)\big|_{\mathcal{I}} &= 0 \quad \text{a.e. in } \mathcal{I},\end{aligned}$$

hold true. In $\mathcal{A}$, we have

$$\lambda^n \geq \lambda^n + c(\varphi^n - \varphi^{n-1}) > 0 \quad \text{a.e. in } \mathcal{A},$$

almost everywhere, which immediately yields $\lambda^n > 0$ a.e. in $\mathcal{A}$. Due to previous findings, we consequently have $\varphi^n - \varphi^{n-1} = 0$ a.e. in $\mathcal{A}$, and obtain

$$\begin{aligned}C(\varphi^n, \lambda^n)\big|_{\mathcal{A}} &= \lambda^n - \max\{0,\, \lambda^n + c(\varphi^n - \varphi^{n-1})\} \\ &= \lambda^n - \lambda^n - c(\varphi^n - \varphi^{n-1}) \\ &= -c(\varphi^n - \varphi^{n-1}) = 0,\end{aligned}$$

a.e. in $\mathcal{A}$. On $\mathcal{I}$ we have

$$c(\varphi^n - \varphi^{n-1}) \leq \lambda^n + c(\varphi^n - \varphi^{n-1}) \leq 0 \quad \text{a.e. in } \mathcal{I},$$

which yields $\varphi^n - \varphi^{n-1} \leq 0$ a.e. in $\mathcal{I}$. With the same argumentation as before, we conclude $\lambda^n = 0$ a.e. in $\mathcal{I}$ and obtain

$$C(\varphi^n, \lambda^n)\big|_{\mathcal{I}} = \lambda^n - \max\{0,\, \lambda^n + c(\varphi^n - \varphi^{n-1})\} = \lambda^n - 0 = 0,$$

a.e. in $\mathcal{I}$. Summarizing, (3.2) is fulfilled.
($\Leftarrow$) Let (3.2) be fulfilled. As before, we have

$$\lambda^n + c(\varphi^n - \varphi^{n-1}) > 0 \quad \text{a.e. in } \mathcal{A}, \tag{3.7}$$

and

$$C(\varphi^n, \lambda^n) = \lambda^n - \lambda^n - c(\varphi^n - \varphi^{n-1}) = -c(\varphi^n - \varphi^{n-1}) = 0,$$

a.e. in $\mathcal{A}$, which is equivalent to $\varphi^n - \varphi^{n-1} = 0$ a.e. in $\mathcal{A}$. Inserting this into (3.7) yields $\lambda^n > 0$ a.e. in $\mathcal{A}$. On $\mathcal{I}$ we have $\lambda^n + c(\varphi^n - \varphi^{n-1}) \leq 0$ a.e. in $\mathcal{I}$, and thus, (3.2) yields $\lambda^n = 0$ a.e. in $\mathcal{I}$. Thus, we find $\varphi^n - \varphi^{n-1} \leq 0$ a.e. in Ω. To obtain (3.5), we observe

$$(\lambda^n, \varphi^n - \varphi^{n-1}) = (\lambda^n, \varphi^n - \varphi^{n-1})_{\mathcal{A}} + (\lambda^n, \varphi^n - \varphi^{n-1})_{\mathcal{I}} = (\lambda^n, 0)_{\mathcal{A}} + (0, \varphi^n - \varphi^{n-1})_{\mathcal{I}} = 0.$$

With this, the proof is finished. □

In the following, the final system is stated and this is the starting point for the primal-dual active regularization.

Problem 15. *(Variational system with complementarity condition) Given φ^0 and for the incremental steps t_n with $n = 1, ..., N$, find $U^n = \{u^n, \varphi^n\} \in V_u^0 \times V_\varphi$ and $\lambda^n \in N_+$ such that*

$$\begin{aligned} A(U^n)(\Psi) + (\lambda^n, \psi^\varphi) = 0 \quad & \forall \Psi = \{\psi^u, \psi^\varphi\} \in V_u^0 \times V_\varphi \cap L^\infty, \\ C(\varphi^n, \lambda^n) = 0 \quad & \text{a.e. in } \Omega, \end{aligned}$$

with $A(U^n)(\Psi)$ and $C(\varphi^n, \lambda^n)$ defined as before.

3.2 Nonlinear solutions: Newton scheme and primal dual active set

In this short section, Newton's method and the primal-dual active set method are introduced on their respective continuous level formulations. Newton's method is employed for the typical nonlinear solution, while the primal-dual active set method (which can be related under suitable mathematical assumptions being a semi-smooth Newton method [78]) is used for treating the crack irreversibility constraint. After the spatial discretizations, the discrete nonlinear systems are described in more detail, and specifically recent improvements on the choice of the active set constant c.

3.2.1 Newton's method

In each incremental step, the first equation of Problem 15 can be solved via a Newton method. Considering incremental step n, we seek for $U^n := \{u^n, \varphi^n\} \in V_u^0 \times V_\varphi$ and $\lambda^n \in N_+$. The solution U^n is found via iterating over $k = 1, 2, 3, \dots$ until convergence, such that

$$A'(U^{n,k})(\delta U^{n,k+1}, \Psi) + (\lambda^{n,k}, \psi^\varphi) = -A(U^{n,k})(\Psi) \quad \forall \Psi \in V_u^0 \times V_\varphi$$

with respect to

$$C(\varphi^{n,k} + \delta\varphi^{n,k+1}, \lambda^{n,k}) = 0 \quad \text{a.e. in } \Omega,$$

for the update $\delta U^{n,k+1}$ and the Lagrange multiplier $\lambda^{n,k+1}$ and updating via

$$U^{n,k+1} = U^{n,k} + \delta U^{n,k+1}.$$

The Jacobian $A'(U^{n,k})(\delta U^{n,k+1}, \Phi)$ is given by

$$\begin{aligned} A'(U^{n,k})(\delta U^{n,k+1}, \Psi) = & \left(g(\tilde{\varphi}^n)\sigma^+(\delta u^{n,k+1}), e(\psi^u)\right) + \left(\sigma^-(\delta u^{n,k+1}), e(\psi^u)\right) \\ & + (1-\kappa)\left(\delta\varphi^{n,k+1}\sigma^+(u^{n,k}) : e(u^{n,k}), \psi^\varphi\right) \\ & + (1-\kappa)\left(2\varphi^{n,k}\sigma^+(\delta u^{n,k+1}) : e(u^{n,k}), \psi^\varphi\right) \\ & + G_C\left(\frac{1}{\varepsilon}(\delta\varphi^{n,k+1}, \psi^\varphi) + \varepsilon(\nabla\delta\varphi^{n,k+1}, \nabla\psi^\varphi)\right), \end{aligned}$$

and $A(U^{n,k})(\Phi)$ is defined as before. To treat the complementarity condition, we introduce the primal-dual active set method.

3.2.2 The primal-dual active set method

The primal-dual active set method (PDAS), introduced for constrained inequality systems in [19, 20, 82, 83], and shown under certain assumptions to be a semi-smooth Newton method [78], and applied on the phase-field fracture model in [74], is based on considerations made in Section 3.1.2. The idea is to split the domain into two subdomains in each incremental step n. On one subdomain, the inactive set $\mathcal{I}^n$, the inequality constraint $\varphi^n - \varphi^{n-1} \leq 0$ is fulfilled strictly. On the other subdomain, the active set $\mathcal{A}^n$, it holds $\varphi^n - \varphi^{n-1} = 0$. A priori, these two sets are not known but combined with the previously introduced Newton method, we obtain a prediction algorithm. Based on the complementarity condition, i.e., (3.2)

$$C(\varphi^{n,k} + \delta\varphi^{n,k+1}, \lambda^{n,k}) = 0,$$

we want to determine the active set $\mathcal{A}^{n,k}$ and the inactive set $\mathcal{I}^{n,k}$ such that

$$\lambda^{n,k} + c(\varphi^{n,k} - \varphi^{n-1}) > 0 \quad \text{a.e. in } \mathcal{A}^{n,k}, \quad \lambda^{n,k} + c(\varphi^{n,k} - \varphi^{n-1}) \leq 0 \quad \text{a.e. in } \mathcal{I}^{n,k}, \tag{3.8}$$

and iterate until the active set does not change within two consecutive Newton iterations. As before, $\mathcal{A}^n$ can be understood as the union of all subsets of Ω on which $\lambda^n + c(\varphi^n - \varphi^{n-1}) > 0$ is fulfilled almost everywhere. The inactive set $\mathcal{I}^n$ is then the complement of $\mathcal{A}^n$ with respect to Ω. If $\mathcal{A}^n$ and $\mathcal{I}^n$ are known, we can set $\lambda^n = 0$ on $\mathcal{I}^n$, see Lemma 2, and treat the problem as an unconstrained problem. On $\mathcal{A}^n$, we set $\varphi^n = \varphi^{n-1}$ and there is nothing to do (for the phase-field). The resulting scheme is given in Algorithm 1.

Algorithm 1: (Primal-dual active set method)

Set iteration index $k = 0$;
while $\mathcal{A}^{n,k} \neq \mathcal{A}^{n,k+1}$ **do**
  Determine the active set $\mathcal{A}^{n,k}$ and inactive set $\mathcal{I}^{n,k}$ with (3.8) Find $\delta U^{n,k+1} \in V_u^0 \times V_\varphi$ and $\lambda^{n,k+1} \in N_+$ with solving

$$\begin{aligned} A'(U^{n,k})(\delta U^{n,k+1}, \Phi) + (\lambda^{n,k+1}, \psi) &= -A(U^{n,k})(\Phi), \quad \forall \Phi \coloneqq \{v, \psi\} \in V_u^0 \times V_\varphi, \\ \delta\varphi^{n,k+1} &= 0 \quad \text{on } \mathcal{A}^k, \\ \lambda^{n,k+1} &= 0 \quad \text{on } \mathcal{I}^k; \end{aligned}$$

  Update the solution to obtain $U^{n,k+1}$ via

$$U^{n,k+1} = U^{n,k} + \delta U^{n,k+1};$$

  Update iteration index $k = k + 1$;
end

3.3 Spatial discretization with finite elements

3.3.1 Discrete system

We discretize Problem 15 using a finite element method with bilinear (2d) or trilinear (3d) elements Q_c^1 [42] for both, the displacement function and the phase-field function. By introducing H^1 conforming discrete spaces, we once again use a Galerkin finite element scheme for the spatial discretization. In the following and specifically Chapter 5, we consider the two dimensional case only, with quadrilateral elements K forming the mesh $\mathcal{T}_h = \{K\}$. Herein h_K is the spatial discretization parameter denoting the diameter of the element K. The set of shape functions $Q_s(K)$ is obtained as bilinear transformations of functions defined on the master element $\hat{K} = (0,1)^2$, where $\hat{Q}_s(\hat{K})$ denotes the space tensor product polynomials up to degree s in d dimensions,

$$\hat{Q}_s(\hat{K}) \coloneqq \operatorname{span}\left\{ \prod_{i=1}^{d} \hat{x}_i^{\alpha_i} \colon \alpha_i \in \{0, 1 \ldots, s\} \right\}.$$

Especially, for $s = 1$ and $d = 2$ we have

$$\hat{Q}_1(\hat{K}) = \operatorname{span}\{1, \hat{x}_1, \hat{x}_2, \hat{x}_1\hat{x}_2\}.$$

The discrete function spaces read

$$\begin{aligned}
V_{uh}^0 &\coloneqq \left\{ u_h \in V_u^0,\, u_h\big|_K \in [Q_1^c(K)]^d\,, \quad \forall\, K \in \mathcal{T}_h \right\},\\
V_{\varphi h} &\coloneqq \left\{ \varphi_h \in V_\varphi,\, \varphi_h\big|_K \in Q_1^c(K), \quad \forall\, K \in \mathcal{T}_h \right\},\\
N_h &\coloneqq \left\{ \lambda_h \in N_+,\, \lambda_h\big|_K \in Q_1^c(K), \quad \forall\, K \in \mathcal{T}_h \right\},
\end{aligned}$$

where $K \in \mathcal{T}_h$ is the finite element and $\mathcal{T}_h$ denotes the decomposition of the domain Ω into a mesh, e.g., [42]. The spatially discretized system is formulated as follows:

Problem 16. *(Discretized system with complementarity condition) Given φ_h^0 and for the incremental steps t_n with $n = 1, ..., N$, find $(u_h^n, \varphi_h^n, \lambda_h^n) \in V_{uh}^0 \times V_{\varphi h} \times N_h$ such that*

$$\begin{aligned}
A(u_h^n, \varphi_h^n)(\Phi_h) + (\lambda_h^n, \psi_h) = 0 \quad &\forall \Phi_h \coloneqq (v_h, \psi_h) \in V_{uh}^0 \times V_{\varphi h},\\
C(\varphi_h^n, \lambda_h^n) = 0 \quad &\forall x \in \Omega,
\end{aligned}$$

with $A(u_h^n, \varphi_h^n)(v_h, \psi_h)$ and $C(\varphi_h^n, \lambda_h^n)$ defined as before in Lemma 2 with the point-wise maximum operation.

Remark 29. *We notice that the choice of the finite elements must be taken with greater care, when it comes to saddle-point structures such as in the nearly-incompressible or incompressible solids [113, 17, 108].*

3.3.2 Parameter interactions

With regard to the discrete systems let us briefly make some comments. The bulk regularization parameter κ is necessary to avoid irregularities in the system matrix. If the phase-field function φ

is 0, we obtain zero-entries on the diagonal of the system matrix. To avoid this, we employ $\kappa > 0$. We have to ensure that κ is not too large since it yields a perturbation of the physics of the system, but it needs to be large enough to prevent irregularities. The second regularization parameter ε appears due to the Ambrosio Tortorelli approximation [8, 9]. The Γ-convergence theory, e.g [30], states on an energy-level that the regularized terms (under certain assumptions) converge to the underlying unregularized model as $\varepsilon \to 0$. A rigorous proof of pressurized phase-field fracture of the one dimensional case is done in [53], a proof in higher dimensions is established in [150]. For the discretized problem, we also have to require $h = o(\varepsilon)$ for the discretization parameter h. Finding an optimal setting for the regularization parameters ε and κ, which yields the best compromise between computational cost and Γ-convergence theory needs some work and is highly test dependent [92]. In practice, we usually must choose $h < \varepsilon$ and often realized with $\varepsilon = 2h$. Finally, we refer to [169][Section 5.5] for more thoughts and facts on the interaction of ε, κ and h and our summary provided in Section 3.5.

3.3.3 Discrete block matrix and discrete right hand side

The application of a Galerkin ansatz with primitive ansatz and test functions of the form

$$\Phi_{h,i} = \begin{bmatrix} \chi_i^u \\ 0 \end{bmatrix} \text{ for } i = 1, ..., N_u,$$
$$\Phi_{h,N_u+i} = \begin{bmatrix} 0 \\ \chi_i^\varphi \end{bmatrix} \text{ for } i = 1, ..., N_\varphi,$$

where N_u is the number of degrees of freedom in u_h and N_φ is the number of degrees of freedom in φ_h, leads to a system of the form

$$\begin{bmatrix} M & B \\ B^T & 0 \end{bmatrix} \begin{bmatrix} \delta U_h^{n,k+1} \\ \lambda_h^{k+1} \end{bmatrix} = \begin{bmatrix} F \\ 0 \end{bmatrix},$$

where B is a mass matrix and M and F are given by

$$M = \begin{bmatrix} M^{uu} & M^{u\varphi} \\ M^{\varphi u} & M^{\varphi\varphi} \end{bmatrix}, \quad F = \begin{bmatrix} F^u \\ F^\varphi \end{bmatrix},$$

with the block entries

$$\begin{aligned}
M_{ij}^{uu} &= \left(g(\tilde{\varphi}^n)\sigma^+(\chi_j^u), e(\chi_i^u)\right) + \left(\sigma^-(\chi_j^u), e(\chi_i^u)\right), \\
M_{ij}^{\varphi u} &= 2(1-\kappa)\left(\varphi_h^{n,k}\sigma^+(\chi_j^u) : e(u_h^{n,k}), \chi_i^\varphi\right), \\
M_{ij}^{u\varphi} &= 0, \\
M_{ij}^{\varphi\varphi} &= (1-\kappa)\left(\sigma^+(u_h^{n,k}) : e(u_h^{n,k})\chi_j^\varphi, \chi_i^\varphi\right) + G_C\left(\frac{1}{\varepsilon}\left(\chi_j^\varphi, \chi_i^\varphi\right) + \varepsilon\left(\nabla\chi_j^\varphi, \nabla\chi_i^\varphi\right)\right),
\end{aligned}$$

and

$$F_{ij}^u = -A(U_h^{n,k})(\chi_i^u) = -\left(\left[(1-\kappa)(\tilde{\varphi}_h^n)^2 + \kappa\right]\sigma^+(u_h^{n,k}), e(\chi_i^u)\right) - \left(\sigma^-(u_h^{n,k}), e(\chi_i^u)\right)$$

$$\begin{aligned}
F_{ij}^\varphi = -A(U_h^{n,k})(\chi_i^\varphi) = &-(1-\kappa)\left(\varphi_h^{n,k}\sigma^+(u_h^{n,k}) : e(u_h^{n,k}), \chi_i^\varphi\right) \\
&- G_C\left(\frac{1}{\varepsilon}\left(1 - \varphi_h^{n,k}, \chi_i^\varphi\right) + \varepsilon\left(\nabla\varphi_h^{n,k}, \nabla\chi_i^\varphi\right)\right).
\end{aligned}$$

We notice that the block $M_{ij}^{u\varphi}$ is zero due to the previously applied linearization in φ in the displacement equation in Problem 13. Consequently, in the Newton system matrix, the corresponding directional derivative vanishes and it holds $M_{ij}^{u\varphi} = 0$. The main purpose is a robust nonlinear and linear solution; see also Remark 33.

Since the $u_h^{n,k}$, $\varphi_h^{n,k}$, $\lambda_h^{n,k}$ are element-wise of polynomial structure, we can compute the active and inactive set point-wise:

$$\mathcal{A}^{n,k} = \left\{ x \,|\, \lambda_h^{n,k}(x) + c(\varphi_h^{n,k}(x) - \varphi_h^{n-1}(x)) > 0 \right\},$$
$$\mathcal{I}^{n,k} = \left\{ x \,|\, \lambda_h^{n,k}(x) + c(\varphi_h^{n,k}(x) - \varphi_h^{n-1}(x)) \leq 0 \right\}.$$

3.4 Predictor-corrector mesh adaptivity

This section is concerned with local mesh adaptivity with a focus on the crack path. Phase-field approaches require fine meshes around the interface (here, the fracture) in order to provide solutions of sufficient accuracy. However, the crack path is a priori unknown in most cases. Therefore, uniform mesh refinement should be the method of choice. We present an approach suggested in [74] in which the crack path is first predicted, followed by a second computation with the required accuracy. The goal is quite simple: we want to refine exclusively the fracture zone in order to work with a small regularization parameter ε.

3.4.1 The main algorithm

In the following we describe the predictor-corrector mesh refinement algorithm in more detail. The basic idea is to pick a single, small ε, and then decide on an adaptive refinement level r for the crack region that ensures $h < \varepsilon$. We then refine the mesh adaptively during the computation so that it is on level r in the crack region. To handle fast growing cracks with a priori unknown paths, we employ a predictor-corrector scheme that keeps repeating the current time step to guarantee the finest mesh level r in the crack region.

Algorithm 1 (At a single time step t_n)**.** *Let the solution to time step t_n be given; see Figure 3.2 top left.*

1. *Solve the full problem with a prediction of the new crack path at time step t_{n+1}; see Figure 3.2 top right.*
2. *If the crack is not resolved adequately, i.e., we have elements in which $h > \varepsilon$, we employ a predictor-corrector cycle:*
   (a) *First, we refine the mesh based on the new solution and interpolate the old solution (at t_n) onto the new mesh (Figure 3.2, bottom left). The refinement is done using a chosen threshold $0 < C < 1$ ($C = 1$ corresponds to global mesh refinement) for the phase-field φ. Each element that has at least one support point with value $\varphi(x_i) < C$ will be refined unless we are already at the maximum desired refinement level r.*
   (b) *Then we solve for the solution at t_{n+1} again, but on the refined mesh (Figure 3.2, bottom right).*
   (c) *Go to (a) and repeat refinement until maximum refinement level is reached.*

Remark 30. *The computational cost includes additional solves when the crack is growing, but the method is robust and efficient as proven in several studies [74, 106].*

In summary, our proposed predictor-corrector scheme - forcing the growing crack region to always be resolved with a fine mesh - reads:

Algorithm 2 (Predictor-corrector mesh adaptivity)**.** *Choose a fixed refinement level r for the crack region. On level r, determine $h_{max}^{(r)}$ and pick an appropriate $\varepsilon := \varepsilon^{(r)} > h_{max}^{(r)}$. Select a bound $0 < C < 1$ for φ to be considered inside the crack. For each time step do:*

1. *Solve for solution (u^{n+1}, φ^{n+1}) at t_{n+1}.*
2. *If elements need to be refined (element with level $k < r$ has $\varphi^{n+1}(x) < C$):*
   refine and transfer solution from t_n, go to 1.

Remark 31. *The parameter ε needs to chosen relative to the largest element size h that can appear on level r during the computation. For refinement of a quadrilateral mesh this quantity can be computed from the set of coarse elements $\mathcal{T}$ using*

$$h_{max}^{(r)} = \max_{T \in \mathcal{T}} 2^{-r} h_T$$

where h_T is the size of element T.

3.4.2 Goals and illustrations

Proposition 16. *The predictor-corrector algorithm asks for the following properties [74]:*

1. ***Keep a single fixed, regularization parameter ε during the entire computation.*** *Most importantly ε is a model parameter, and we do not want to change the fracture model during a computation! Decreasing ε (locally) during the computation will not allow for an increase in the accuracy of the solution. While reducing ε would result in a thinner crack mushy zone - thus changing the model. As a consequence, ε should not be changed during the computation.*
2. ***Ensure $\varepsilon > h$ inside the crack region.*** *It is required to have a sufficiently small mesh size h to resolve the transition of the phase field variable. The width of this zone is controlled by the choice of ε. Importantly, the ε-h relationship is only required to be satisfied inside or directly around the current crack region and not in the whole computational domain.*
3. ***Error is controlled by ε, not h: the interplay of model and discretization errors***
   In contrast to standard a-posteriori or goal-oriented adaptive mesh refinement, just refining the mesh does not reduce the discretization error significantly. This is because the choice of ε determines the width of the mushy zone around the crack path. Ideally, an adaptive method would try to minimize ε and pick an appropriate h to minimize the discretization error introduced by the mesh size.
4. ***No requirement of prior knowledge about the crack location(s).*** *Typically, specifically for more realistic problems, the final location of the cracks is unknown. While it is an option to repeat the whole computation on a finer mesh that is determined using the first computation, this is too expensive to be practical. Therefore, the predictor-corrector algorithm should detect during the computation in which direction the cracks are growing.*

5. ***Handling fast growing cracks.*** *Only adapting the mesh based on the current crack location before moving on to the next time step may result that the adaptive mesh lags behind in time and does not resolve the crack region adequately, in particular, if the crack is growing rapidly.*

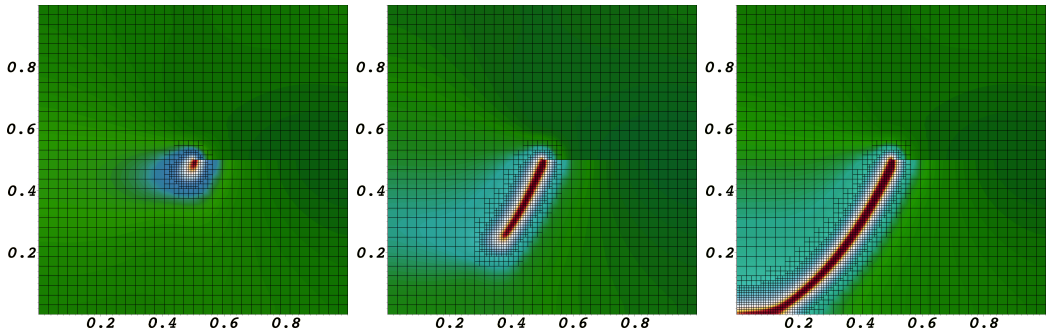

Figure 3.1: Functionality of predictor-corrector mesh refinement in two spatial dimensions: the mesh grows with the fracture. Here the transition zone with $0 < \varphi < 1$ determines the region in which the mesh has to be refined. If the fracture (in red) grows faster than the fine mesh, such that $\varepsilon > h$ is violated, we first refine the mesh (the predictor step) according to the transition zone and than perform a second computation to determine the precise fracture location inside the refined mesh.

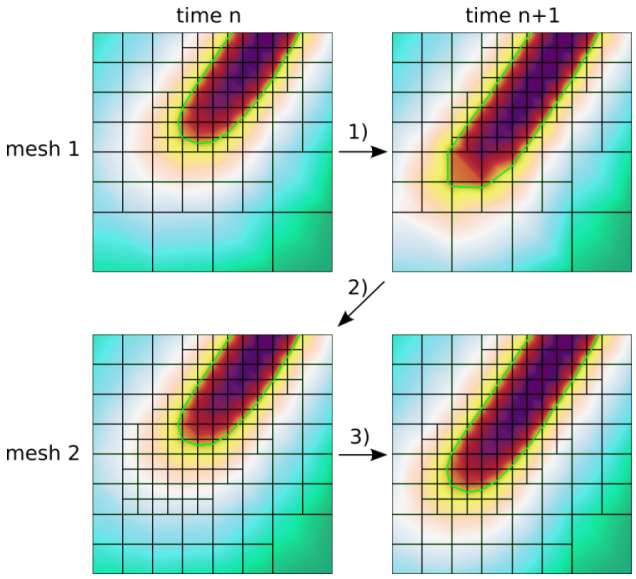

Figure 3.2: Predictor-corrector scheme: 1. advance in time, crack leaves fine mesh. 2. refine and go back in time (interpolate old solution). 3. advance in time on new mesh. Repeat until mesh doesn't change anymore. Refinement is triggered for $\varphi < C = 0.2$ (green contour line) here.

3.4.3 Performance

For the single edge notched shear test, we used an Intel(R) Core(TM) i5-3320M CPU @ 2.60GHz machine with two processors. The following results presented in Table 3.1 were obtained in [74].

Table 3.1: Single edge notched shear test: Comparison of computational cost for different refinement strategies. The numbers in the prec/corr strategy indicate the phase-field threshold value used for mesh refinement.

Strategy	Time [s]	Time [min]	Number of loading steps	DoFs: min/avg/max
global refinement	5036	84	151	50115
local prerefinement	1277	21	151	19746
predictor/corrector (0.8)	233	4	151+63	3315/4731/8286
predictor/corrector (0.6)	184	3	151+53	3315/4225/6666

Remark 32. *We notice that the accuracy of the different simulations was comparable as shown in [74]. Thus it is really worth to use predictor-corrector mesh refinement for this numerical example.*

3.5 Relationship of material, model, and discretization parameters

As the governing phase-field regularization was taken from image segmentation in the early days [24], an analysis of the governing parameters can be found in [22], with the result shown in the left column in Table 3.2. A numerical analysis of a simplified problem statment was carried out in [169][Section 5.5] yielding the results in column No. 2. In practice from experiences, reading other papers, and numerous discussions on conferences, the third column is relevant and mostly used. When it comes to physical interpretations of ε, then it seems to be some small fixed number that is obtained from calibrations; see e.g., the overview [49] for general discussions and pointing to specific references.

MATHEMATICALLY	NUMERICALLY	PRACTICE (often used)	ENGINEERING
$h \ll \kappa \ll \varepsilon$ $h = o(\varepsilon),\ h = o(\kappa),\ \kappa = o(\varepsilon)$	$h \ll \varepsilon,\ h \ll \kappa$	$\kappa \sim 10^{-10}$ and $\varepsilon = 2h$ or $\varepsilon = 4h$	ε length-scale (micro-cracks)

Table 3.2: The sizes of h, κ and ε depend on each other.

Considering dynamic fracture (Section 2.12.2) or space-time formulations (Section 3.10), then also the temporal discretization parameter Δt_m must be considered as well. Moreover, on the model side the crack irreversibility penalization parameter γ (or active set constant c) have a relation to the previously mentioned paramteres. Finally, in Chapter 4, we introduce the optimal control Tikhonov regularization parameter α as well as an additional phase-field regularization parameter η (with $\eta \ll \gamma$) that are required for the sake of mathematical (not proven here, but known) and numerical purposes. The latter reasons is necessary for obtaining stable computational results. It

is clear, that a deeper inside from all directions, mathematical, numerical, and engineering wise how to relate all parameters is of great interest.

3.6 Combined Newton scheme for discrete nonlinear systems

Given the fully discretized system, we can formulate a combined Newton method, namely addressing all nonlinearities simultaneously. This is implemented in `pfm-cracks` utilizing Algorithm 2.

Algorithm 2: (Primal-dual active set method with backtracking line search)

Set iteration index $k = 0$;
while $\left(\mathcal{A}^{n,k-1} \neq \mathcal{A}^{n,k}\right)$ ***or*** $\left(\tilde{R}(U_h^{n,k}) > TOL_N\right)$ **do**
  Assemble the residual $R(U_h^{n,k})$;
  Compute the active set $\mathcal{A}^{n,k} = \left\{ x_i \middle| [B]_{ii}^{-1} \left[R(U_h^{n,k})\right]_i + c(\varphi_{h,i}^{n,k} - \varphi_{h,i}^{n-1}) > 0 \right\}$ Set $\varphi_h^{n,k} = \varphi_h^{n-1}$ on $\mathcal{A}^{n,k}$;
  Assemble the system matrix M (Newton Jacobian) and the right-hand side $F = R(U_h^{n,k})$;
  Eliminate rows/columns in $\mathcal{A}^{n,k}$ from M and F to obtain $\tilde{M}$ and $\tilde{F} = \tilde{R}(U_h^{n,k})$;
  Solve the linear system $\tilde{M}\delta U_h^{n,k+1} = \tilde{F}$ with GMRES and AMG preconditioner [76];
  Choose maximum number of line search iterations $l_{\max}$;
  Choose line search damping parameter $0 < \omega \leq 1$;
  for $l = 1 : l_{\max}$ **do**
    Update the solution with $U_h^{n,k+1} = U_h^{n,k} + \delta U_h^{n,k+1}$;
    Assemble the new residual $\tilde{R}(U_h^{n,k+1})$;
    if $\|\tilde{R}(U_h^{n,k+1})\|_2 < \|\tilde{R}(U_h^{n,k})\|_2$ **then**
      break;
    end
    else
      Adjust the Newton update with $\delta U_h^{n,k+1} := \omega^l \delta U_h^{n,k+1}$;
    end
  end
  Update iteration index $k = k + 1$;
end

Remark 33. *In line 8, the reduced linear system is solved with a GMRES (generalized minimal residual) method [143] and algebraic multigrid preconditioning (AMG) [77]. In this work, the implementation as it is from* `pfm-cracks` *[76] is utilized. In our numerical tests (Section 5.1), we observe in all simulations between* $10 - 40$ *linear iterations. This is in agreement with the results obtained in [75][Table 1]. The main reason for the excellent performance is twofold. First, it is the triangular block structure of* $\tilde{M}$ *due to the zero block* $M_{ij}^{u\varphi}$ *as previously discussed. Second, the diagonal terms in* $\tilde{M}$ *are of elliptic type, which is well-known that multigrid methods perform very well.*

Remark 34. *The lines 9-19 describe a classical backtracking line search algorithm, where the Newton update is damped with a damping parameter* $\omega \in (0, 1]$*, if the updated solution* $U_h^{n,k+1} = U_h^{n,k} + \delta U_h^{n,k+1}$ *does not reduce the residual norm. In all experiments in Section 5.1, we use* $l_{\max} = 10$ *and* $\omega = 0.6$*.*

Remark 35. *Note that we deal with two systems of equations in Algorithm 2: the global nonlinear system and the reduced linear system. The nonlinear system consists of the matrix* M *and the right-hand-side* F*. The reduced linear system, defined by the matrix* $\tilde{M}$ *and* $\tilde{F}$ *only contains the equations of the nonlinear system, which belong to the inactive set. The residual of the full nonlinear system is then given by* R *whereas* $\tilde{R}$ *denotes the residual of the reduced linear system. From an implementation point of view, this is realized by setting constraints to the system such that we enforce the phase-field to remain the same on the active degrees of freedom.*

3.7 Modified combined Newton active set algorithms

This section is dedicated to presenting adjustments to the primal-dual active set method based on an analysis of the active set constant $c > 0$ (see again Lemma 2 and Algorithm 1). In [85], the authors prove for an obstacle problem that the primal-dual active set converges for any sufficiently large $c > 0$. Furthermore, they point out that c only influences the first active set iteration in theory. Similar observations were made in [81, 137, 146]. The authors state on the one hand that a constant c of magnitude around the Youngs modulus is reasonable from an engineer's perspective, while they also point out on the other hand, that different settings for c do not affect the solution but only the algorithmic performance. These results are a motivation to further investigate the influence of c for our primal-dual active set phase-field fracture formulation. We start by pointing out the bottleneck of the above described primal-dual active set algorithm. Specifically on fine meshes, we often run into convergence issues of the active set, whereas the residual converges comparably fast (see e.g., [74][Fig. 14]).

3.7.1 Investigation of the active set constant c

In the following, our objective is to illustrate the influence of the active set constant c and how to adjust it to reduce the number of active set iterations. To this end, we begin with an investigation of the role of the active set constant c in the algorithm. It is involved in the classification of the active set $\mathcal{A}^k$ as a degree of freedom x_i is classified as active (in iteration k within the current incremental step), if

$$\lambda_{h,i}^k + c(\varphi_{h,i}^k - \varphi_{h,i}^{\text{old}}) > 0,$$

where $\varphi_{h,i}^{\text{old}}$ is the value of the phase field solution of the previous incremental step at degree of freedom i. We identify nine different situations, depending on the sign of $\lambda_{h,i}^k$ and $(\varphi_{h,i}^k - \varphi_{h,i}^{\text{old}})$:

1. $\varphi_{h,i}^k - \varphi_{h,i}^{\text{old}} = 0$, and $\lambda_{h,i}^k > 0 \Rightarrow \varphi_{h,i}^k = \varphi_{h,i}^{\text{old}}$, $\delta\varphi_{h,i}^{k+1} = 0$ and $\lambda_{h,i}^{k+1} = B_{ii}^{-1} F_i$
2. $\varphi_{h,i}^k - \varphi_{h,i}^{\text{old}} = 0$, and $\lambda_{h,i}^k = 0 \Rightarrow \delta\varphi_{h,i}^{k+1}$ as solution of the system and $\lambda_{h,i}^{k+1} = 0$
3. $\varphi_{h,i}^k - \varphi_{h,i}^{\text{old}} = 0$, and $\lambda_{h,i}^k < 0 \Rightarrow \varphi_{h,i}^k = \varphi_{h,i}^{\text{old}}$, $\delta\varphi_{h,i}^{k+1} = 0$ and $\lambda_{h,i}^{k+1} = B_{ii}^{-1} F_i$
4. $\varphi_{h,i}^k - \varphi_{h,i}^{\text{old}} > 0$, and $\lambda_{h,i}^k > 0 \Rightarrow \delta\varphi_{h,i}^{k+1} = 0$ and $\lambda_{h,i}^{k+1} = B_{ii}^{-1} F_i$

5. $\varphi_{h,i}^k - \varphi_{h,i}^{\text{old}} > 0$, and $\lambda_{h,i}^k = 0 \Rightarrow \varphi_{h,i}^k = \varphi_{h,i}^{\text{old}}$, $\delta\varphi_{h,i}^{k+1} = 0$ and $\lambda_{h,i}^{k+1} = B_{ii}^{-1} F_i$

6. $\varphi_{h,i}^k - \varphi_{h,i}^{\text{old}} > 0$, and $\lambda_{h,i}^k < 0 \Rightarrow \begin{cases} \varphi_{h,i}^k = \varphi_{h,i}^{\text{old}},\ \delta\varphi_i^{k+1} = 0, \\ \qquad\qquad \lambda_{h,i}^{k+1} = B_{ii}^{-1} F_i \\ \delta\varphi_{h,i}^{k+1} \text{ as solution},\ \lambda_{h,i}^{k+1} = 0 \end{cases} \begin{array}{l} \text{if } |\lambda_{h,i}^k| < c(\varphi_{h,i}^k - \varphi_{h,i}^{\text{old}}), \\ \text{otherwise.} \end{array}$

7. $\varphi_{h,i}^k - \varphi_{h,i}^{\text{old}} < 0$, and $\lambda_{h,i}^k > 0 \Rightarrow \begin{cases} \delta\varphi_{h,i}^{k+1} \text{ as solution},\ \lambda_{h,i}^{k+1} = 0 \\ \varphi_{h,i}^k = \varphi_{h,i}^{\text{old}},\ \delta\varphi_{h,i}^{k+1} = 0, \\ \qquad\qquad \lambda_{h,i}^{k+1} = B_{ii}^{-1} F_i \end{cases} \begin{array}{l} \text{if } \lambda_{h,i}^k \le |c(\varphi_{h,i}^k - \varphi_{h,i}^{\text{old}})|, \\ \\ \text{otherwise} \end{array}$

8. $\varphi_{h,i}^k - \varphi_{h,i}^{\text{old}} < 0$, and $\lambda_{h,i}^k = 0 \Rightarrow \delta\varphi_{h,i}^{k+1}$ as solution, $\lambda_{h,i}^{k+1} = 0$

9. $\varphi_{h,i}^k - \varphi_{h,i}^{\text{old}} < 0$, and $\lambda_{h,i}^k < 0 \Rightarrow \delta\varphi_{h,i}^{k+1}$ as solution, $\lambda_{h,i}^{k+1} = 0$.

We observe that the active set constant c only has an influence on the classification when $\lambda_{h,i}^k$ and $\varphi_{h,i}^k - \varphi_{h,i}^{\text{old}}$ have different signs. In situation No. 6, $\varphi_{h,i}^k$ shows crack healing behaviour, thus we do not want to accept it as a solution and set it to $\varphi_{h,i}^{\text{old}}$. We achieve this, if

$$|\lambda_{h,i}^k| < c(\varphi_{h,i}^k - \varphi_{h,i}^{\text{old}}),$$

i.e.

$$\frac{|\lambda_{h,i}^k|}{(\varphi_{h,i}^k - \varphi_{h,i}^{\text{old}})} < c.$$

In situation No. 7, we do not violate the constraint with the solution of the kth iteration, thus, we still want to classify this degree of freedom as inactive. This can be achieved via

$$\lambda_{h,i}^k \le c|(\varphi_{h,i}^k - \varphi_{h,i}^{\text{old}})|,$$

i.e.

$$\frac{\lambda_{h,i}^k}{|(\varphi_{h,i}^k - \varphi_{h,i}^{\text{old}})|} < c.$$

Summarizing, we can formulate a condition for c:

$$\left| \frac{\lambda_{h,i}^k}{(\varphi_{h,i}^k - \varphi_{h,i}^{\text{old}})} \right| < c.$$

Thus, any c larger than the lower bound is sufficiently large.

3.7.2 Proposed adjustments and definition of four cases

In the following, we propose four different cases for implementing the Newton active set algorithm. The basis for these cases is Algorithm 2. For better readability and since the concepts are the same in each incremental step, we drop the incremental index n. Both stopping criteria, i.e., if not stated otherwise, require the active set to converge and the residual-norm to fall below a certain tolerance. For our adjustment, we choose

$$c = c^k := 2 \left| \frac{\lambda_{h,i}^k}{(\varphi_{h,i}^k - \varphi_{h,i}^{\text{old}})} \right|,$$

thus, in contrast to before, c changes in every Newton iteration. This could be avoided by iterating until convergence, saving the largest c^k and then restarting the iteration. But this is an unnecessary computational cost and in our opinion, a varying c^k does not lead to any conflicts. In Section 5.1, we will perform several experiments to observe the performance boost of this adjustment. Based on the previous findings, we suggest four different cases:

- **Case 1:** We iterate as long as the active set does not change within 2 iterations with a constant $c = 10E$, where E is Young's modulus. Let k be the iteration index and $\mathcal{A}^k$ the active set of iteration k, we stop, when $\mathcal{A}^k = \mathcal{A}^{k+1}$ and $\|\tilde{R}(U_h^{k+1})\|_2 < \mathrm{TOL}_N$.
- **Case 2:** The classification of active/inactive set proceeds as in **Case 1**, but with the modified c set as
$$c = c^k = 2\left|\frac{\lambda_{h,i}^k}{(\varphi_{h,i}^k - \varphi_{h,i}^{\mathrm{old}})}\right|.$$
Apart from this, everything is similar to Algorithm 2 including the stopping criteria: we stop, when $\mathcal{A}^k = \mathcal{A}^{k+1}$ and $\|\tilde{R}(U_h^{k+1})\|_2 < \mathrm{TOL}_N$.
- **Case 3:** The classification of the active/inactive set proceeds as in **Case 1** with $c = 10E$. But in this case, we weaken the active set stopping criterion, i.e. we do not enforce $\mathcal{A}^k = \mathcal{A}^{k+1}$ for termination anymore. Instead, we perform as much Newton active set iterations as needed to achieve $\|\tilde{R}(U_h^{k+1})\|_2 < \mathrm{TOL}_N$. When this is fulfilled, we only perform 10 more Newton active set iterations until we stop. The number 10 is chosen heuristically based on our experiences made in [93]. It is a compromise between sufficiently many iterations to guess that we may have converged and computational cost by not adding too many additional iterations.
- **Case 4:** The classification of the active/inactive set proceeds as in **Case 1** with $c = 10E$. But in this case, we completely omit the active set stopping criteria. This means, we do not require $\mathcal{A}^k = \mathcal{A}^{k+1}$ but stop immediately as soon as $\|\tilde{R}(U_h^{k+1})\|_2 < \mathrm{TOL}_N$ is reached.

3.8 Linear solution

In this section, we concentrate on the linear systems arising at each Newton step. Formally, Newton's defect step reads
$$MU = F,$$
(respectively $\tilde{M}\tilde{U} = \tilde{F}$ in the case of the primal dual active set method) and has the block structure
$$M = \begin{pmatrix} M^{uu} & M^{u\varphi} \\ M^{\varphi u} & M^{\varphi\varphi} \end{pmatrix}, \qquad F = \begin{pmatrix} F^u \\ F^\varphi \end{pmatrix}.$$
Therein, the Jacobian M is composed by the directional derivatives
$$\begin{aligned}
M_{i,j}^{uu} &= \Big(\big((1-\kappa)\tilde{\varphi}^2 + \kappa\big)\,\sigma^+(\chi_j^u), e(\chi_i^u)\Big) + (\sigma^-(\chi_j^u), e(\chi_i^u)),\\
M_{i,j}^{\varphi u} &= 2(1-\kappa)(\varphi\,\sigma^+(\chi_j^u) : e(u), \chi_i^\varphi)\\
M_{i,j}^{u\varphi} &= 0,\\
M_{i,j}^{\varphi\varphi} &= (1-\kappa)(\sigma^+(u) : e(u)\chi_j^\varphi, \chi_i^\varphi) + G_c\Big(\frac{1}{\varepsilon}(\chi_j^\varphi, \chi_i^\varphi) + \varepsilon(\nabla\chi_j^\varphi, \nabla\chi_i^\varphi)\Big).
\end{aligned}$$

The term $M_{i,j}^{u\varphi} = 0$ arises due to the linearization in the degradation function; see Section 3.1.1. In a fully monolithic form [168, 166], this block would be non-zero. The Newton right hand side F (the actual residual) consists of:

$$F_i^u = -\widetilde{A}(U_k)(\chi_i^u), \quad F_i^\varphi = -\widetilde{A}(U_k)(\chi_i^\varphi).$$

In order to make iterative linear solvers efficient, we need to apply a preconditioner. First of all, the linear systems $MU = F$ are solved with GMRES (generalized minimal residual) [143, 142]. For the preconditioner, we need to analyze the structure of the Jacobian M and specifically the block entries. Here, it can be observed that the diagonal blocks mainly consist of elliptic terms (which are besides mass matrices, the nicest entries one can have):

$$P^{-1} = \begin{pmatrix} (P^{uu})^{-1} & 0 \\ 0 & (P^{\varphi\varphi})^{-1} \end{pmatrix}$$

Indeed, in [74, 75], we found that a straighforward application of an AMG multigrid solver works sufficiently well. Approximately, we have:

$$P_{uu} \approx -\nabla \cdot (\varphi^2 \nabla u), \qquad P_{\varphi\varphi} \approx \varepsilon \Delta \varphi - \frac{1}{\varepsilon}(1-\varphi),$$

which both are of elliptic type and are therefore 'nice' terms to deal with.

3.9 Parallelization

Working with the software library deal.II, parallelization is very well documented and very well tested. The 'standard implementation' using MPI was applied to the previously described systems. The meshes are handled with p4est (parallel dynamic management of a collection of adaptive octrees). With these parts, the `pfm-cracks` code was parallelized with relative ease in the year 2015 [75], including adaptively refined meshes. Scalability studies for Sneddon's example (see later Chapter 5 for more descriptions) were conducted in [75] and shown in Table 3.3. Therein the overall numerical solver is based on the descriptions of the previous sections.

		NP							
ref	Dofs	16	32	64	128	256	512	1024	2048
1	867	2	2	2	2	2	2	2	2
2	3267	10	10	9	9	8	8	8	8
3	12675	13	13	13	13	12	12	19	19
4	49923	17	17	16	17	14	15	14	14
5	198'147	19	19	19	18	18	18	17	19
6	789'507	24	23	25	24	25	23	24	23
7	3'151'875	33	27	29	28	27	27	25	37
8	12'595'203	-	-	31	31	33	32	30	32
9	50'356'227	-	-	43	43	44	48	40	52

Table 3.3: Number of GMRES iterations of a single Newton step for the Sneddon 2d test with global refinement. Iterations are nearly independent of problem size (h) and number of processors NP. The relative residual is 1e-8.

In Figure 3.3 a graphical illustration of four different processors is provided. Specifically, we point to the distribution of the parts of domain to each processors in order to have loading balancing, e.g., each processors has a similar amount of computational work to do.

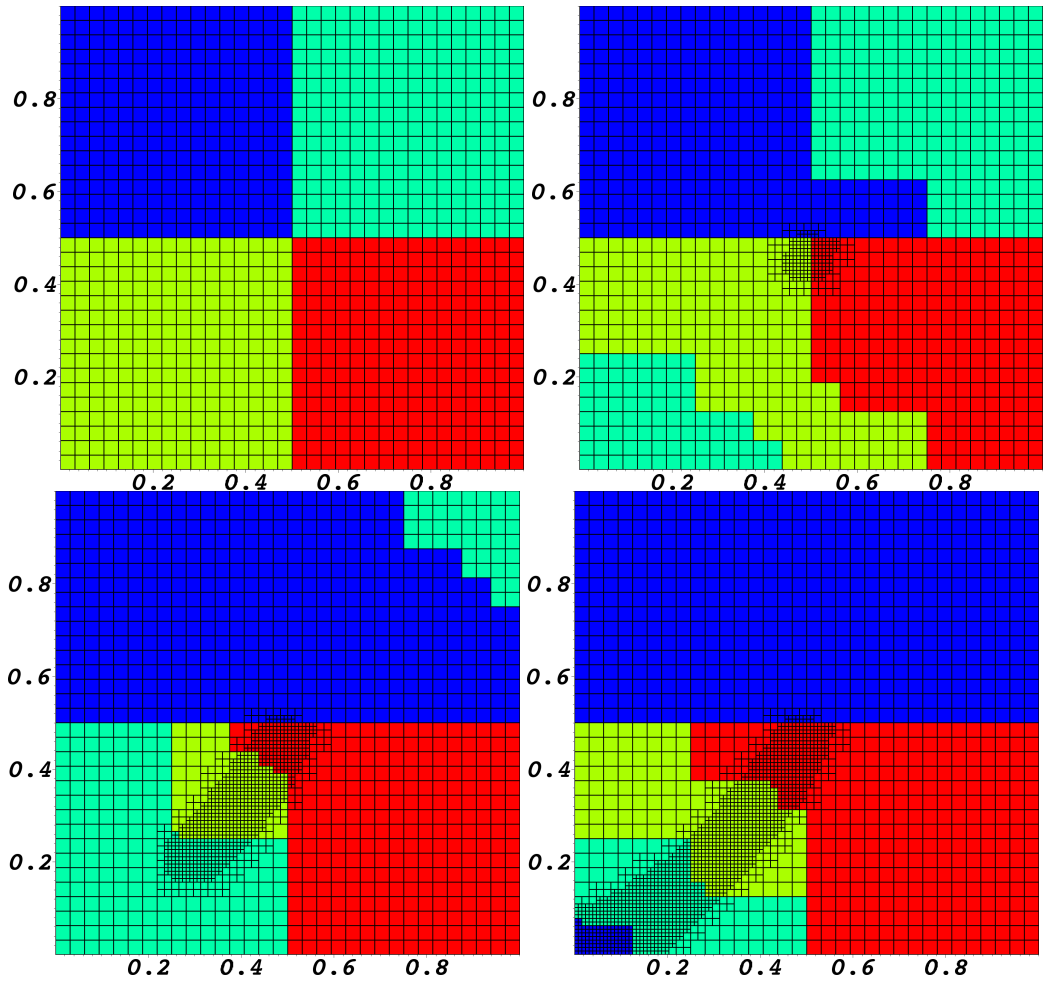

Figure 3.3: Exemplified visualization of parallel computing on 4 processors. The different subdomains are associated with different processors. Depending on mesh refinement, the workload for each processor is adjusted dynamically at each time step.

3.10 Space-time Galerkin finite element discretization

In this section, we start from Proposition 15. The new part is concerned with the temporal discretization, which is based on a discontinuous Galerkin (dG) finite element method. The spatial part is as before, i.e., using continuous Galerkin (cG) finite elements. Using dG, we need to introduce jump terms, which require additional notations and make the problem statements rather heavy. On the other hand, having a Galerkin scheme in time yields all the concepts we already have for the spatial discretizations, such as best approximation properties, finite element error estimates, consistent derivation of adjoints (Chapter 4), solver developments [61, 144], and an holistic view on the model.

3.10.1 Temporal discretization

For $T > 0$, we partition $I = [0, T]$ into M left-open subintervals $I_m = (t_{m-1}, t_m]$ using the time grid $0 = t_0 < \cdots < t_M = T$,

$$I = \{0\} \cup I_1 \cup \cdots \cup I_M.$$

In order to apply discontinuous Galerkin methods, here dG(0), we define the space X_k^0 of piecewise polynomials of degree 0,

$$X_k^0 \coloneqq \{V \in X \colon V(0) \in V \text{ and } V|_{I_m} \in \mathbb{P}_0(I_m, V),\ m = 1, \dots, M\}. \tag{3.9}$$

Consequently we seek a solution U in the space X_k^0, where the subindex k indicates the time-discretized function space. For the temporal jump terms arising from dicontinuous Galerkin methods we use the standard notation

$$V_m^+ \coloneqq V(t_m+), \qquad V_m^- \coloneqq V(t_m-) = V(t_m), \qquad [V]_m \coloneqq V_m^+ - V_m^-.$$

Remark 36. *Since we use piece-wise constant functions in time (dG(0)), we have*

$$\partial_t V = V_m^- - V_{m-1}^+ = 0 \quad \forall V \in X_k^0\ \forall m = 1, \dots, M.$$

Next, the two equations from (2.14) are combined to form the discretized state equation. To shorten the notation we sum up all, the energy-related terms in a semi-linear form $a \colon Q \times V \times V \to \mathbb{R}$,

$$\begin{aligned} a(U)(\Phi) \coloneqq\ & g(\varphi) \cdot (\mathbb{C}e(u), e(\Phi_u)) \\ & + G_c \varepsilon (\nabla\varphi, \nabla\Phi_\varphi) - \frac{G_c}{\varepsilon}(1 - \varphi, \Phi_\varphi) \\ & + (1 - \kappa)(\varphi \cdot \mathbb{C}e(u) : e(u), \Phi_\varphi). \end{aligned}$$

For a given initial value $U_0 = (u_0, \varphi_0) \in V$, the fully discretized state equation consists of finding a function $U \in X_k^0$ that solves (3.10) for every $\Phi \in X_k^0$

$$0 = \sum_{m=1}^{M} \left[\gamma(\partial_t\varphi, \Phi_\varphi)_{\{\partial_t\varphi > 0, I_m\}} + \eta(\partial_t\varphi, \Phi_\varphi)_{I_m}\right] \tag{3.10a}$$

$$+ \sum_{m=0}^{M-1} \left[\gamma([\varphi]_m, \Phi_{\varphi,m}^+)_{\{\varphi_{m+1}^- > \varphi_m^-\}} + \eta([\varphi]_m, \Phi_{\varphi,m}^+)\right] \tag{3.10b}$$

$$+ \sum_{m=1}^{M} a(U(t_m))(\Phi(t_m))\Delta t_m \tag{3.10c}$$

$$+ (u_0^- - u_0, \Phi_{u,0}^-) + (\varphi_0^- - \varphi_0, \Phi_{\varphi,0}^-). \tag{3.10d}$$

The right-sided box rule has been used to approximate the time integral in (3.10c), where $\Delta t_m \coloneqq t_m - t_m - 1$. The jump terms in (3.10b) represent the discontinuities of the functions in X_k^0. These jump terms can be reformulated as

$$\sum_{m=1}^{M} \big[\gamma(\varphi_{m-1}^+ - \varphi_{m-1}^-, \Phi_{\varphi,m-1}^+)_{\{\varphi_m^- > \varphi_{m-1}^-\}} + \eta(\varphi_{m-1}^+ - \varphi_{m-1}^-, \Phi_{\varphi,m-1}^+)\big]. \tag{3.11}$$

Additionally, because we are using a dG(0) scheme, our test functions satisfy

$$\Phi_{m-1}^+ = \Phi_m^- \quad \forall m = 1, \dots, M.$$

The first sum (3.10a) vanishes entirely by remark 36 and the two terms in (3.11) containing φ_{m-1}^+ become $(\varphi_m^-, \Phi_{\varphi,m}^-)_{\{\varphi_m^- > \varphi_{m-1}^-\}}$ and $(\varphi_m^-, \Phi_{\varphi,m}^-)$, respectively. In combination with (3.10b) and (3.10d), the discrete state equation (3.10) reads

$$\begin{aligned} 0 = \sum_{m=1}^{M} \Big(& \gamma\big[(\varphi_m^-, \Phi_{\varphi,m}^-)_{\{\varphi_m^- > \varphi_{m-1}^-\}} - (\varphi_{m-1}^-, \Phi_{\varphi,m}^-)_{\{\varphi_m^- > \varphi_{m-1}^-\}}\big] \\ & + \eta\big[(\varphi_m^-, \Phi_{\varphi,m}^-) - (\varphi_{m-1}^-, \Phi_{\varphi,m}^-)\big] \\ & + a(U(t_m))(\Phi(t_m))\Delta t_m \Big) \\ + (u_0^- - u_0, \Phi_{u,0}^-) & + (\varphi_0^- - \varphi_0, \Phi_{\varphi,0}^-) \quad \forall \Phi \in X_k^0. \end{aligned} \tag{3.12}$$

We solve (3.12) by obtaining $U_0^- = U(0)$ from the initial condition

$$(U(0), \Phi_0^-) = (U_0, \Phi_0^-) \quad \forall \Phi_0^- \in V. \tag{3.13}$$

Then we obtain $U(t_m)$ for $m = 1, \dots, M$ from

$$\begin{aligned} 0 = {} & \gamma(\varphi(t_m), \Phi_\varphi(t_m))_{\{\varphi(t_m) > \varphi(t_{m-1})\}} + \eta(\varphi(t_m), \Phi_\varphi(t_m)) \\ & - \gamma(\varphi(t_{m-1}), \Phi_\varphi(t_m))_{\{\varphi(t_m) > \varphi(t_{m-1})\}} - \eta(\varphi(t_{m-1}), \Phi_\varphi(t_m)) \\ & + a(U(t_m))(\Phi(t_m))\Delta t_m \quad \forall \Phi \in X_k^0. \end{aligned} \tag{3.14}$$

3.10.2 Spatial discretization

As in Section 3.3, we construct a finite element spaces $V_h \coloneqq V_{uh} \times V_{\varphi h}$ on the mesh $\mathcal{T}_h$ as usual:

$$\begin{aligned} V_{uh} &\coloneqq \{v \in H_D^1(\Omega; \mathbb{R}^2) \colon v|_K \in Q_s(K) \text{ for } K \in \mathcal{T}_h\}, \\ V_{\varphi h} &\coloneqq \{v \in H^1(\Omega) \colon v|_K \in Q_s(K) \text{ for } K \in \mathcal{T}_h\}. \end{aligned}$$

Based on (3.9) we can use these preparations to define the fully discrete function space

$$X_{hk}^0 \coloneqq \{V \in X \colon V_h(0) \in V_h \text{ and } V|_{I_m} \in \mathbb{P}_0(I_m, V_h),\ m = 1, \dots, M\}.$$

In order to find a solution U_h for the fully discrete system we solve the initial condition

$$(U_h(0), \Phi_{h,0}^-) = (U_{h,0}, \Phi_{h,0}^-) \quad \forall \Phi_{h,0}^- \in V_h \tag{3.15}$$

first, and then we obtain $U_h(t_m)$ for $m = 1, \dots, M$ by solving

$$\begin{aligned} 0 = {} & \gamma(\varphi_h(t_m), \Phi_{\varphi,h}(t_m))_{\{\varphi_h(t_m) > \varphi_h(t_{m-1})\}} + \eta(\varphi_h(t_m), \Phi_{\varphi,h}(t_m)) \\ & - \gamma(\varphi_h(t_{m-1}), \Phi_{\varphi,h}(t_m))_{\{\varphi_h(t_m) > \varphi_h(t_{m-1})\}} - \eta(\varphi_h(t_{m-1}), \Phi_{\varphi,h}(t_m)) \\ & + a(U_h(t_m))(\Phi_h(t_m))\Delta t_m \quad \forall \Phi_h \in X_{hk}^0. \end{aligned} \tag{3.16}$$

3.11 Excursus II: Numerical modeling and implementation of the obstacle problem

In this section, we continue from Section 2.4 our developments in order to demonstrate regularization and Newton's method for a 'simple' model problem; namely the obstacle problem. The obstacle setting shares important similarities with phase-field fracture as we discussed previously: indeed the crack irreversibility constraint can be seen as an 'obstacle' condition in time. In the following, several details of the discretization, implementation, and simulation results are provided.

3.11.1 Problem statement

As in Section 2.4, we consider $\Omega = (0,1)^2$ and the following setting:

$$\begin{aligned} -\Delta u &\geq f \quad \text{in } \Omega, \\ u &\geq g \quad \text{in } \Omega, \\ (f + \Delta u)(g - u) &= 0 \quad \text{in } \Omega, \\ u &= 0 \quad \text{on } \partial\Omega, \end{aligned}$$

with a right hand side $f = -1$. For comparison, we also recall the classical Poisson problem:

$$\begin{aligned} -\Delta u &= f \quad \text{in } \Omega, \\ u &= 0 \quad \text{on } \partial\Omega, \end{aligned}$$

with $f = -1$. Plots of the numerical solutions are provided in Figure 3.4.

Variational forms

We set

$$\begin{aligned} a(u,\varphi) &= (\nabla u, \nabla\varphi), \\ l(\varphi) &= (f,\varphi). \end{aligned}$$

Define a convex set:

$$K := \{u \in H_0^1(\Omega) |\, u \geq g \text{ a.e. in } \Omega\}$$

and $V := H_0^1(\Omega)$. Then:

$$u \in K: \quad a(u,\varphi) \geq l(\varphi) \quad \forall \varphi \in K.$$

Regularization (penalization) of the inequality constraint

We regularize $u \geq g$ as follows:

$$\gamma([g-u]^+, \varphi),$$

with the (simple) penalization parameter $\gamma > 0$.

Remark 37. *Obviously, this term is non-smooth and renders the overall nonlinear problem for which we need a nonlinear solver (for instance Newton).*

Then:

$$u \in V: \quad a(u,\varphi) - \gamma([g-u]^+, \varphi) = l(\varphi) \quad \forall \varphi \in V.$$

Newton's method

We now formulate a root-finding problem. Redefine from before:

$$a_N(u)(\varphi) := a(u,\varphi) - \gamma([g-u]^+,\varphi) - l(\varphi).$$

Then:

$$u \in V: \quad a_N(u)(\varphi) = 0 \quad \forall \varphi \in V.$$

Newton: Initial guess $u_0 \in V$. Then iteration: for $k = 0, 1, 2, \ldots$:

$$u_k \in V: \quad a_N'(u_k)(\delta u, \varphi) = -a_N(u_k)(\varphi) \quad \forall \varphi \in V$$
$$u_{k+1} = u_k + \omega \delta u$$

with a line search parameter $\omega \in (0, 1]$. And with

$$a_N'(u_k)(\delta u, \varphi) := (\nabla \delta u, \nabla \varphi) + \gamma(\delta u, \varphi)_{B(u_k)}$$

with the set

$$B(u_k) := \{x \in \Omega | u_k(x) < g(x)\}.$$

Discretization

We employ a conforming finite element method: $V_h \subset V$ with $V_h := \{\varphi_1, \ldots, \varphi_M\}$ and $\dim(V_h) = M$. Take as FEM, for instance, linear (bilinear) elements, i.e., hat functions in 1D.

For a usual linear problem, we would try to solve for $u_{h,k} \in V_h$. Since the problem is nonlinear, we cannot determine $u_{h,k}$ directly, but use the nonlinear Newton iteration. Here, we determine $\delta u_h \in V_h$, which means:

$$\delta u_h = \sum_{j=1}^{M} u_j \varphi_j.$$

Then:

$$u_{h,k} \in V_h: \quad a_N'(u_{h,k})(\delta u_h, \varphi_h) = -a_N(u_{h,k})(\varphi_h) \quad \forall \varphi_h \in V_h$$
$$u_{h,k+1} = u_{h,k} + \omega \delta u_h$$

The defect solution (first line of Newton's method) can be re-written as:

$$\begin{aligned}
& a_N'(u_{h,k})(\sum_{j=1}^{M} u_j \varphi_j, \varphi_h) = -a_N(u_{h,k})(\varphi_h) \quad \forall \varphi_h \in V_h \\
\Leftrightarrow \quad & \sum_{j=1}^{M} u_j \, a_N'(u_{h,k})(\varphi_j, \varphi_h) = -a_N(u_{h,k})(\varphi_h) \quad \forall \varphi_h \in V_h \\
\Leftrightarrow \quad & \sum_{j=1}^{M} u_j \, a_N'(u_{h,k})(\varphi_j, \varphi_i) = -a_N(u_{h,k})(\varphi_i) \quad i = 1, \ldots, M. \quad \Leftrightarrow \quad A\delta U = B.
\end{aligned}$$

Specifically,

$$A := \underbrace{(a_N'(u_{h,k})(\varphi_j, \varphi_i))_{i,j=1}^{M}}_{\in \mathbb{R}^{M \times M}}, \quad \delta U = \underbrace{(u_j)_{j=1}^{M}}_{\in \mathbb{R}^M}, \quad B := \underbrace{a_N(u_{h,k})(\varphi_i)_{i=1}^{M}}_{\in R^M}.$$

In explicit matrix notation:

$$A = \begin{pmatrix} (\nabla\varphi_1, \nabla\varphi_1) + \gamma(\varphi_1, \varphi_1)_B & \dots & (\nabla\varphi_M, \nabla\varphi_1) + \gamma(\varphi_M, \varphi_1)_B \\ \vdots & \ddots & \vdots \\ (\nabla\varphi_1, \nabla\varphi_M) + \gamma(\varphi_1, \varphi_M)_B & \dots & (\nabla\varphi_M, \nabla\varphi_M) + \gamma(\varphi_M, \varphi_M)_B \end{pmatrix}$$

Recall: test functions determine the row.

Details and discussions

We provide a bit more details in terms of heuristic discussions in this section. It is trivial to see that:

$$(\nabla\varphi_1, \nabla\varphi_1) = \int_\Omega \nabla\varphi_1 \cdot \nabla\varphi_1 \, dx \quad \rightarrow \quad \text{Laplacian},$$

and

$$\gamma(\varphi_1, \varphi_1) = \int_\Omega \varphi_1 \cdot \varphi_1 \, dx \quad \rightarrow \quad \text{(weighted) mass term.}$$

For $\gamma \gg 0$ (heavy enforcement of the constraint) and $u \ll g$ (large violations of the constraint), the linear system in the defect of Newton's method becomes ill-conditioned and Newton's method itself more nonlinear. Indeed

$$\gamma(\varphi_j, \varphi_i)_B$$

only acts in rows and columns in which the constraint is violated. We therefore have a large condition number

$$cond_2(A) \gg 1.$$

Furthermore, the condition numbers of the Laplacian and the mass term are:

$$(\nabla\varphi_j, \nabla\varphi_i) \sim \frac{1}{h}, \quad (\varphi_j, \varphi_i) \sim h$$

and for the right hand (f, φ_i), it holds:

$$(f, \varphi_i) \sim h.$$

For an asymptotic equilibrium we thus need:

$$\gamma \sim \frac{1}{h^2}.$$

In addition if we have material parameters (for instance Young's modulus or the critical energy release rate G_C if we have the phase-field system in mind), which enter into the Laplacian

$$(\alpha(x)\nabla\varphi_j, \nabla\varphi_i).$$

From this we can follow that

$$\gamma \sim \frac{\alpha(x)}{h^2}.$$

Implementation in DOpElib

For details on DOpElib within these lecture notes, we refer to [112][Chapter 15]. The programming code used for this example can be found on

`http://www.thomaswick.org/links/Example_Obstacle_Simple_Penalization.zip`

and is based on the official DOpElib example `dopelib/Examples/PDE/StatPDE/Example4/` (classical Poisson problem on the unit square).

- Some parameters are provided in `dope.prm`;
- The grid and important setups are in `main.cc`;
- The equations, g and γ are implemented in `local_pde.h`.

The number of DoFs is 4 225, the obstacle function is $g = -0.01$ and the penalization is chosen as $\gamma = \frac{\bar{\gamma}}{h^2}$ with $\bar{\gamma} = 0.1$.

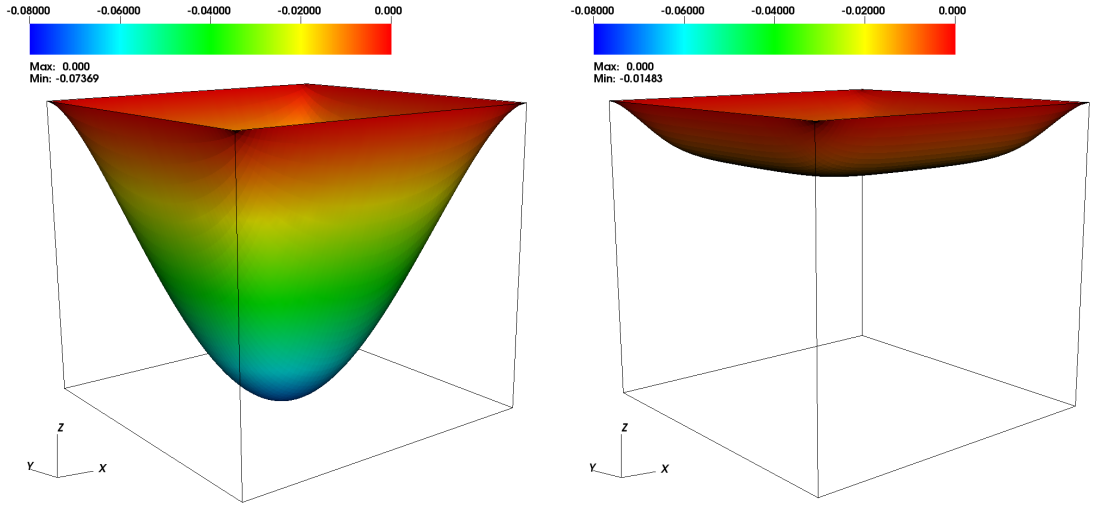

Figure 3.4: Left: 3d surface plot solution of the classical Poisson problem in $(0,1)^2$ and right hand side $f = -1$, as in Section 3.11.1. Right: obstacle problem with $g = -0.01$ and simple penalization.

The nonlinear solver behaves as follows:

```
Newton step: 0  Residual (abs.):   2.4414e-04
Newton step: 0  Residual (rel.):   1.0000e+00
Newton step: 1  Residual (rel.):   9.7262e-01   LineSearch {2}
Newton step: 2  Residual (rel.):   4.8631e-01   LineSearch {1}
Newton step: 3  Residual (rel.):   2.6331e-01   LineSearch {0}
Newton step: 4  Residual (rel.):   5.1674e-03   LineSearch {0}
Newton step: 5  Residual (rel.): < 1.0000e-11   LineSearch {0}
```

Evaluating the solution in the middle point yields

$$u(0.5, 0.5) = -0.0148305.$$

This shows that the constraint works, but it slightly relaxed the solution. This is a well-known shortcoming of simple penalization.

For a fair comparison, we briefly state the results for the classical Poisson problem:

```
Newton step: 0  Residual (abs.):   2.4414e-04
Newton step: 0  Residual (rel.):   1.0000e+00
Newton step: 1  Residual (rel.): < 1.0000e-11   LineSearch {0}
```

The solution value at the middle point is

$$u(0.5, 0.5) = -0.0736855.$$

Mesh refinement studies with $\gamma = \frac{\bar{\gamma}}{h^2}$

We now briefly investigate the behavior of the solution with respect to (uniform) mesh refinement. The numbers of DoFs are

```
4225 (above), 33282, 132098
```

We run the same code as before and obtain for the middle point and number of Newton iterations:

```
DoFs      u(0.5,0.5)          Newton iter.
-----------------------------------------
4225      -0.0148305          5
33282     -0.0112206          10
132098    -0.0103052          19
```

Thus we observe a dependence on h of both the solution and the solver performance.

Mesh refinement studies with $\gamma = \frac{\bar{\gamma}}{h^2_{\mathbf{coarse}}}$

Here, we remove the dependency of h in the penalization constraint. We take the coarsest h_{coarse} and evaluate

$$\gamma = \frac{\bar{\gamma}}{h^2_{\text{coarse}}} = 204.8$$

On the finer levels, we take the same γ. Then we obtain:

```
DoFs      u(0.5,0.5)          Newton iter.
-----------------------------------------
4225      -0.0148305          5
33282     -0.01483            6
132098    -0.0148299          6
```

Here, the nonlinear solver shows constant iteration numbers. Moreover, the middle point $u(0.5, 0.5)$ converges qualitatively. However, of course, the constraint itself $g = -0.01$ is not that well approximated.

Further implementation exercises

In order to study the previous problem in more detail, here are some tasks:

1. Refine the mesh and observe the Newton iteration numbers and the displacement value $u(0.5, 0.5)$.
2. Change γ. What do you observe?
3. Change g. For instance, $g = -0.1$ and $g = -0.005$. What do you observe?
4. Introduce a material coefficient in the Laplacian. What do you observe for the numerical solution, the number of Newton iterations and $u(0.5, 0.5)$?
5. Implement an iteration scheme that allows to increase γ successively. Why is this useful? What do you observe for the Newton iteration numbers and $u(0.5, 0.5)$?

3.12 Exercises

Exercise 5. *Derive a staggered solution scheme for Proposition 14 and compare it with the (quasi-) monolithic scheme presented in this chapter. What are differences of both schemes? What are advantages and shortcomings of one or the other?*

Exercise 6.

1. *By formal Gauss elimination, derive a block-triangular system of M in Section 3.8.*
2. *The matrix obtained by these elimentary operations, constitutes an (optimal) preconditioner matrix P^{-1}. Double-check that the result $P^{-1}M$ yields identities on the diagonal.*
3. *Discuss the differences to the block-diagonal preconditioner that is currently suggested in Section 3.8.*

Exercise 7. *Calculate and verify all steps up to the linear system for the finite element discretization of the obstacle problem in Section 3.11.*

Chapter 4

Optimization (Session 3)

In this section, we follow [87][1] and introduce an optimal control configuration based on the previously introduced space-time formulation. Therein a certain cost functional (e.g., matching a given crack pattern φ_d) shall be minimized, while adapting the boundary conditions, i.e., the control variables, in a certain way. For general overviews of PDE-based optimization, we refer the reader to [79] and [18, 116].

In the following, we introduce the reduced solution approach. Here, the primal solution (state variable) U is eliminated by a solution operator and represented through the control variable q. Thus, the solution process is reduced to the control variable. Therein, the primal forward problem plus three additional equations must be solved. Their combination yields the final solution algorithm.

4.1 Optimization problem

In this chapter, we introduce separable NLP (Non-Linear Program) with a tracking type const functional. The goal of this NLP is to find a suitable control q which leads to a desired crack path described by a given phase-field fracture pattern φ_d. We introduce the space-time weak formulation with some optimal control in the following way. Let $Q \coloneqq L^2(\Gamma_N)$ be the function space for the control function q and the space $W \coloneqq C(I, Q)$. Then, with the preliminary work carried out in Section 3.10, we have

Proposition 17. *Given initial values $U_0 = (u_0, \varphi_0) \in V$ and a control $q \in W$, we seek $U \in X$ that solves*

$$\begin{aligned} (g(\varphi)\mathbb{C}e(u), e(\Phi_u))_I - (q, \Phi_{u:\perp})_{\Gamma_N, I} = 0, \\ G_c\varepsilon(\nabla\varphi, \nabla\Phi_\varphi)_I - \frac{G_c}{\varepsilon}(1-\varphi, \Phi_\varphi)_I + (1-\kappa)(\varphi\mathbb{C}e(u) : e(u), \Phi_\varphi)_I \\ + \gamma(\partial_t\varphi, \Phi_\varphi)_{\{\partial_t\varphi > 0, I\}} + \eta(\partial_t\varphi, \Phi_\varphi)_I = 0, \end{aligned} \tag{4.1}$$

for every test function $\Phi = (\Phi_u, \Phi_\varphi) \in X$.

The discretized phase-field fracture system is given by

[1] Large parts are taken from [87] for which permission from Elsevier is gratefully acknowledged.

Problem 17. *Let the initial condition in weak form (see Section 3.10)*

$$(U(0), \Phi_0^-) = (U_0, \Phi_0^-) \quad \forall \Phi_0^- \in V, \tag{4.2}$$

be given. Then we compute $U(t_m)$ for $m = 1, \dots, M$ from

$$\begin{aligned} 0 &= \gamma(\varphi(t_m), \Phi_\varphi(t_m))_{\{\varphi(t_m) > \varphi(t_{m-1})\}} + \eta(\varphi(t_m), \Phi_\varphi(t_m)) \\ &\quad - \gamma(\varphi(t_{m-1}), \Phi_\varphi(t_m))_{\{\varphi(t_m) > \varphi(t_{m-1})\}} - \eta(\varphi(t_{m-1}), \Phi_\varphi(t_m)) \\ &\quad + a(q(t_m), U(t_m))(\Phi(t_m))\Delta t_m \quad \forall \Phi \in X_k^0. \end{aligned} \tag{4.3}$$

The resulting minimization problem reads as:

$$\begin{aligned} \min_{q,U} \quad & \mathcal{J}(q, U) \coloneqq \frac{1}{2} \sum_{m=1}^{M} \|\varphi(t_m) - \varphi_d(t_m)\|^2 + \frac{\alpha}{2} \sum_{m=1}^{M} \|q(t_m) - q_d(t_m)\|_{\Gamma_N}^2 \\ \text{s.t.} \quad & (q, U) \text{ solve (4.2) and (4.3) for } m = 1, \dots, M, \end{aligned} \tag{4.4}$$

with $(u_0, \varphi_0) \in V$ and $(q, U) \in W \times X$. Here $\varphi_d \in L^\infty(\Omega)$ is some desired phase-field and q_d is a suitable nominal control used for numerical stabilization. The second sum denotes a classical Tikhonov regularization with the positive parameter α. For functions that are non-negative and weakly semi-continuous, it was shown in [128, Theorem 4.3] that there exists a global solution of (4.4) in $L^2(I, Q) \times X$.

4.2 Reduced optimization problem

In order to apply the reduced approach to (4.4), we assume the existence of a solution operator $S \colon W \to X$ for the PDE (4.1). Using this operator the state variable U can be eliminated from the cost functional $\mathcal{J}(q, U)$ and we obtain a reduced cost functional $j \colon W \to \mathbb{R}$, $j(q) \coloneqq \mathcal{J}(q, S(q))$. The NLP (4.4) is the replaced by the unconstrained optimization problem

$$\min_q \; j(q). \tag{4.5}$$

Specifically, we have

$$j'(q)(\delta q) = 0 \quad \forall \delta q \in W,$$

for which the linear system (within Newton's method) reads

$$j''(q)(\delta q_1, \delta q_2) = -j'(q)(\delta q_2) \quad \forall \delta q_1, \delta q_2 \in W.$$

To solve $j'(q) = 0$ by Newton's method, we compute representations of j' and j'' using the established approach in [18]. These representations require the solution of four auxiliary equations, which involve the derivatives of the Lagrangian defined as $\mathcal{L} \colon W \times X_k^0 \times X_k^0 \to \mathbb{R}$,

$$\begin{aligned} \mathcal{L}(q, U, Z) \coloneqq \mathcal{J}(q, U) &- \gamma(\partial_t \varphi, z_\varphi)_{\{\partial_t \varphi > 0, I\}} - \eta(\partial_t \varphi, z_\varphi)_I \\ &- \int_I a(q(t), U(t))(Z(t)) \, \mathrm{d}t \\ &- \eta_0(u(0) - u_0, z_u(0)) - \eta(\varphi(0) - \varphi_0, z_\varphi(0)), \end{aligned} \tag{4.6}$$

in the continuous case and

$$\begin{aligned}\mathcal{L}(q,U,Z) \coloneqq \mathcal{J}(q,U) &- \sum_{m=1}^{M}\left(\gamma(\partial_t\varphi, z_\varphi)_{\{\partial_t\varphi>0, I_m\}} + \eta(\partial_t\varphi, z_\varphi)_{I_m}\right)\\ &- \sum_{m=0}^{M-1}\left(\gamma([\varphi]_m, z^+_{\varphi,m})_{\{\varphi^-_{m+1}>\varphi^-_m\}} + \eta([\varphi]_m, z^+_{\varphi,m})\right)\\ &- \int_I a(q(t),U(t))(Z(t))\,\mathrm{d}t\\ &- \eta_0(u(0)-u_0, z_u(0)) - \eta(\varphi(0)-\varphi_0, z_\varphi(0)),\end{aligned} \tag{4.7}$$

within the dG(r) setting.

4.3 State, adjoint, tangent, adjoint Hessian

The four equations that must be solved in order to determine j' and j'' are presented in this section.

1. *State equation:* given control $q \in W$, find state $U = S(q) \in X$ such that the PDE (4.1) holds:

$$\mathcal{L}'_Z(q,U,Z)(\Phi) = 0 \quad \forall \Phi \in X.$$

2. *Adjoint equation:* given control $q \in W$ and state solution $U = S(q)$, find adjoint solution $Z \in X$ such that

$$\mathcal{L}'_U(q,U,Z)(\Phi) = 0 \quad \forall \Phi \in X. \tag{4.8}$$

3. *Tangent equation:* given control $q \in W$, state solution $U = S(q)$, adjoint solution Z and a direction $\delta q \in W$, find $\delta U \in X$ such that

$$\mathcal{L}''_{qZ}(q,U,Z)(\delta q,\Phi) + \mathcal{L}''_{UZ}(q,U,Z)(\delta U,\Phi) = 0 \quad \forall \Phi \in X. \tag{4.9}$$

4. *Adjoint Hessian equation:* given control $q \in W$, state solution $U = S(q)$, adjoint solution $Z \in X$ from (4.8), a direction $\delta q \in W$, and $\delta U \in X$ from (4.9), find $\delta Z \in X$ such that

$$\mathcal{L}''_{qU}(q,U,Z)(\delta q,\Phi) + \mathcal{L}''_{UU}(q,U,Z)(\delta U,\Phi) + \mathcal{L}''_{ZU}(q,U,Z)(\delta Z,\Phi) = 0 \quad \forall \Phi \in X. \tag{4.10}$$

The representations of the derivatives that we require for Newton's method are then obtained by solving these equations in a specific order, see for example [18, 116]:

$$\begin{aligned} j'(q)(\delta q) &= \mathcal{L}'_q(q,U,Z)(\delta q) \quad \forall \delta q \in W,\\ j''(q)(\delta q_1,\delta q_2) &= \mathcal{L}''_{qq}(q,U,Z)(\delta q_1,\delta q_2) + \mathcal{L}''_{Uq}(q,U,Z)(\delta U,\delta q_2)\\ &\quad + \mathcal{L}''_{Zq}(q,U,Z)(\delta Z,\delta q_2) \quad \forall \delta q_1,\delta q_2 \in W.\end{aligned} \tag{4.11}$$

4.4 Adjoint time-stepping scheme

In order to derive the adjoint time-stepping scheme we have to compute the derivative of $\mathcal{L}$. We formulate it directly in the weak form

$$\begin{aligned}\mathcal{L}'_U(q,U,Z)(\Phi) = \mathcal{J}'_U(q,U)(\Phi) \\ - \gamma(\partial_t\Phi_\varphi, z_\varphi)_{\{\partial_t\varphi>0,I\}} - \eta(\partial_t\Phi_\varphi, z_\varphi)_I \\ - \int_I a'_U(q(t),U(t))(\Phi(t),Z(t))\,\mathrm{d}t \\ - \eta_0(\Phi_u(0), z_u(0)) - \eta(\Phi_\varphi(0), z_\varphi(0)).\end{aligned} \tag{4.12}$$

Herein the partial derivative of a reads

$$\begin{aligned}a'_U(q,U)(\Phi,Z) = ((1-\kappa)\varphi^2+\kappa)\cdot(\mathbb{C}e(\Phi_u), e(z_u)) \\ + 2\varphi(1-\kappa)\Phi_\varphi(\mathbb{C}e(u), e(z_u)) \\ + G_c\varepsilon(\nabla\Phi_\varphi, \nabla z_\varphi) + \frac{G_c}{\varepsilon}(\Phi_\varphi, z_\varphi) \\ + (1-\kappa)(\Phi_\varphi\cdot\mathbb{C}e(u) : e(u), z_\varphi) \\ + 2\varphi(1-\kappa)(\mathbb{C}e(\Phi_u) : e(u), z_\varphi).\end{aligned} \tag{4.13}$$

The main problem now is that the time derivatives are applied to the test function Φ, which is usual for the adjoint. Thus, we use integration by parts to convert the time derivatives to Z. Then the second line in (4.12) becomes

$$\begin{aligned}\gamma(\Phi_\varphi, \partial_t z_\varphi)_{\{\partial_t\varphi>0,I\}} + \eta(\Phi_\varphi, \partial_t z_\varphi)_I \\ + \gamma(\Phi_\varphi(0), z_\varphi(0))_{\{\partial_t\varphi(0)>0\}} + \eta(\Phi_\varphi(0), z_\varphi(0)) \\ - \gamma(\Phi_\varphi(T), z_\varphi(T))_{\{\partial_t\varphi(T)>0\}} - \eta(\Phi_\varphi(T), z_\varphi(T)).\end{aligned} \tag{4.14}$$

In the next step we want to apply the procedure that we applied to the state equation, i.e state a dG(0) formulation. This will require an approximation of $\partial_t\varphi(t_m)$. While $\partial_t\varphi(t_m)$ for $m = 1,\dots,M$ is easily approximated by the backward difference

$$\partial_t\varphi(t_m) \approx \frac{\varphi(t_m)-\varphi(t_{m-1})}{t_m - t_{m-1}},$$

this procedure will not work for the first mesh point $t_0 = 0$. The forward difference

$$\partial_t\varphi(0) \approx \frac{\varphi(t_1)-\varphi(t_0)}{t_1 - t_0}$$

is a good choice because it simplifies the condition $\partial_t\varphi(t_0) > 0$ to $\varphi(t_1) > \varphi(t_0)$ and leads to desired cancellations. Finally we obtain the derivative in a dG(0) setting.

$$\begin{aligned}\mathcal{L}'_U(q,U,Z)(\Phi) = \mathcal{J}'_U(q,U)(\Phi)\\ &- \gamma(\Phi^-_{\varphi,M}, z^-_{\varphi,M})_{\{\varphi(t_M)>\varphi(t_{M-1})\}} - \eta(\Phi^-_{\varphi,M}, z^-_{\varphi,M})\\ &+ \sum_{m=1}^{M} \big[\gamma(\Phi^-_{\varphi,m-1}, z^+_{\varphi,m-1} - z^-_{\varphi,m-1})_{\{\varphi^-_m>\varphi^-_{m-1}\}}\\ &\qquad + \eta(\Phi^-_{\varphi,m-1}, z^+_{\varphi,m-1} - z^-_{\varphi,m-1})\big]\\ &- \sum_{m=1}^{M} a'_U(q(t_m),U(t_m))(\Phi(t_m),Z(t_m))\Delta t_m\\ &- \eta_0(\Phi^-_{u,0}, z^-_{u,0}).\end{aligned} \tag{4.15}$$

From this point on, we make use of the separable structure of $\mathcal{J}(q,U) = \sum_m J(q(t_m),U(t_m))$. We begin the solution procedure by separating all terms related to the last time point t_M from (4.15).

$$\begin{aligned}&a'_U(q(t_M)U(t_M))(\Phi(t_M),Z(t_M))\Delta t_M\\ &\quad+\gamma(\Phi^-_{\varphi,M}, z^-_{\varphi,M})_{\{\varphi^-_m>\varphi^-_{m-1}\}} + \eta(\Phi^-_{\varphi,M}, z^-_{\varphi,M})\\ &\quad= J'_U(q(t_M),U(t_M))(\Phi(t_M)) \quad \forall\Phi\in X^0_k.\end{aligned} \tag{4.16}$$

Next, we add up what is left, multiply by -1 and use the X_k0 property ($z^+_{\varphi,m-1} = z^-_{\varphi,m}$) to obtain:

$$\begin{aligned}0 = &\sum_{m=1}^{M} \big[\gamma(\Phi^-_{\varphi,m-1}, z^-_{\varphi,m-1} - z^-_{\varphi,m})_{\{\varphi^-_m>\varphi^-_{m-1}\}} + \eta(\Phi^-_{\varphi,m-1}, z^-_{\varphi,m-1} - z^-_{\varphi,m})\big]\\ &+ \sum_{m=1}^{M-1} a'_U(q(t_m),U(t_m))(\Phi(t_m),Z(t_m))\Delta t_m\\ &- \sum_{m=1}^{M-1} J'_U(q(t_m),U(t_m))(\Phi(t_m))\\ &+ \eta_0(\Phi^-_{u,0}, z^-_{u,0}) \quad \forall\Phi\in X^0_k.\end{aligned} \tag{4.17}$$

Now we want to rewrite the entire equation as a single sum in order to derive the equations that are solved in each time step. Consequently, we separate the terms for $m = 0$ and shift down the index of the first sum:

$$\begin{aligned}0 = &\sum_{m=1}^{M-1} \Big(\big[\gamma(\Phi^-_{\varphi,m}, z^-_{\varphi,m} - z^-_{\varphi,m+1})_{\{\varphi^-_{m+1}>\varphi^-_m\}} + \eta(\Phi^-_{\varphi,m}, z^-_{\varphi,m} - z^-_{\varphi,m+1})\big]\\ &\qquad + a'_U(q(t_m),U(t_m))(\Phi(t_m),Z(t_m))\Delta t_m\\ &\qquad - J'_U(q(t_m),U(t_m))(\Phi(t_m))\Big)\\ &+ \gamma(\Phi^-_{\varphi,0}, z^-_{\varphi,0} - z^-_{\varphi,1})_{\{\varphi^-_1>\varphi^-_0\}} + \eta(\Phi^-_{\varphi,0}, z^-_{\varphi,0} - z^-_{\varphi,1})\\ &+ \eta_0(\Phi^-_{u,0}, z^-_{u,0}).\end{aligned}$$

Finally we solve for $m = M-1, M-2, \ldots, 1$ the equation

$$\begin{aligned} &a'_U(q(t_m), U(t_m))(\Phi(t_m), Z(t_m))\Delta t_m \\ &\quad + \gamma(\Phi^-_{\varphi,m}, z^-_{\varphi,m} - z^-_{\varphi,m+1})_{\{\varphi^-_{m+1} > \varphi^-_m\}} + \eta(\Phi^-_{\varphi,m}, z^-_{\varphi,m} - z^-_{\varphi,m+1}) \\ &\quad = J'_U(q(t_m), U(t_m))(\Phi(t_m)) \quad \forall \Phi \in X^0_k. \end{aligned} \tag{4.18}$$

For $m = 0$ the three remaining terms are,

$$\gamma(\Phi^-_{\varphi,0}, z^-_{\varphi,0} - z^-_{\varphi,1})_{\{\varphi^-_1 > \varphi^-_0\}} + \eta(\Phi^-_{\varphi,0}, z^-_{\varphi,0} - z^-_{\varphi,1}) + \eta_0(\Phi^-_{u,0}, z^-_{u,0}) = 0. \tag{4.19}$$

The last term of (4.19) can be omitted for $\eta_0 \ll \eta$ small enough and the following equation can be solved in its place:

$$(\Phi^-_{\varphi,0}, z^-_{\varphi,1}) = (\Phi^-_{\varphi,0}, z^-_{\varphi,0}). \tag{4.20}$$

Remark 38 (Algorithmic realization)**.** *It can be helpful to add the initial condition* $(\Phi^-_{u,0}, z^-_{u,1}) = (\Phi^-_{u,0}, z^-_{u,0})$ *to prevent singular matrices that would cause a loss of convergence in the linear solvers. In total,* $(\Phi^-_0, Z^-_1) = (\Phi^-_0, Z^-_0)$ *is used to replace* (4.20)*.*

4.5 Tangent time-stepping schemes

Similar to the state equation we start by solving the initial conditions,

$$\begin{aligned} (\delta u^-_0, \Phi^-_{u,0}) &= 0, \\ (\delta \varphi^-_0, \Phi^-_{\varphi,0}) &= 0, \end{aligned}$$

in short

$$(\delta U(t_0), \Phi^-_0) = 0 \quad \forall \Phi^-_0 \in V. \tag{4.21}$$

An application of the X^0_k property to $\delta\varphi^+_{m-1}$ leads to the following equation that is solved for $m = 1, \ldots, M$

$$\begin{aligned} &\gamma(\delta\varphi^-_m, \Phi^-_{\varphi,m})_{\{\varphi^-_m > \varphi^-_{m-1}\}} + \eta(\delta\varphi^-_m, \Phi^-_{\varphi,m}) \\ &\qquad + a'_U(q(t_m), U(t_m))(\delta U(t_m), \Phi(t_m))\Delta t_m \\ &\qquad = \eta(\delta\varphi^-_{m-1}, \Phi^-_{\varphi,m}) + \gamma(\delta\varphi^-_{m-1}, \Phi^-_{\varphi,m})_{\{\varphi^-_m > \varphi^-_{m-1}\}} \\ &\qquad - a'_q(q(t_m), U(t_m))(\delta q(t_m), \Phi(t_m))\Delta t_m \quad \forall \Phi \in X^0_k. \end{aligned} \tag{4.22}$$

4.6 Adjoint Hessian time-stepping schemes

The procedure for the adjoint Hessian equation is similar to the adjoint equation. In dG(r) terms the equation reads as

$$\begin{aligned}
0 = \sum_{m=1}^{M} \Big(& \mathcal{J}''_{UU}(q(t_m), U(t_m))(\delta U(t_m), \Phi(t_m)) \\
& - a''_{UU}(q(t_m), U(t_m))(\delta U(t_m), \Phi(t_m), Z(t_m))\Delta t_m \\
& - a'_{U}(q(t_m), U(t_m))(\Phi(t_m), \delta Z(t_m))\Delta t_m \\
& + \gamma(\Phi^-_{\varphi,m-1}, \delta z^+_{\varphi,m-1} - \delta z^-_{\varphi,m-1})_{\{\varphi^-_m > \varphi^-_{m-1}\}} \\
& + \eta(\Phi^-_{\varphi,m-1}, \delta z^+_{\varphi,m-1} - \delta z^-_{\varphi,m-1}) \Big) \\
- \gamma(\Phi^-_{\varphi,M}, \delta z^-_{\varphi,M})_{\{\varphi^-_M > \varphi^-_{M-1}\}} & - \eta(\Phi^-_{\varphi,M}, \delta z^-_{\varphi,M}) \\
- \eta_0(\Phi^-_{u,0}, \delta z^-_{u,0}) \quad & \forall \Phi \in X^0_k.
\end{aligned} \tag{4.23}$$

First we collect all containing the last time point t_M and solve

$$\begin{aligned}
0 = & J''_{UU}(q(t_M), U(t_M))(\delta U(t_M), \Phi(t_M)) \\
& - a'_{U}(q(t_M), U(t_M))(\Phi(t_M), \delta Z(t_M))\Delta t_M \\
& - a''_{UU}(q(t_M), U(t_M))(\delta U(t_M), \Phi(t_M), Z(t_M))\Delta t_M \\
& - \gamma(\Phi^-_{\varphi,M}, \delta z^-_{\varphi,M})_{\{\varphi^-_M > \varphi^-_{M-1}\}} - \eta(\Phi^-_{\varphi,M}, \delta z^-_{\varphi,M}) \quad \forall \Phi \in X^0_k.
\end{aligned} \tag{4.24}$$

Then (4.23) is reformulated as

$$\begin{aligned}
0 = & \sum_{m=1}^{M-1} \Big(J''_{UU}(q(t_m), U(t_m))(\delta U(t_m), \Phi(t_m)) \\
& - a''_{UU}(q(t_m), U(t_m))(\delta U(t_m), \Phi(t_m), Z(t_m))\Delta t_m \\
& - a'_{U}(q(t_m), U(t_m))(\Phi(t_m), \delta Z(t_m))\Delta t_m \Big) \\
& + \sum_{m=1}^{M} \Big(\gamma(\Phi^-_{\varphi,m-1}, \delta z^+_{\varphi,m-1} - \delta z^-_{\varphi,m-1})_{\{\varphi^-_m > \varphi^-_{m-1}\}} \\
& + \eta(\Phi^-_{\varphi,m-1}, \delta z^+_{\varphi,m-1} - \delta z^-_{\varphi,m-1}) \Big) \\
& - \eta_0(\Phi^-_{u,0}, \delta z^-_{u,0}) \quad \forall \Phi \in X^0_k.
\end{aligned} \tag{4.25}$$

Finally the index of the second sum is shifted and all terms corresponding to $m = 0$ are separated

$$\begin{aligned}
0 = & \sum_{m=1}^{M-1} \Big(J''_{UU}(q(t_m), U(t_m))(\delta U(t_m), \Phi(t_m)) \\
& - a''_{UU}(q(t_m), U(t_m))(\delta U(t_m), \Phi(t_m), Z(t_m))\Delta t_m \\
& - a'_{U}(q(t_m), U(t_m))(\Phi(t_m), \delta Z(t_m))\Delta t_m \\
& + \gamma(\Phi^-_{\varphi,m}, \delta z^+_{\varphi,m} - \delta z^-_{\varphi,m})_{\{\varphi^-_{m+1} > \varphi^-_m\}} \\
& + \eta(\Phi^-_{\varphi,m}, \delta z^+_{\varphi,m} - \delta z^-_{\varphi,m}) \Big) \\
& + \gamma(\Phi^-_{\varphi,0}, \delta z^+_{\varphi,0} - \delta z^-_{\varphi,0})_{\{\varphi^-_1 > \varphi^-_0\}} + \eta(\Phi^-_{\varphi,0}, \delta z^+_{\varphi,0} - \delta z^-_{\varphi,0}) \\
& - \eta_0(\Phi^-_{u,0}, \delta z^-_{u,0}) \quad \forall \Phi \in X^0_k.
\end{aligned} \tag{4.26}$$

As a result, we determine $\delta Z(t_m)$ for $m = M-1, M-2, \ldots, 1$ from

$$\begin{aligned}
0 &= J''_{UU}(q(t_m), U(t_m))(\delta U(t_m), \Phi(t_m)) \\
&\quad - a''_{UU}(q(t_m), U(t_m))(\delta U(t_m), \Phi(t_m), Z(t_m))\Delta t_m \\
&\quad - a'_U(q(t_m), U(t_m))(\Phi(t_m), \delta Z(t_m))\Delta t_m \\
&\quad + \gamma(\Phi^-_{\varphi,m}, \delta z^+_{\varphi,m} - \delta z^-_{\varphi,m})_{\{\varphi^-_{m+1} > \varphi^-_m\}} \\
&\quad + \eta(\Phi^-_{\varphi,m}, \delta z^+_{\varphi,m} - \delta z^-_{\varphi,m}) \quad \forall \Phi \in X^0_k.
\end{aligned}$$

Consequently the only remaining terms in (4.26) are

$$\gamma(\Phi^-_{\varphi,0}, \delta z^+_{\varphi,0} - \delta z^-_{\varphi,0})_{\{\varphi^-_1 > \varphi^-_0\}} + \eta(\Phi^-_{\varphi,0}, \delta z^+_{\varphi,0} - \delta z^-_{\varphi,0}) - \eta_0(\Phi^-_{u,0}, \delta z^-_{u,0}). \tag{4.27}$$

The final step is to use the assumption $\eta_0 \ll \eta$ once more and eliminate the last term in the equation (4.27):

$$\begin{aligned}
(\Phi^-_{\varphi,0}, \delta z^-_{\varphi,0}) &= (\Phi^-_{\varphi,0}, \delta z^-_{\varphi,1}), \\
(\Phi^-_{u,0}, \delta z^-_{u,0}) &= (\Phi^-_{u,0}, \delta z^-_{u,1}).
\end{aligned}$$

4.7 Final complete algorithm

The complete method given in Algorithm 3 is obtained by combining the optimization problem statement and the space-time discretizations from the previous sections, as well as the resulting time-stepping schemes for the four equations.

Algorithm 3: Overall space-time phase-field fracture control algorithm

Data: Domain Ω, mesh $\mathcal{T}_h$, number of time intervals M, parameters ε, κ, G_c, μ, λ, γ, η, α, initial value U_0, initial control guess q^0.

Result: Optimal control q and admissible solution U.

1: Set $k = 0$ and $q^k = q^0$ and solve the state equation for U: $\mathcal{L}'_Z(q^k, U, Z)(\Phi) = 0 \ \forall \Phi$. Specifically, obtain $U(t_0)$ from (4.2) and then $U(t_1), \dots, U(t_M)$ from (4.3);

2: Solve the adjoint equation for Z: $\mathcal{L}'_U(q^k, U, Z)(\Phi) = 0 \ \forall \Phi$. Obtain $Z(t_M)$ from (4.16), then $Z(t_{M-1}), \dots, Z(t_1)$ from (4.18), and finally $Z(t_0)$ from (4.19);

3: Construct the coefficient vector $\boldsymbol{f} \in \mathbb{R}^n$ for the reduced gradient $\nabla j(q^k)$ by solving $\boldsymbol{G}\boldsymbol{f} = [j'(q^k)(q_i)]_{i=1}^n$. Here q_i denotes the i-th basis function of the discrete control space Q_h and $\boldsymbol{G}_{ij} = (q_i, q_j)$ defines the mass matrix. The derivatives $j'(q^k)(q_i)$ for the right hand side are computed from the representation (4.11);

while $\|\boldsymbol{f}\|_2 > TOL$ **do**

4: Obtain δq from the Newton equation, $j''(q^k)(\delta q, q_i) = -j'(q^k)(q_i) \ \forall q_i$, by minimizing $m(q^k, \boldsymbol{d}) = j(q^k) + \langle \boldsymbol{f}, \boldsymbol{d} \rangle + \frac{1}{2}\langle \boldsymbol{H}\boldsymbol{d}, \boldsymbol{d} \rangle$ for a vector $\boldsymbol{d} \in \mathbb{R}^n$ using the CG-method (matrix free). Here $\boldsymbol{H} \in \mathbb{R}^{n \times n}$ denotes the coefficient matrix of $\nabla^2 j(q^k)\delta q$;

for *every CG step* **do**

5: Solve the tangent equation for δU: $\mathcal{L}''_{qZ}(q^k, U, Z)(\delta q, \Phi) + \mathcal{L}''_{UZ}(q^k, U, Z)(\delta U, \Phi) = 0 \ \forall \Phi$. Obtain $\delta U(t_0)$ from (4.21) and then $\delta U(t_1), \dots, \delta U(t_M)$ from (4.22);

6: Solve the adjoint Hessian equation for δZ: $\mathcal{L}''_{qU}(q^k, U, Z)(\delta q, \Phi) + \mathcal{L}''_{UU}(q^k, U, Z)(\delta U, \Phi) + \mathcal{L}''_{ZU}(q^k, U, Z)(\delta Z, \Phi) = 0 \ \forall \Phi$. Obtain $\delta Z(t_M)$ from (4.24), then $\delta Z(t_{M-1}), \dots, \delta Z(t_1)$ from (4.25), and finally $\delta Z(t_0)$ from (4.26);

7: Construct the coefficient vector $\boldsymbol{h} \in \mathbb{R}^n$ for $\nabla^2 j(q^k)\delta q$ by solving $\boldsymbol{G}\boldsymbol{h} = j''(q^k)(\delta q, q_i)_{i=1}^n$, where $j''(q^k)(\delta q, q_i)$ is represented via (4.11);

end

8: Choose a step length ν by an Armijo backtracking method;

9: Set $q^{k+1} = q^k + \nu \delta q$;

10: Repeat steps 1, 2, 3 for the new control q^{k+1} to obtain $\boldsymbol{f}$ for $\nabla j(q^{k+1})$.;

11: Increment $k = k + 1$;

end

4.8 Exercises

Exercise 8. *1. Discuss the physical meaning of* (4.4)*.*

2. Discuss and formulate other tracking type functionals, e.g., for the displacements.

3. Discuss and formulate other control variables q, e.g., in the right hand side or Dirichlet boundary conditions.

Exercise 9. *1. Given the Lagrangian* (4.6)*, calculate the directional derivative into the direction of u, namely derive the adjoint equation.*

2. What does the adjoint tell us?

3. What are the properties of the adjoint?

Chapter 5

Numerical simulations and current developments (Session 4)

In this chapter, we introduce some current developments made in our group and collaborations. The focus is on numerical aspects such as iteration numbers, convergence studies, robustness in parameters, and computational cost. We provide findings of recently published work, ongoing and future research as well as links to research software developments.

5.1 Modified combined Newton scheme: improving nonlinear efficiency

In the first example[1], we test the performance of the modified active set approach proposed in Section 3.7. For this, we consider a stationary benchmark test [145], where a constant pressure is applied in the inner of a pre-existing crack in the middle of a domain, and only the crack width varies. This test setup is motivated by Sneddon [148], and Sneddon and Lowengrub [149]. This results into the system

Problem 18. *(Linearized Euler-Lagrange equations with stress-splitting) Let $p^n \in L^\infty(\Omega)$ be a given pressure. For a given φ^0 and for every incremental step t_n with $n = 1, ..., N$, find $U^n := \{u^n, \varphi^n\} \in V_u^0 \times K$ such that it holds for $\Phi := \{0, \varphi^n\} \in V_u^0 \times K$*

$$A(U^n)(\Psi - \Phi) \geq 0 \quad \forall \Psi := \{\psi^u, \psi^\varphi\} \in V_u^0 \times K \cap L^\infty,$$

where $A(U^n)(\Psi - \Phi)$ is defined as

$$\begin{aligned} A(U^n)(\Psi - \Phi) := \big(g(\tilde{\varphi}^n)\sigma^+(u^n), e(\psi^u)\big) + \big(\sigma^-(u^n), e(\psi^u)\big) + ((\tilde{\varphi}^n)^2 p^n, \operatorname{div} \psi^u) \\ + (1-\kappa)(\varphi^n \sigma^+(u^n) : e(u^n), \psi^\varphi - \varphi^n) \\ + 2(\varphi^n p^n \operatorname{div} u^n, \psi^\varphi - \varphi^n) \\ + G_C \left(\frac{1}{\varepsilon}(1 - \varphi^n, \psi^\varphi - \varphi^n) + \varepsilon(\nabla \varphi^n, \nabla(\psi^\varphi - \varphi^n)) \right). \end{aligned}$$

[1] Permission from Elsevier to reprint [93] is gratefully acknowledged.

We restrict ourselves to a one dimensional fracture C on a two dimensional domain $\Omega = (-10, 10)^2$ as depicted in Figure 5.1 on the left. The fracture is centered horizontally within Ω and has a constant half crack length $l_0 = 0.25$ and varying width. Precisely, the crack width corresponds to $2h$, where h is the minimal element diameter of the mesh. The mesh is pre-refined geometrically in the crack zone, as depicted exemplarily for one adaptive refinement step in Figure 5.1 on the right, where the crack zone is resolved with the smallest mesh size. The driving force is given by a constant pressure $\rho = 10^{-3}$ Pa in the inner crack. The parameter setting is given in Table 5.1.

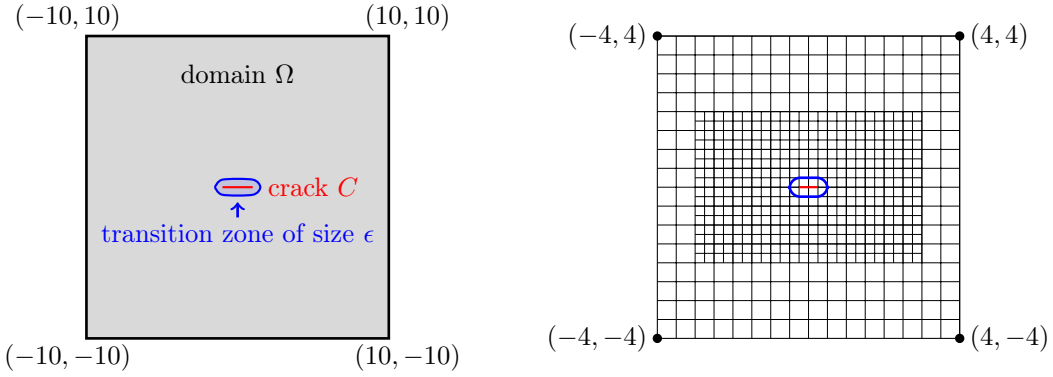

Figure 5.1: Left: geometry of the two dimensional Sneddon test. Right: zoom-in to the pre-refined crack zone in $[-4, 4] \times [-4, 4]$ with two global refinement steps and one local refinement step (geometrically pre-refined). Reprinted from [93] with permission of Elsevier.

The spatial discretization parameter, i.e. the minimal element diameter, is set as

$$h = 0.022,\ 0.011,\ 0.0055,\ 0.0027,\ 0.0013.$$

The quantity of interest, called total crack volume (TCV), can be computed numerically via

$$\mathrm{TCV} = \int_\Omega u(x, y) \nabla \varphi(x, y)\, d(x, y).$$

The analytical solution [149] is given by

$$\mathrm{TCV}_{\mathrm{ref}} = \frac{2\pi\rho l_0^2}{E'}.$$

The Figures 5.2 - 5.5 visualize the average active-set iterations required per time-step for **Case 1**-**Case 4** and $h = 0.022, 0.011, 0.0055, 0.0027$. We observe, that with a smaller h, the number of iterations can become comparatively large in **Case 1** in comparison to the other cases. We also ran a test with a minimal element diameter $h = 0.0013$ which leads to around 40 million degrees of freedom. There, the Newton active set method did not achieve convergence within 500 Newton active set iterations with **Case 1** in the 2nd incremental step. In contrast, with the modified constant c from **Case 2**, the Newton method terminates within 46, 26, 18, 7 and 4 iterations to converge at each incremental step. With **Case 3** $10-11$ Newton active set iterations are needed in each timestep on each refinement level. With **Case 4** only 1 iteration is needed. The latter shows that the Newton method only needs 1 iteration to converge, which underlines the assumption that

Parameter	Definition	Value
Ω	Domain	$(-10, 10)^2$
h	Diagonal element diameter	test-dependent
l_0	Half crack length	0.25
G_C	Material toughness	1.0
E	Young's modulus	1.0
μ	Lamé parameter	0.42
λ	Lamé parameter	0.28
ν	Poisson's ratio	0.2
p	Applied pressure	10^{-3}
ε	Bandwidth of the initial crack	$2h$
κ	Regularization parameter	10^{-10}
	Number of global refinements	2
	Number of local refinements	5, 6, 7, 8, 9
TOL_N	Tolerance outer Newton solver	10^{-7}
	Tolerance inner linear solver	$\|\tilde{R}(U_h^{n,k})\|_2 10^{-8}$

Table 5.1: The setting of the material and numerical parameters for the Sneddon 2d test. Reprinted from [93] with permission of Elsevier.

the active set stopping criterion is indeed the reason for the slow convergence in **Case 1**. The speed-up coming along with **Case 3**, **Case 4** and especially **Case 2** has a noticeable impact in the computation time, which is summarized for all settings in Table 5.2. The speed-up of **Case 3** and **Case 4** must be treated with caution since we do not iterate until full convergence of the active set in these cases, which may lead to reduced accuracy.

	Total wallclock time | Sneddon 2d				
Case	$h = 0.022$ | 4 cores	$h = 0.011$ | 4 cores	$h = 0.0055$ | 16 cores	$h = 0.0027$ | 32 cores	$h = 0.0013$ | 64 cores
Case 1	587.983s	2243.164s	2275.481s	11682.962s	–
Case 2	161.765s	976.391s	784.019s	2590.394s	6562.554s
Case 3	117.775s	458.664s	572.438s	1228.499s	4132.350s
Case 4	22.833s	77.788s	87.405s	208.310s	940.686s

Table 5.2: Total wallclock time of the Sneddon 2d test for different refinement levels on different numbers of cores. Reprinted from [93] with permission of Elsevier.

As it can be observed in Table 5.3, the error in the TCV is not affected, even though we completely ignore the active set stopping criterion (**Case 4**). But in this case, we may obtain a non-smooth phase-field solution. This phenomenon is depicted in Figure 5.6. The slight increase of the TCV error for $h < 0.0055$ can be attributed to the fact that the analytical solution is based on an infinite domain. Thus, the solution does not converge to the exact solution for $h \to 0$ since the domain-error due to the finite domain will become dominant if h is small enough, which is the case for $h < 0.0055$, as we assume. This phenomenon was further investigated in [75].

Lastly, a brief parallel study is conducted. The framework is parallelized with MPI. Since it is based on the `pfm-cracks` code [76], extensive scalability analyses can be found in [75]. We compare the CPU time for one representative incremental step for $h = 0.022$ (168 609 degrees of

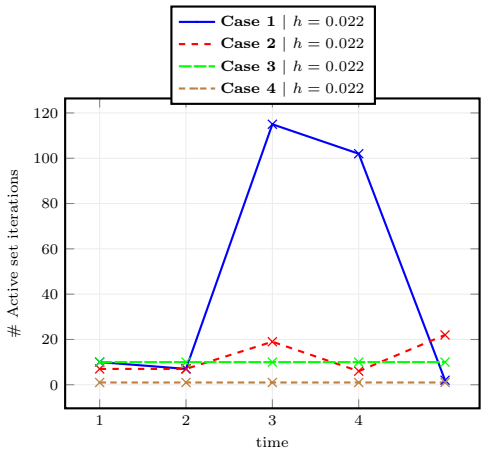

Figure 5.2: Number of active set iterations for **Case 1**-**Case 4** and $h = 0.022$ in the Sneddon 2d test. Reprinted from [93] with permission of Elsevier.

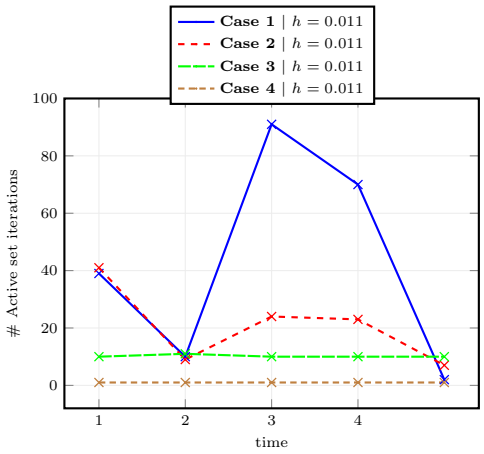

Figure 5.3: Number of active set iterations for **Case 1** to **Case 4** and $h = 0.011$ in the Sneddon 2d test. Reprinted from [93] with permission of Elsevier.

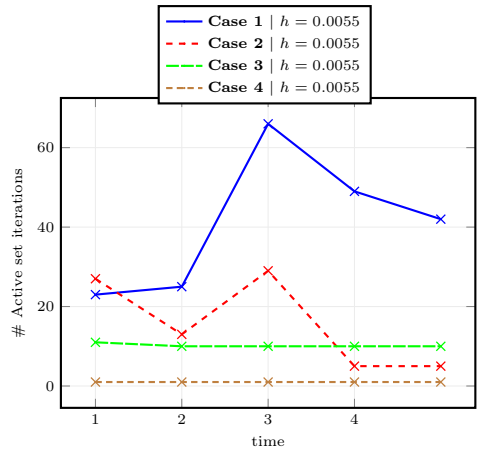

Figure 5.4: Number of active set iterations for **Case 1**-**Case 4** and $h = 0.0055$ in the Sneddon 2d test. Reprinted from [93] with permission of Elsevier.

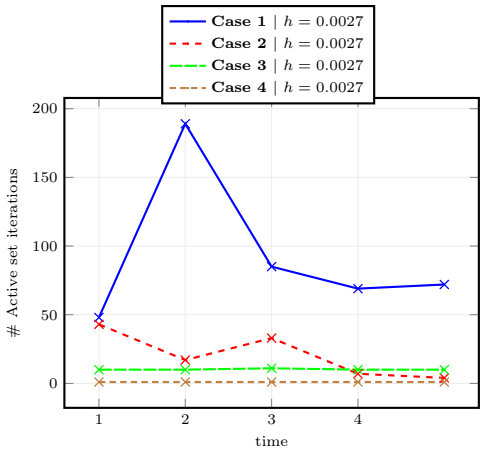

Figure 5.5: Number of active set iterations for **Case 1**-**Case 4** and $h = 0.0027$ in the Sneddon 2d test. Reprinted from [93] with permission of Elsevier.

	TCV error | Sneddon 2d				
Case	$h = 0.022$	$h = 0.011$	$h = 0.0055$	$h = 0.0027$	$h = 0.0013$
Case 1	0.000173649	3.72255e-05	3.03573e-05	6.45367e-05	–
Case 2	0.000173649	3.72255e-05	3.03573e-05	6.45367e-05	8.19169e-05
Case 3	0.000173649	3.72255e-05	3.03573e-05	6.45367e-05	8.19169e-05
Case 4	0.000173649	5.33208e-05	3.03573e-05	6.14307e-05	8.19169e-05

Table 5.3: Error in the TCV for different mesh size parameters and **Case 1** - Case 4. Reprinted from [93] with permission of Elsevier.

Figure 5.6: Visualization of the nonsmooth phase-field solution of the two dimensional Sneddon test with $h = 0.011$ and **Case 4**. Red represents the fully intact part of the domain, blue the fully broken part and white stands for the transition zone. Reprinted from [93] with permission of Elsevier.

freedom) computed on 1 core and 16 cores. On 1 core, the CPU time of one incremental step is 2386s (approx. 18h) and on 16 cores, the CPU time is 142s.

5.2 Space-time phase-field fracture optimal control

In this second numerical experiment[2] we employ a tracking type cost functional (4.4) and solve it by the formulations and algorithms laid out in Chapter 4. to compute an optimal control that approximately generates a desired phase-field. The open source software libraries `deal.II` [12, 13] and DOpElib [50] are used for the numerical calculations in this section.

Since a major part of the published work deals with forward phase-field fracture, where the cracks propagate through large areas of the domain and even reach the domain boundaries, we emphasize that short fractures are specifically considered in our optimal control settings. Especially the desired crack pattern φ_d is set to be small enough such that we can clearly distinguish between our optimal control final fractures and non-controlled fractures.

In this experiment we want to find an optimal control which connects some (but not all) initial notches in a given domain. Herein we consider the rectangle $\Omega = (0, 2.2) \times (0, 0.4)$ with four initial horizontal notches $\mathcal{N}_1 := (0.3, 0.5) \times \{0.2\}$, $\mathcal{N}_2 := (0.7, 0.9) \times \{0.2\}$, $\mathcal{N}_3 := (1.3, 1.5) \times \{0.2\}$, $\mathcal{N}_4 := (1.7, 1.9) \times \{0.2\}$, see Fig. 5.7. By combining these notches $\mathcal{N} := \bigcup_{i=1}^{4} \mathcal{N}_i$ we define the initial phase-field as

$$\varphi_0(x, y) := \begin{cases} 0, & (x, y) \in \mathcal{N}, \\ 1, & \text{else.} \end{cases}$$

[2]Reprinting text, figures, and tables from [87] is gratefully acknowledged and with permission from Elsevier.

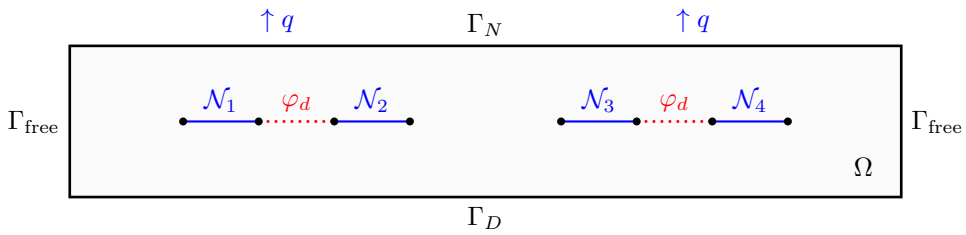

Figure 5.7: Domain $\Omega = (0, 2.2) \times (0, 0.4)$ with boundary partition $\partial\Omega = \Gamma_D \cup \Gamma_N \cup \Gamma_{free}$, four initial notches $\mathcal{N}_1, \ldots, \mathcal{N}_4$, and the desired phase-field φ_d. Reprinted from [87], with permission from Elsevier.

Table 5.4: Regularization and penalty parameters (left), model and material parameters (right).

Par.	Definition	Value
ε	Regul. (crack) $\approx 4h$	0.035
κ	Regul. (crack)	1.0e−10
η	Regul. (viscosity)	1.0e3
γ	Penalty	1.0e5
α	Tikhonov	2.1e−10

Par.	Definition	Value
G_c	Fracture toughness	1.0
ν_s	Poisson's ratio	0.2
E	Young's modulus	1.00e6
q_0	Initial control	1.0
q_d	Nominal control	6.53e3

The desired phase-field φ_d is defined as the connection of $\mathcal{N}_1$ with $\mathcal{N}_2$ and $\mathcal{N}_3$ with $\mathcal{N}_4$, thus we write

$$\varphi_d(x, y) := \begin{cases} 0, & x \in (0.5, 0.7) \cup (1.5, 1.7) \text{ and } y \in (0.2 - 4h, 0.2 + 4h), \\ 1, & \text{else.} \end{cases}$$

We partition the boundary $\partial\Omega$ as shown in Fig. 5.7, and the spatial mesh consists of 352×64 square elements with diameter $h = \sqrt{2} \times 0.4/64 \approx 0.00884$. We discretize the time interval $[0, 1]$ into 2001 equidistant time points, i.e., $T = 1$ and $M = 2000$. Table 5.4 contains all relevant parameters for this experiment.

For a tolerance 2.0e−9 the results are shown in Table 5.5. The final optimal phase-field in Fig. 5.8 (bottom) shows that the desired phase-field has been reached, because $\mathcal{N}_1$ is connected to $\mathcal{N}_2$ and $\mathcal{N}_3$ is connected to $\mathcal{N}_4$. The corresponding optimal control force shown in Fig. 5.11 has two maxima right between the notches that should be connected. This behaviour can be expected from a mechanical standpoint. The decreasing control at the end points can explain the four cracks propagating from both ends of each pair of connected notches. Due to the decreasing control we get a different principal axis of tension which leads to a non-horizontal crack growth.

Table 5.5: Experiment 3: number of CG iterations, residuals, cost terms and maximal force during NLP iteration.

Iter	CG	Relative residual	Absolute residual	Cost	Tracking	Tikhonov	Force
0	–	1.0	2.00e−6	2.3850e−2	1.4302e−2	9.5483e−3	100.00
1	2	0.110	2.20e−7	1.2839e−2	1.2839e−2	3.4223e−8	6550.69
2	2	3.13e−2	6.27e−8	1.2428e−2	1.2309e−2	1.1897e−4	7899.32
3	2	1.22e−2	2.44e−8	1.2330e−2	1.2139e−2	1.9136e−4	8264.47
4	2	9.34e−3	1.87e−8	1.2292e−2	1.2066e−2	2.2519e−4	8403.51
5	2	1.44e−3	2.89e−9	1.2263e−2	1.2011e−2	2.5205e−4	8501.55
6	2	9.20e−4	1.84e−9	1.2261e−2	1.2006e−2	2.5478e−4	8514.26

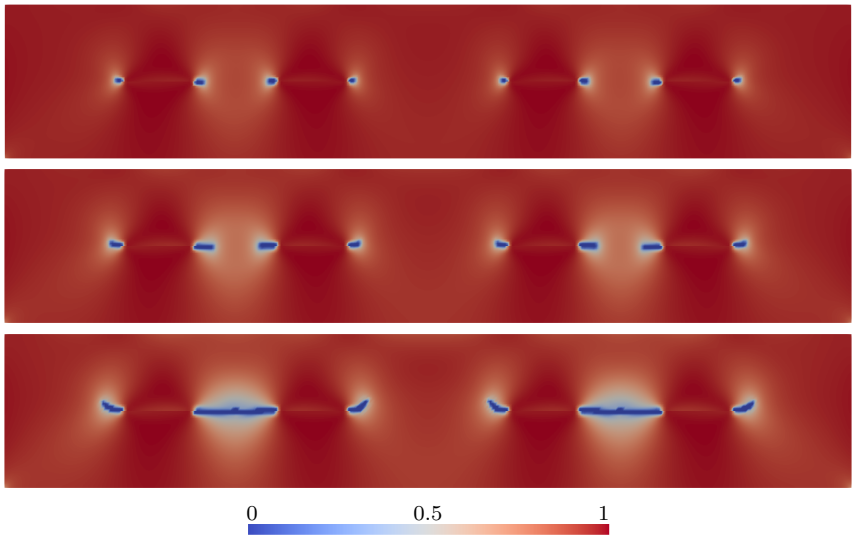

Figure 5.8: Optimal phase-field φ at times 1400, 1800, and 2000. Reprinted from [87], with permission from Elsevier.

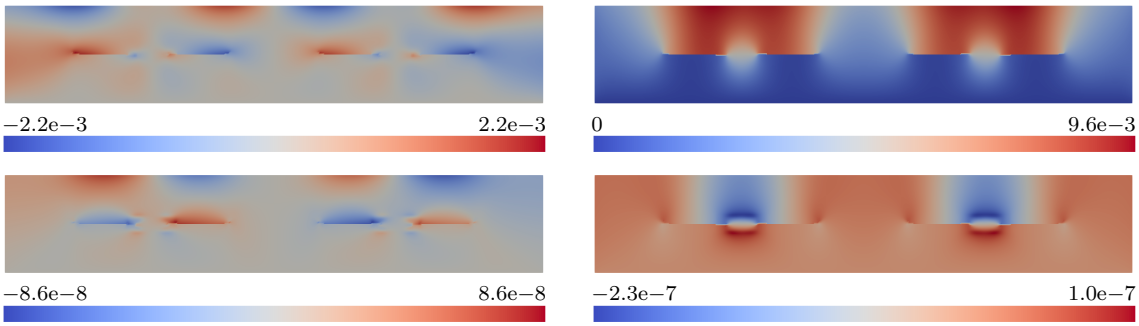

Figure 5.9: Optimal displacement field u (top: x left, y right) and adjoint field z_u (bottom: x left, y right) at time 1800. Reprinted from [87], with permission from Elsevier.

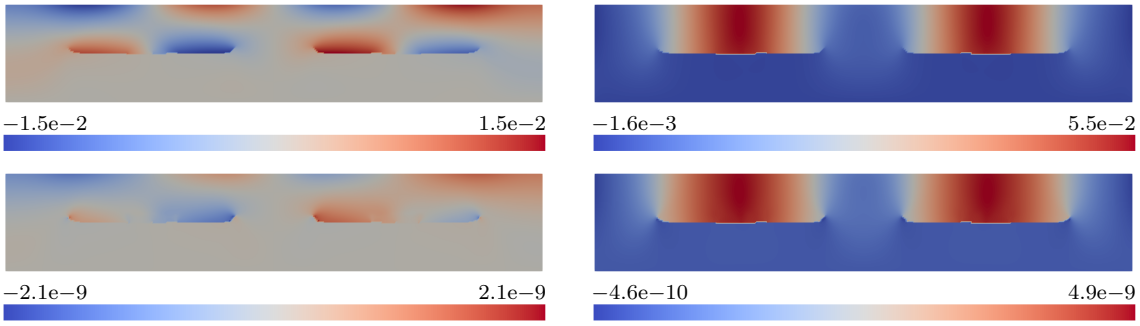

Figure 5.10: Optimal displacement field u (top: x left, y right) and adjoint field z_u (bottom: x left, y right) at time 2000. Reprinted from [87], with permission from Elsevier.

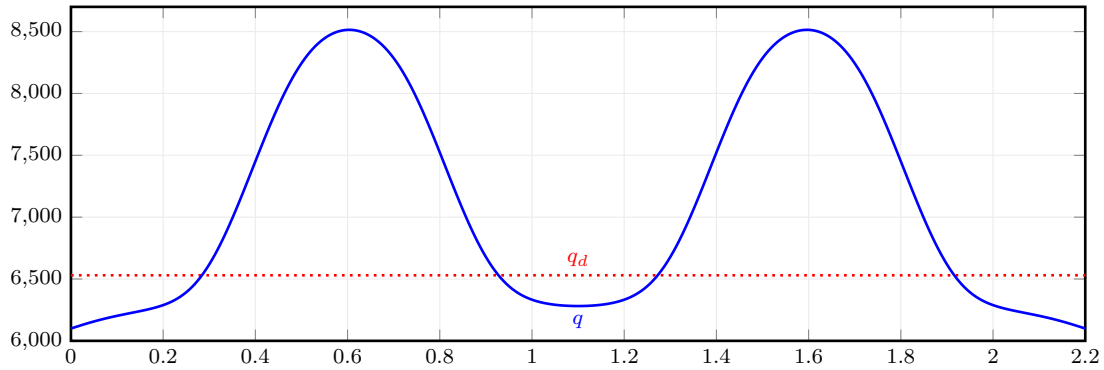

Figure 5.11: Optimal control force (solid) and nominal control force (dotted) on upper boundary Γ_N. Reprinted from [87], with permission from Elsevier.

The optimal displacement fields at the end time are shown in Fig. 5.10 (top). Both displacement fields reach their maxima, similar to the control force, right at the two sections between the notches $\mathcal{N}_1 - \mathcal{N}_2$ and $\mathcal{N}_3 - \mathcal{N}_4$. In Fig. 5.9 we present the displacement fields before the cracks join at time step 1800.

5.3 Phase-field fracture simulations on the CARPIUC benchmark

One important goal[3] is to use numerical simulations to predict the behavior of components within developments of new materials or work tools. [4] We can validate the quality and accuracy of those simulations by a direct comparison with experimental data.

The CARPIUC benchmark [37] is a series of experiments that is specifically designed for the validation of numerical models of mixed mode crack propagation in quasi-brittle materials and is therefore perfectly suited to verify the several capabilities of phase-field fracture models. In this campaign, square specimens made of mortar are fixed inside of a 6-axis testing machine, also called "Hexapod". While the bottom boundary of the sample is kept steady, a varying combination of vertical and horizontal translation, as well as in-plane rotation was applied. During the whole test several thousand images were acquired, such that the measuring technique "digital image correlation" (DIC) [153] allowed for the assessment of the displacement fields of the specimens for the duration of the test.

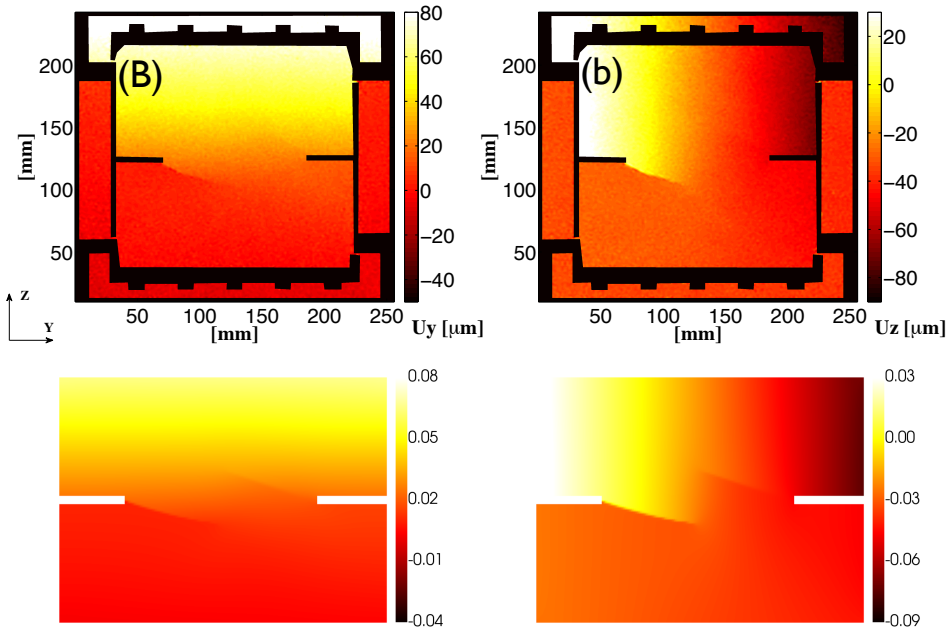

Figure 5.12: The measured displacement field of the IT2 test in [µm](top: y left, z right), reprinted from [114] according to the Creative Commons Attribution 4.0 International Public License, and the simulated displacement field of a sub-region of the sample in [mm](bottom: y left, z right).

[3]Continuing discussions and ongoing work with Amélie Fau and Francois Hild (ENS Université Paris-Saclay, France) is gratefully acknowledged.

[4]This setting was newly implemented in `pfm-cracks` and the phase-field results shown in this section are not published elsewhere.

5.3.1 Computation 1: two notches

In the following we take the measured displacement of the top and bottom face of the sample, acquired from [114], as the boundary conditions of our simulation, which were performed with `pfm-cracks`. The direct comparison of the displacement field of the simulation and the displacement field acquired from DIC is in Figure 5.12.

From the measured displacement field we can see two cracks propagating, one from the left nodge to the bottom right corner and another from the right nodge to the top left corner. Not only does the displacement field of the simulation match very well the measured one, but also matches the phase-field solution the observed crack pattern; see Figure 5.13. Even though the boundary conditions are not smooth and change continuously, the number of nonlinear iterations are relatively low and comparable to synthetic tests, as for example the single edge nodge shear test [168].

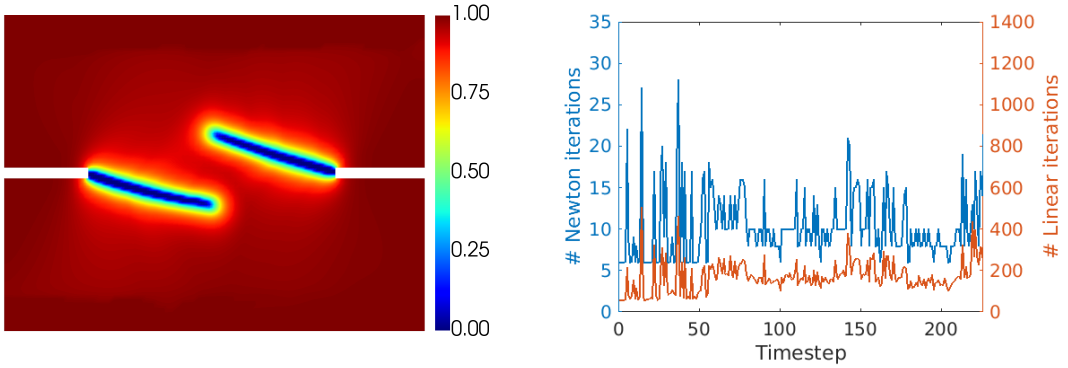

Figure 5.13: Solution of the phase-field variable for the IT2 test (left) and a comparison of the number of Newton iterations per time step with the number of iterations of the linear solver (right).

5.3.2 Computation 2: right side notch

In another setup the experiment was controlled such that a crack is propagating from the right to the left in form of a sinus curve up to the point, where the crack started to bifurcate; see Figure 5.14.

While the displacement fields around the bifurcation are very similar, it seems that the simulation did not properly capture the initialization of the crack. Moreover, from the phase-field solution, Figure 5.15, we can see, that it is quite thick at the area of the nodge. But solutions of previous time steps show, that the crack was captured well in the beginning, but was smeared when the bifurcation started. This behaviour is presented in more detail in [175]. In comparison to the two notch test, the computational cost increased. Not only are almost always more than 16 Newton iterations needed until convergence, but also does the number of iterations of the linear solver increase significantly up to about 1400 iterations. This increase of linear iterations is related to the moment before the crack started to bifurcate.

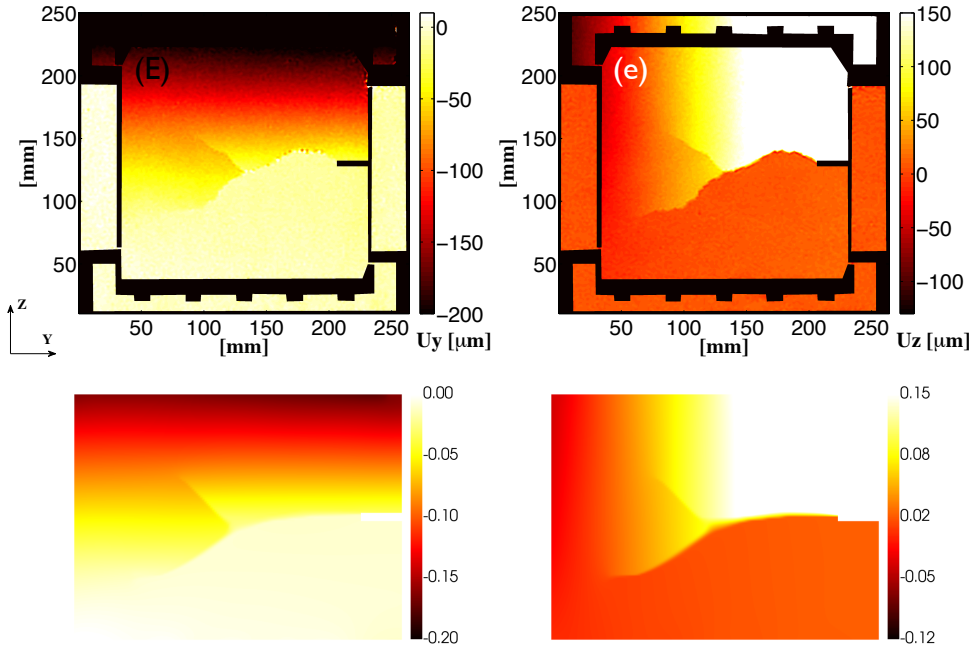

Figure 5.14: The measured displacement field of the IT3 test in [µm](top: y left, z right), reprinted from [114] according to the Creative Commons Attribution 4.0 International Public License, and the simulated displacement field of a sub-region of the sample in [mm](bottom: y left, z right).

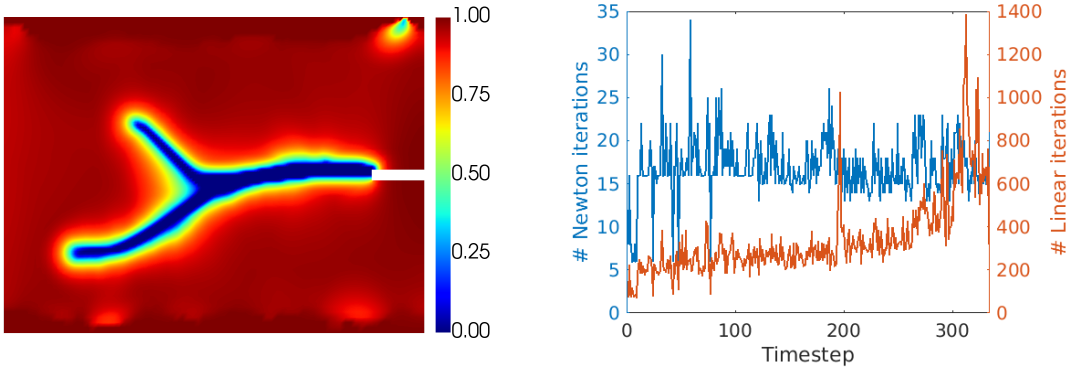

Figure 5.15: Solution of the phase-field variable for the IT3 test (left) and a comparison of the number of Newton iterations per time step with the number of iterations of the linear solver (right).

5.4 A predictor-corrector non-intrusive global-local approach

Often, the interest of numerical simulations is in some domain as we have seen previously, but the 'dynamics' play a role in a smaller subdomain.[5] However, due to the influence of boundary conditions or changing dynamics, the 'dynamics' may evolve.

Previously, we already introduced predictor-corrector adaptivity (Section 3.4), where the focus was on an accurate representation on the crack path and small regularization parameters ε. In this section, we extend this concept to situations that the entire physics can change, such that the full-physics problem is considered in some smaller subdomain. This situation is addressed with a non-intrusive global-local approach [62]. This approach was extended to phase-field fracture in [64]. The global (macroscale) problem is linearized elasticity without phase-field and the local (microscale) problem is elasticity with stress-splitting (of the solid stress tensor; e.g., [121, 11, 152]) and phase-field. The coupling between both domains is based on a non-overlapping domain decomposition approach (see [154]) and Lagrange multipliers on the interface. An important role plays 'non-intrusiveness', which means that existing codes shall not be changed and only the coupling on the interface must be realized. This procedure shall also allow for easier coupling of different software codes.

In phase-field fracture the crack however grows and the crack path is a priori unknown, which leads to the problem that the global and local domains may change during the simulation time. One approach is a predictor-corrector technique in which the new crack path is first predicted and in a second calculation the actual solution is computed (corrected). This was first developed for adaptive mesh refinement in [74]. In [131] this idea was extended to an adaptive predictor-corrector scheme for a non-intrusive global-local approach. Therein, local fine-scale problems are chosen dynamically depending on the fracture path.

Problem 19 (Macro-scale/global problem)**.** *Find $u \in V_u^D$ such that*

$$A_M(u)(w) = l(w) \quad \forall w \in V_u^0,$$

with $A_M(u)(w) := (\sigma(u), \nabla w)$ and $l(w) := (f, w)$ and for instance the linearized stress tensor $\sigma(u) = 2\mu e(u) + \lambda tr(e)I$. We notice that no phase-field solution φ is sought.

On the microscale, the full phase-field model with nonlinear constitutive models is considered, i.e., Proposition 14. Here, we have the CVIS

Problem 20 (Micro-scale/local problem)**.** *Find $U = (u, \varphi) \in V_u \times V_\varphi$ such that*

$$A_m(U)(\Psi - \Phi) \geq 0 \quad \Phi \in V_u \times V_\varphi.$$

A challenge is linked to propagating fractures such that the crack may grow out of the fine-scale problem. Consequently, the local and global subdomains are time-dependent and change during a simulation. This is challenging in terms of an algorithmic realization and implementation because the interface conditions between the local and global subdomains must be updated during time. A flexible choice is provided by using Lagrange multipliers. For details, we refer the reader to [64].

[5] This section is largely taken from [169] for the mathematical descriptions. The numerical results are taken from [131] with permission from Elsevier.

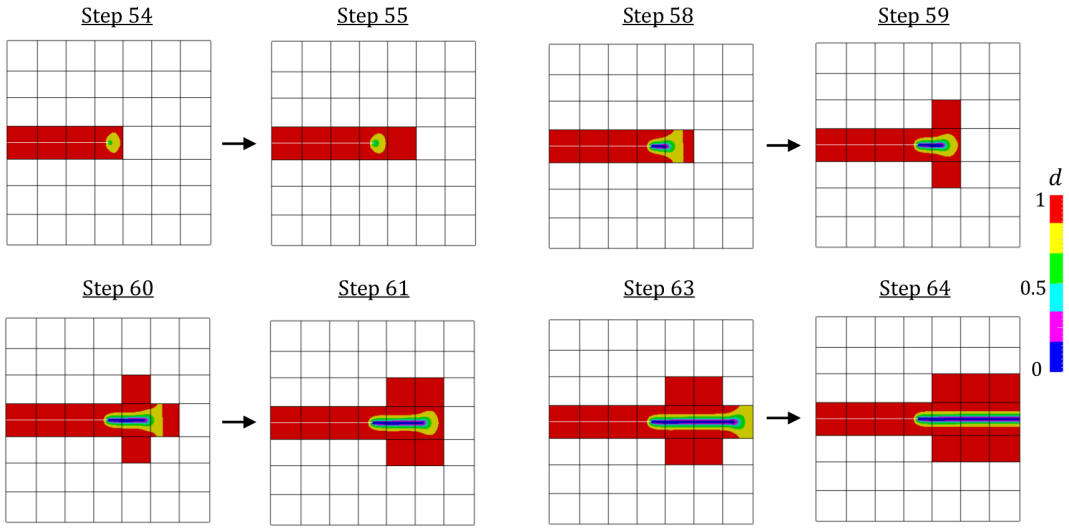

Figure 5.16: Illustration of the predictor-corrector adaptive global-local approach for eight different time points. Reprinted from [131] with permission from Elsevier.

The question remains how to determine the local and global subdomains for growing fractures. Here, we base ourselves on the previous predictor-corrector suggested in [74]. The mode of operation for the global-local approach is illustrated in Figure 5.16. The basic adaptive global-local algorithm is provided in the following and worked out in [131]. The numerical analysis is open and not yet addressed.

From [131][Section 4], we extract the key algorithm and re-write the main steps in the notation used in these lecture notes.

Algorithm 3 (Adaptive global-local scheme)**.** *The adaptive global-local scheme consists of the following steps:*

1. *Solve the coupled global-local problem at time t_n:*

$$\begin{aligned} \text{Find } \tilde{u} \in V_u: \quad & A_M(\tilde{u})(w) = 0 \quad w \in V_u \\ \text{Find } \tilde{U} \in V_u \times V_\varphi: \quad & A_m(\tilde{U})(\Psi) = 0 \quad \Psi \in V_u \times V_\varphi. \end{aligned}$$

2. *Predictor step:*
   - *If $\tilde{\varphi} < \eta_C$ at an internal edge ∂K of an global element K_M and a local element K_m of the current decomposition $\mathcal{T}_n$, then $K_M \to K_m$ to obtain a new global-local decomposition $\mathcal{T}_{n+1}$*
   - *Else increment time $n \to n+1$ and go to Step 1.*
3. *Interpolate global solution u onto the newly assigned local mesh element K_m. We notice that u is now known on the new local element K_m, but φ is not.*
4. *Corrector step: Solve on the new global-local decomposition $\mathcal{T}_{n+1}$:*

$$\begin{aligned} \text{Find } u_{n+1} \in V_u: \quad & A_M(u_{n+1})(w) = 0 \quad w \in V_u, \\ \text{Find } U_{n+1} \in V_u \times V_\varphi: \quad & A_m(U_{n+1})(\Psi) = 0 \quad \Psi \in V_u \times V_\varphi. \end{aligned}$$

5. *Increment time* $n \to n+1$ *and go to Step 1.*

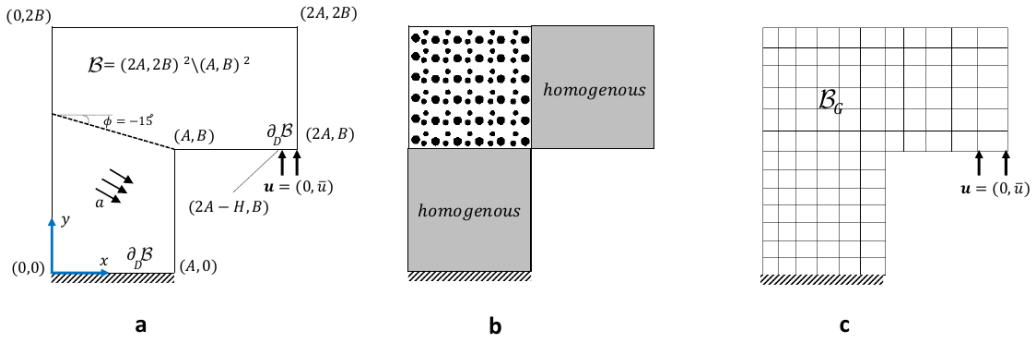

Figure 5.17: Heterogeneous L-shaped panel test. (a) Geometry and loading setup with a structural director a inclined under an angle $\phi = -15$ (b) partitioning of domain into the heterogeneity and homogeneity counterparts and (c) global finite element mesh without potential fictitious zones. Reprinted from [131] with permission from Elsevier.

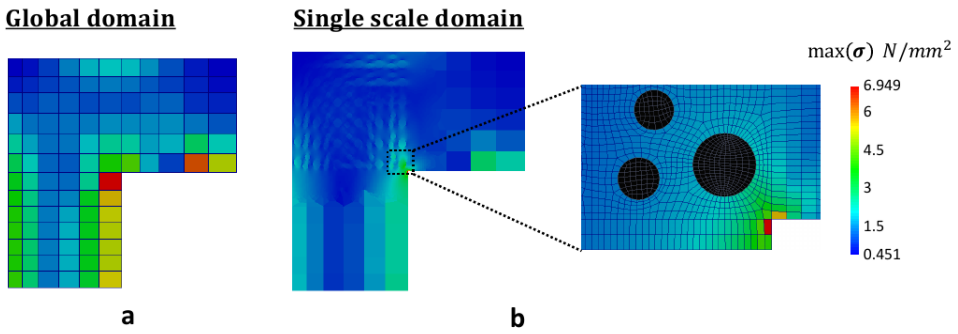

Figure 5.18: Maximum stress state in the heterogeneous L-shaped panel test. (a) Global stress state and (b) single scale stress state. Reprinted from [131] with permission from Elsevier.

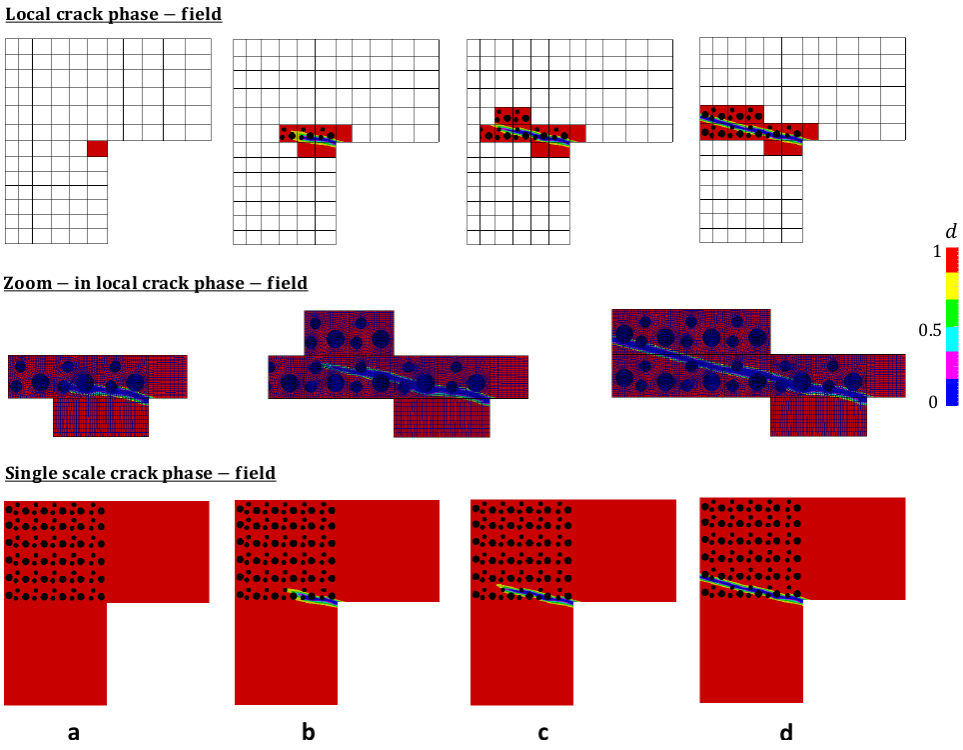

Figure 5.19: Crack phase-field pattern for the transversely isotropic heterogeneous L-shaped panel test with fiber direction angle of $\phi = -15°$. First row: local crack phase-field based on the adaptive scheme; Second row: mesh evolution for local domain by considering the influence of inclusions; Third row: resulting single scale phase-field solution at (a) $\bar{u} = 0.15\ mm$, (b) $\bar{u} = 0.324\ mm$, (c) $\bar{u} = 0.333\ mm$ and (d) $\bar{u} = 0.58\ mm$. Reprinted from [131] with permission from Elsevier.

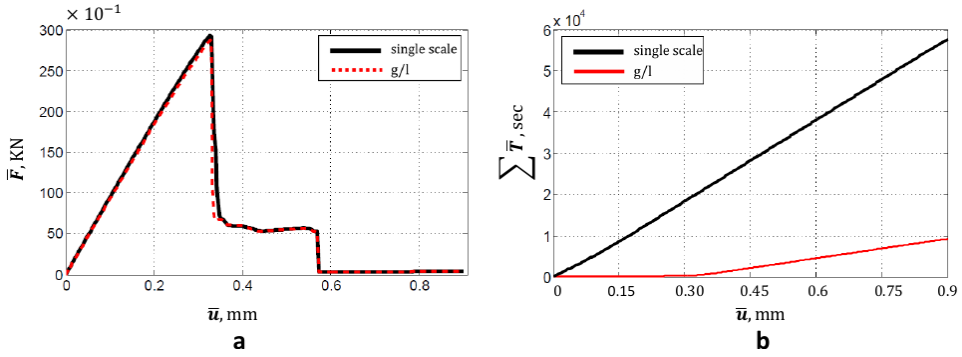

Figure 5.20: Heterogeneous L-shaped panel test. (a) Comparison of the load-displacement curves and (b) accumulated time-displacement curves. Reprinted from [131] with permission from Elsevier.

5.5 Ongoing developments

Ongoing and future developments in our group and collaborations include:

- Realization an implementation of the space-time phase-field fracture complementarity system [86];
- A fully robust-efficient monolithic solution (in our opinion [166, 168, 63] can be further improved; see also more recent developments [97, 96]);
- Extending matrix-free multigrid [84] to adaptive finite elements and using it as module in multiphysics phase-field fracture such as IPACS [163];
- Parameter identification in phase-field fracture with digital image correlation (collaboration between V. Kosin, A. Fau, C. Jailin, F. Hild, Wick; within the IRTG 2657 Leibniz University Hannover and Université Paris-Saclay) [98];
- Extending the multiphysics phase-field fracture in-house code IPACS [163] to THMC (thermo-hydro-mechanical-chemical) phase-field fracture;
- High-accuracy frameworks by transfer from interface-capturing phase-field fracture as crack predictor, via mesh reconstruction, to sharp interface (interface-tracking) representations, where additionally accurate physics can be described in sufficiently refined crack meshes [160].

5.6 Open-access materials and research software engineering

Based on the open-source finite element library deal.II [13, 14, 16], three projects are currently maintained and further developed:

- `pfm-cracks` [76];
- Phase-field fracture in DOpElib (Denis) [67];
- IPACS [163] (some moduls open-source; other in-house).

Chapter 6

Wrap-up: Quiz

In this final chapter, we consolidate what we learned through some questions:

1. Formulate a simplified phase-field fracture problem (Laplacian, scalar-valued).
2. Given the simplified strong form, derive a weak formulation.
3. How is the energy formulation given?
4. Provide a brief idea of Griffth's model.
5. What was the achievement of Francfort and Marigo in 1998?
6. Describe in words the idea of phase-field fracture.
7. Describe in your own words the meaning and purpose of the phase-field variable.
8. What is the length scale parameter?
9. List some properties and purpose of the length scale parameter.
10. Please give some own examples in which damage or fracture arise in nature, research or daily life.
11. What are challenges (or drawbacks) in using a phase-field method for fracture propagation? Please give one or two examples.
12. Interprete the crack irreversibility constraint physically and give a relationship to the obstacle problem.
13. Explain one method to treat the crack irreversibility constraint numerically.
14. What are typical difficulties when using (simple) penalization for regularizing an inequality constraints?
15. What is the role of the penalization constant?
16. What are the active and non-active sets in the obstacle problem?
17. Describe the phase-field fracture complementarity system.

18. What is a primal-dual active set formulation?
19. What is the role of the active set constant?
20. What is the difference between quasi-static and dynamic fracture modeling?
21. What are Euler-Lagrange equations?
22. What is a 'stationary' point?
23. Given a PDE on the continuous level, what are the key steps in the numerical solution process?
24. What are solution algorithms to solve a coupled problem?
25. How can we decouple the displacement/phase-field problem? What do we observe?
26. What are solution algorithms to solve nonlinear problems?
27. Formulate a fixed-point (staggered) iteration.
28. What are the possibilities to improve the efficiency of the numerical solution?
29. List the type of nonlinearities arising in phase-field fracture.
30. Characterize the phase-field fracture problem in terms of the mathematical classifications (type of coupling, nonlinearities, classical PDE or CVIS).
31. Formulate Newton's method for solving the phase-field fracture problem.
32. Using a monolithic formulation for phase-field fracture, why do classical Newton methods have difficulties?
33. Take a monolithic formulation and do a mathematical manipulation in order to linearize the equations.
34. Give a simplified numerical analysis (key ideas) about the relationship between h and ε.
35. Why space-time modeling?
36. Formulate space-time phase-field fracture.
37. Which part(s) of the spatial discretization is(/are) tricky in phase-field fracture?
38. What is optimal control?
39. Give an example of phase-field fracture optimal control.
40. What is a cost functional?
41. Give examples of other cost functionals, which are different than presented.
42. Describe the solution process of the reduced optimization approach.
43. Describe the physics of the adjoint.

44. What is predictor-corrector mesh adaptivity?
45. What is the non-intrusive global-local approach?
46. What is predictor-corrector non-intrusive global-local?
47. Describe the differences between predictor-corrector mesh adaptivity and the predictor-corrector global-local approach.
48. What is the challenge in the CARPIUC benchmark?
49. What is Sneddon's benchmark?
50. Formulate the road map from a strong form (or weak form) phase-field fracture setting up to output functionals. What steps need to be done?

Bibliography

[1] R. A. Adams. *Sobolev Spaces*. Academic Press, 1975.

[2] F. Aldakheel, N. Noii, T. Wick, O. Allix, and P. Wriggers. Multilevel global-local techniques for adaptive ductile phase-field fracture. *Computer Methods in Applied Mechanics and Engineering*, 387:114175, 2021.

[3] F. Aldakheel, N. Noii, T. Wick, and P. Wriggers. A global-local approach for hydraulic phase-field fracture in poroelastic media. *Computers & Mathematics with Applications*, 91:99–121, 2021. Robust and Reliable Finite Element Methods in Poromechanics.

[4] R. Alessi, J.-J. Marigo, C. Maurini, and S. Vidoli. Coupling damage and plasticity for a phase-field regularisation of brittle, cohesive and ductile fracture: One-dimensional examples. *International Journal of Mechanical Sciences*, 2017.

[5] M. Ambati, T. Gerasimov, and L. De Lorenzis. Phase-field modeling of ductile fracture. *Computational Mechanics*, 55(5):1017–1040, 2015.

[6] M. Ambati, T. Gerasimov, and L. De Lorenzis. A review on phase-field models of brittle fracture and a new fast hybrid formulation. *Computational Mechanics*, 55(2):383–405, 2015.

[7] L. Ambrosio and N. Dancer. *Calculus of Variations and Partial Differential Equations*. Springer, 2000.

[8] L. Ambrosio and V. Tortorelli. Approximation of functionals depending on jumps by elliptic functionals via γ-convergence. *Comm. Pure Appl. Math.*, 43:999–1036, 1990.

[9] L. Ambrosio and V. Tortorelli. On the approximation of free discontinuity problems. *Boll. Un. Mat. Ital. B*, 6:105–123, 1992.

[10] L. Ambrosio and E. Virga. A boundary value problem for nematic liquid crystals with variable degree of orientation. *Arch. Rational Mech. Anal.*, 114:335–347, 1991.

[11] H. Amor, J.-J. Marigo, and C. Maurini. Regularized formulation of the variational brittle fracture with unilateral contact: Numerical experiments. *J. Mech. Phys. Solids*, 57:1209–1229, 2009.

[12] D. Arndt, W. Bangerth, T. C. Clevenger, D. Davydov, M. Fehling, D. Garcia-Sanchez, G. Harper, T. Heister, L. Heltai, M. Kronbichler, R. M. Kynch, M. Maier, J.-P. Pelteret, B. Turcksin, and D. Wells. The `deal.II` library, version 9.1. *Journal of Numerical Mathematics*, 27:203–213, 2019.

[13] D. Arndt, W. Bangerth, D. Davydov, T. Heister, L. Heltai, M. Kronbichler, M. Maier, J.-P. Pelteret, B. Turcksin, and D. Wells. The deal.ii finite element library: Design, features, and insights. *Computers & Mathematics with Applications*, 2020.

[14] D. Arndt, W. Bangerth, M. Feder, M. Fehling, R. Gassmöller, T. Heister, L. Heltai, M. Kronbichler, M. Maier, P. Munch, J.-P. Pelteret, S. Sticko, B. Turcksin, and D. Wells. The `deal.II` library, version 9.4. *Journal of Numerical Mathematics*, 30(3):231–246, 2022.

[15] I. Babuska and U. Banerjee. Stable generalized finite element method (sgfem). *Computer Methods in Applied Mechanics and Engineering*, 201-204(0):91 – 111, 2012.

[16] W. Bangerth, R. Hartmann, and G. Kanschat. deal.II – a general purpose object oriented finite element library. *ACM Trans. Math. Softw.*, 33(4):24/1–24/27, 2007.

[17] S. Basava, K. Mang, M. Walloth, T. Wick, and W. Wollner. *Adaptive and Pressure-Robust Discretization of Incompressible Pressure-Driven Phase-Field Fracture*, pages 191–215. Springer International Publishing, Cham, 2022.

[18] R. Becker, D. Meidner, and B. Vexler. Efficient numerical solution of parabolic optimization problems by finite element methods. *Optim. Methods Softw.*, 22(5):813–833, 2007.

[19] M. Bergounioux, M. Haddou, M. Hintermüller, and K. Kunisch. A comparison of a Moreau-Yosida-based active set strategy and interior point methods for constrained optimal control problems. *SIAM J. Optim.*, 11(2):495–521, 2000.

[20] M. Bergounioux, K. Ito, and K. Kunisch. Primal-dual strategy for constrained optimal control problems. *SIAM J. Control Optim.*, 37(4):1176–1194, 1999.

[21] M. J. Borden, C. V. Verhoosel, M. A. Scott, T. J. R. Hughes, and C. M. Landis. A phase-field description of dynamic brittle fracture. *Comput. Meth. Appl. Mech. Engrg.*, 217:77–95, 2012.

[22] B. Bourdin. Image segmentation with a finite element method. *Mathematical Modelling and Numerical Analysis*, 33(2):229–244, 1999.

[23] B. Bourdin. Numerical implementation of the variational formulation for quasi-static brittle fracture. *Interfaces and free boundaries*, 9:411–430, 2007.

[24] B. Bourdin, G. Francfort, and J.-J. Marigo. Numerical experiments in revisited brittle fracture. *J. Mech. Phys. Solids*, 48(4):797–826, 2000.

[25] B. Bourdin, G. Francfort, and J.-J. Marigo. The variational approach to fracture. *J. Elasticity*, 91(1–3):1–148, 2008.

[26] B. Bourdin and G. A. Francfort. Past and present of variational fracture. *SIAM News*, 52(9), 2019.

[27] B. Bourdin, C. Larsen, and C. Richardson. A time-discrete model for dynamic fracture based on crack regularization. *Int. J. Frac.*, 168(2):133–143, 2011.

[28] B. Bourdin, J.-J. Marigo, C. Maurini, and P. Sicsic. Morphogenesis and propagation of complex cracks induced by thermal shocks. *Phys. Rev. Lett.*, 112:014301, Jan 2014.

[29] D. Braess. *Finite Elemente*. Springer-Verlag Berlin Heidelberg, Berlin, Heidelberg, vierte, überarbeitete und erweiterte edition, 2007.

[30] A. Braides. *Approximation of free-discontinuity problems*. Springer Berlin Heidelberg, 1998.

[31] K. Bredies and D. Lorenz. *Mathematische Bildverarbeitung*. Vieweg+Teubner, 2011.

[32] S. C. Brenner and L. R. Scott. *The mathematical theory of finite element methods*. Number 15 in Texts in applied mathematics ; 15 ; Texts in applied mathematics. Springer, New York, NY, 3. ed. edition, 2008.

[33] I. Bronshtein, K. Semendyayev, G. Musiol, and H. Muehlig. *Handbook of Mathematics*. Springer-Verlag Berlin Heidelberg, 5th edition edition, 2007.

[34] M. K. Brun, T. Wick, I. Berre, J. M. Nordbotten, and F. A. Radu. An iterative staggered scheme for phase field brittle fracture propagation with stabilizing parameters. *Computer Methods in Applied Mechanics and Engineering*, 361:112752, 2020.

[35] S. Burke, C. Ortner, and E. Süli. An adaptive finite element approximation of a variational model of brittle fracture. *SIAM J. Numer. Anal.*, 48(3):980–1012, 2010.

[36] C. Burstedde, L. C. Wilcox, and O. Ghattas. P4est: Scalable algorithms for parallel adaptive mesh refinement on forests of octrees. *SIAM J. Sci. Comput.*, 33(3):1103–1133, May 2011.

[37] A. Carpiuc, M. Poncelet, J. Réthoré, and S. Roux. Carpiuc benchmark overview: crack advance, reorientation, propagation and initiation under complex loadings. *Advanced Modeling and Simulation in Engineering Sciences*, 2018.

[38] A. Chambolle. Image segmentation by variational methods: Mumford and shah functional and the discrete approximations. *SIAM J. Appl. Math.*, 55:827–863, 1995.

[39] A. Chambolle and G. D. Maso. Discrete approximation of the mumford-shah functional in dimension two. *ESAIM: Mathematical Modelling and Numerical Analysis - Modélisation Mathématique et Analyse Numérique*, 33(4):651–672, 1999.

[40] C. Chang and M. E. Mear. A boundary element method for two dimensional linear elastic fracture analysis. *International Journal of Fracture*, 74:219–251, 1995.

[41] P. G. Ciarlet. *Mathematical Elasticity. Volume 1: Three Dimensional Elasticity*. North-Holland, 1984.

[42] P. G. Ciarlet. *The finite element method for elliptic problems*. North-Holland, Amsterdam [u.a.], 2. pr. edition, 1987.

[43] P. G. Ciarlet. *Linear and Nonlinear Functional Analysis with Applications*. SIAM, 2013.

[44] S. Conti, M. Focardi, and F. Iurlano. Existence of strong minimizers for the griffith static fracture model in dimension two. *Annales de l'Institut Henri Poincaré C, Analyse non linéaire*, 36(2):455 – 474, 2019.

[45] R. Dautray and J.-L. Lions. *Mathematical Analysis and Numerical Methods for Science and Technology*, volume 5. Springer-Verlag, Berlin-Heidelberg, 2000.

[46] T. A. Davis and I. S. Duff. An unsymmetric-pattern multifrontal method for sparse LU factorization. *SIAM J. Matrix Anal. Appl.*, 18(1):140–158, 1997.

[47] R. de Borst and C. Verhoosel. Gradient damage vs phase-field approaches for fracture: Similarities and differences. *Computer Methods in Applied Mechanics and Engineering*, 312(December):78–94, 2016.

[48] J. Desai, G. Allaire, and F. Jouve. Topology optimization of structures undergoing brittle fracture. *Journal of Computational Physics*, 458:111048, 2022.

[49] P. Diehl, R. Lipton, T. Wick, and M. Tyagi. A comparative review of peridynamics and phase-field models for engineering fracture mechanics. *Computational Mechanics*, 69:1259–1293, 2022.

[50] The Differential Equation and Optimization Environment: DOpElib. `http://www.dopelib.net`.

[51] G. Duvaut and J. L. Lions. *Inequalities in Mechanics and Physics*. Springer, Berlin-Heidelberg-New York., 1976.

[52] C. Engwer, S. I. Pop, and T. Wick. Dynamic and weighted stabilizations of the l-scheme applied to a phase-field model for fracture propagation. arXiv:1912.07096, 2019.

[53] C. Engwer and L. Schumacher. A phase field approach to pressurized fractures using discontinuous galerkin methods. *Mathematics and Computers in Simulation*, pages –, 2016.

[54] L. C. Evans. *Partial differential equations*. American Mathematical Society, 2010.

[55] P. E. Farrell and C. Maurini. Linear and nonlinear solvers for variational phase-field models of brittle fracture. *Int. J. Numer. Meth. Engrg.*, 109:648–667, 2017.

[56] F. Fei, A. Costa, J. E. Dolbow, R. R. Settgast, and M. Cusini. A phase-field model for hydraulic fracture nucleation and propagation in porous media. *International Journal for Numerical and Analytical Methods in Geomechanics*, 47(16):3065–3089, 2023.

[57] G. Francfort. Variational fracture: twenty years after. *International Journal of Fracture*, pages 1–11, 2021.

[58] G. Francfort, N. Le, and S. Serfaty. Critical points of Ambrosio-tortorelli converge to critical points of Mumford-Shah in the one-dimensional Dirichlet case. *ESAIM: COCV*, 15(0):576–598, 2009.

[59] G. Francfort and J.-J. Marigo. Revisiting brittle fracture as an energy minimization problem. *J. Mech. Phys. Solids*, 46(8):1319–1342, 1998.

[60] T.-P. Fries and T. Belytschko. The extended/generalized finite element method: An overview of the method and its applications. *Int. J. Numer. Meth. Engrg.*, 84:253–304, 2010.

[61] M. J. Gander and M. Neumüller. Analysis of a new space-time parallel multigrid algorithm for parabolic problems. *SIAM J. Sci. Comput.*, 38(4):A2173–A2208, 2016.

[62] L. Gendre, O. Allix, P. Gosselet, and F. Comte. Non-intrusive and exact global/local technique for structural problems with local plasticity. *Comput. Mech.*, 44(2):233–245, 2009.

[63] T. Gerasimov and L. D. Lorenzis. A line search assisted monolithic approach for phase-field computing of brittle fracture. *Computer Methods in Applied Mechanics and Engineering*, 312:276 – 303, 2016.

[64] T. Gerasimov, N. Noii, O. Allix, and L. De Lorenzis. A non-intrusive global/local approach applied to phase-field modeling of brittle fracture. *Advanced Modeling and Simulation in Engineering Sciences*, 5(1):14, May 2018.

[65] T. Gerasimov, U. Römer, J. Vondřejc, H. G. Matthies, and L. De Lorenzis. Stochastic phase-field modeling of brittle fracture: Computing multiple crack patterns and their probabilities. *Computer Methods in Applied Mechanics and Engineering*, 372:113353, 2020.

[66] E. D. Giorgi and L. Ambrosio. Un nuovo funzionale del calcolo delle variazioni. *Atti. Accad. Naz. Linccei Rend. Cl. Sci. Fis. Mat. Natur.*, 82:199–210, 1988.

[67] C. Goll, T. Wick, and W. Wollner. DOpElib: Differential equations and optimization environment; A goal oriented software library for solving pdes and optimization problems with pdes. *Archive of Numerical Software*, 5(2):1–14, 2017.

[68] C. Gräser, D. Kienle, and O. Sander. Truncated nonsmooth newton multigrid for phase-field brittle-fracture problems, with analysis. *Comp. Mech.*, 2023.

[69] A. A. Griffith. The phenomena of rupture and flow in solids. *Philos. Trans. R. Soc. Lond.*, 221:163–198, 1921.

[70] C. Großmann, H.-G. Roos, and M. Stynes. *Numerical Treatment of Partial Differential Equations*. Springer, 2007.

[71] F. Hausdorff. Dimension und äußeres maß. *Mathematische Annalen*, 79(1):157–179, Mar 1918.

[72] Y. Heider. A review on phase-field modeling of hydraulic fracturing. *Engineering Fracture Mechanics*, 253:107881, 2021.

[73] Y. Heider and B. Markert. A phase-field modeling approach of hydraulic fracture in saturated porous media. *Mechanics Research Communications*, 80:38 – 46, 2017. Multi-Physics of Solids at Fracture.

[74] T. Heister, M. F. Wheeler, and T. Wick. A primal-dual active set method and predictor-corrector mesh adaptivity for computing fracture propagation using a phase-field approach. *Comp. Meth. Appl. Mech. Engrg.*, 290:466 – 495, 2015.

[75] T. Heister and T. Wick. Parallel solution, adaptivity, computational convergence, and open-source code of 2d and 3d pressurized phase-field fracture problems. *PAMM*, 18(1):e201800353, 2018.

[76] T. Heister and T. Wick. pfm-cracks: A parallel-adaptive framework for phase-field fracture propagation. *Software Impacts*, 6:100045, 2020.

[77] M. A. Heroux, R. A. Bartlett, V. E. Howle, R. J. Hoekstra, J. J. Hu, T. G. Kolda, R. B. Lehoucq, K. R. Long, R. P. Pawlowski, E. T. Phipps, A. G. Salinger, H. K. Thornquist, R. S. Tuminaro, J. M. Willenbring, A. Williams, and K. S. Stanley. An overview of the trilinos project. *ACM Trans. Math. Softw.*, 31(3):397–423, 2005.

[78] M. Hintermüller, K. Ito, and K. Kunisch. The primal-dual active set strategy as a semismooth newton method. *SIAM Journal on Optimization*, 13(3):865–888, 2002.

[79] M. Hinze, R. Pinnau, M. Ulbrich, and S. Ulbrich. *Optimization with PDE constraints*. Number 23 in Mathematical modelling: theory and applications. Springer, Dordrecht u.a., 2009.

[80] G. Holzapfel. *Nonlinear Solid Mechanics: A continuum approach for engineering*. John Wiley and Sons, LTD, 2000.

[81] S. Hüeber and B. Wohlmuth. A primal–dual active set strategy for non-linear multibody contact problems. *Comput. Methods Appl. Mech. Engrg.*, 194(27):3147–3166, 2005.

[82] K. Ito and K. Kunisch. Augmented lagrangian methods for nonsmooth, convex optimization in Hilbert spaces. *Nonlinear Analysis*, 41:591–616, 2000.

[83] K. Ito and K. Kunisch. Optimal control of elliptic variational inequalities. *Appl. Math. Optim.*, 41(3):343–364, 2000.

[84] D. Jodlbauer, U. Langer, and T. Wick. Matrix-free multigrid solvers for phase-field fracture problems. *Computer Methods in Applied Mechanics and Engineering*, 372:113431, 2020.

[85] T. Kärkkäinen, K. Kunisch, and P. Tarvainen. Augmented Lagrangian active set methods for obstacle problems. *J. Optim. Theory Appl.*, 119(3):499–533, 2003.

[86] D. Khimin, J. Lankeit, M. C. Steinbach, and T. Wick. Analysis of a space-time phase-field fracture complementarity model and its optimal control formulation, 2023.

[87] D. Khimin, M. Steinbach, and T. Wick. Space-time formulation, discretization, and computational performance studies for phase-field fracture optimal control problems. *Journal of Computational Physics*, 470:111554, 2022.

[88] D. Khimin, M. Steinbach, and T. Wick. Space-time mixed system formulation of phase-field fracture optimal control problems. *Journal of Optimization Theory and Applications*, 2023, published online.

[89] A. Khodadadian, N. Noii, M. Parvizi, M. Abbaszadeh, T. Wick, and C. Heitzinger. A bayesian estimation method for variational phase-field fracture problems. *Computational Mechanics*, 66:827–849, 2020.

[90] N. Kikuchi and J. Oden. *Contact problems in elasticity*. Studies in Applied Mathematics. Society for Industrial and Applied Mathematics (SIAM), Philadelphia, PA, 1988.

[91] D. Kinderlehrer and G. Stampacchia. *An Introduction to Variational Inequalities and Their Applications*. Classics in Applied Mathematics. Society for Industrial and Applied Mathematics, 2000.

[92] L. Kolditz and K. Mang. On the relation of Gamma-convergence parameters for pressure-driven quasi-static phase-field fracture. *Examples and Counterexamples, in review*, 2021.

[93] L. Kolditz, K. Mang, and T. Wick. A modified combined active-set newton method for solving phase-field fracture into the monolithic limit. *Computer Methods in Applied Mechanics and Engineering*, 414:116170, 2023.

[94] K. Königsberger. *Analysis 1.* Springer Lehrbuch. Springer, Berlin – Heidelberg – New York, 6. auflage edition, 2004.

[95] K. Königsberger. *Analysis 2.* Springer Lehrbuch. Springer, Berlin – Heidelberg – New York, 5. auflage edition, 2004.

[96] A. Kopanicakova and R. Krause. A recursive multilevel trust region method with application to fully monolithic phase-field models of brittle fracture. *Computer Methods in Applied Mechanics and Engineering*, 360:112720, 2020.

[97] A. Kopaničáková, H. Kothari, and R. Krause. Nonlinear field-split preconditioners for solving monolithic phase-field models of brittle fracture. *Computer Methods in Applied Mechanics and Engineering*, 403:115733, 2023.

[98] V. Kosin, A. Fau, C. Jailin, F. Hild, and T. Wick. Parameter identification of a phase-field fracture model using integrated digital image correlation. *Elsevier, in revised review*, page 34, 2023.

[99] P. K. Kristensen and E. Martínez-Pañeda. Phase field fracture modelling using quasi-newton methods and a new adaptive step scheme. *Theoretical and Applied Fracture Mechanics*, 107:102446, 2020.

[100] C. Kuhn and R. Müller. A continuum phase field model for fracture. *Engineering Fracture Mechanics*, 77(18):3625 – 3634, 2010. Computational Mechanics in Fracture and Damage: A Special Issue in Honor of Prof. Gross.

[101] A. Kumar, B. Bourdin, G. A. Francfort, and O. Lopez-Pamies. Revisiting nucleation in the phase-field approach to brittle fracture. *Journal of the Mechanics and Physics of Solids*, 142:104027, 2020.

[102] P. Kumar, P. Steinmann, and J. Mergheim. A graded interphase enhanced phase-field approach for modeling fracture in polymer composites. *Forces in Mechanics*, 9:100135, 2022.

[103] O. Lampron, D. Therriault, and M. Lévesque. An efficient and robust monolithic approach to phase-field quasi-static brittle fracture using a modified newton method. *Computer Methods in Applied Mechanics and Engineering*, 386:114091, Dec 2021.

[104] S. Lee, A. Mikelić, M. Wheeler, and T. Wick. Phase-field modeling of two phase fluid filled fractures in a poroelastic medium. *Multiscale Modeling & Simulation*, 16(4):1542–1580, 2018.

[105] S. Lee, A. Mikelić, M. F. Wheeler, and T. Wick. Phase-field modeling of proppant-filled fractures in a poroelastic medium. *Computer Methods in Applied Mechanics and Engineering*, 312:509 – 541, 2016. Phase Field Approaches to Fracture.

[106] S. Lee, M. F. Wheeler, and T. Wick. Pressure and fluid-driven fracture propagation in porous media using an adaptive finite element phase field model. *Computer Methods in Applied Mechanics and Engineering*, 305:111 – 132, 2016.

[107] J. L. Lions and E. Magenes. *Problèmes aux limites non homogènes et applications.* Travaux et Recherches Mathématiques, Paris, 1968.

[108] K. Mang. *Phase-field fracture modeling, numerical solution, and simulations for compressible and incompressible solids.* PhD thesis, Leibniz University Hannover, 2022.

[109] K. Mang, A. Fehse, N. H. Kröger, and T. Wick. A mixed phase-field fracture model for crack propagation in punctured epdm strips. *Theoretical and Applied Fracture Mechanics*, 115:103076, 2021.

[110] K. Mang, M. Walloth, T. Wick, and W. Wollner. Mesh adaptivity for quasi-static phase-field fractures based on a residual-type a posteriori error estimator. *GAMM-Mitteilungen*, 43(1):e202000003, 2020.

[111] K. Mang, M. Walloth, T. Wick, and W. Wollner. Adaptive numerical simulation of a phase-field fracture model in mixed form tested on an l-shaped specimen with high poisson ratios. In F. J. Vermolen and C. Vuik, editors, *Numerical Mathematics and Advanced Applications ENUMATH 2019*, pages 1185–1193, Cham, 2021. Springer International Publishing.

[112] K. Mang and T. Wick. Numerical methods for variational phase-field fracture problems. Hannover : Institutionelles Repositorium der Leibniz Universität Hannover, DOI: https://doi.org/10.15488/5129, July 2019.

[113] K. Mang, T. Wick, and W. Wollner. A phase-field model for fractures in nearly incompressible solids. *Computational Mechanics*, 65:61–78, 2020.

[114] P. Martin, C. Andreea, J. Clément, K. Kyryl, L. Hugo, and F. Hild. Concrete mixed mode fracture test carpiuc benchmark « interactive loadings » it1, it2, it3 [data set]. https://doi.org/10.5281/zenodo.2625006, 2019.

[115] H.-G. Maschke and M. Kuna. A review of boundary and finite element methods in fracture mechanics. *Theoretical and Applied Fracture Mechanics*, 4(3):181 – 189, 1985.

[116] D. Meidner. *Adaptive Space-Time Finite Element Methods for Optimization Problems Governed by Nonlinear Parabolic Systems*. PhD thesis, University of Heidelberg, 2008.

[117] J. Melenk and I. Babuška. The partition of unity finite element method: Basic theory and applications. *Computer Methods in Applied Mechanics and Engineering*, 139(1):289 – 314, 1996.

[118] C. Miehe, M. Hofacker, L.-M. Schaenzel, and F. Aldakheel. Phase field modeling of fracture in multi-physics problems. part ii. coupled brittle-to-ductile failure criteria and crack propagation in thermo-elastic–plastic solids. *Computer Methods in Applied Mechanics and Engineering*, 294:486 – 522, 2015.

[119] C. Miehe, M. Hofacker, and F. Welschinger. A phase field model for rate-independent crack propagation: Robust algorithmic implementation based on operator splits. *Comput. Meth. Appl. Mech. Engrg.*, 199:2765–2778, 2010.

[120] C. Miehe, F. Welschinger, and M. Hofacker. A phase field model of electromechanical fracture. *J. Mech. Phys. Solids*, 58:1716–1740, 2010.

[121] C. Miehe, F. Welschinger, and M. Hofacker. Thermodynamically consistent phase-field models of fracture: variational principles and multi-field fe implementations. *Int. J. Numer. Methods Engrg.*, 83:1273–1311, 2010.

[122] A. Mikelić, M. Wheeler, and T. Wick. A phase-field approach to the fluid filled fracture surrounded by a poroelastic medium. ICES Report 13-15, Jun 2013.

[123] A. Mikelić, M. F. Wheeler, and T. Wick. A quasi-static phase-field approach to pressurized fractures. *Nonlinearity*, 28(5):1371–1399, 2015.

[124] A. Mikelić, M. F. Wheeler, and T. Wick. Phase-field modeling through iterative splitting of hydraulic fractures in a poroelastic medium. *GEM - International Journal on Geomathematics*, 10(1), Jan 2019.

[125] L. Modica and S. Mortola. Il limite nella γ-convergenza di una famiglia di funzionali ellittici. *Boll. Un. Mat. Ital. A (5)*, 14(3):526–529, 1977.

[126] N. Moes, J. Dolbow, and T. Belytschko. A finite element method for crack growth without remeshing. *Int. J. Numer. Meth. Engrg.*, 46:131–150, 1999.

[127] D. Mumford and J. Shah. Optimal approximations by piecewise smooth functions and associated variational problems. *Comm. Pure Appl. Math.*, 42:577–685, 1989.

[128] I. Neitzel, T. Wick, and W. Wollner. An optimal control problem governed by a regularized phase-field fracture propagation model. *SIAM Journal on Control and Optimization*, 55(4):2271–2288, 2017.

[129] I. Neitzel, T. Wick, and W. Wollner. An optimal control problem governed by a regularized phase-field fracture propagation model. part ii: The regularization limit. *SIAM Journal on Control and Optimization*, 57(3):1672–1690, 2019.

[130] J. Nocedal and S. J. Wright. *Numerical optimization*. Springer Ser. Oper. Res. Financial Engrg., 2006.

[131] N. Noii, F. Aldakheel, T. Wick, and P. Wriggers. An adaptive global-local approach for phase-field modeling of anisotropic brittle fracture. *Computer Methods in Applied Mechanics and Engineering*, 361:112744, 2020.

[132] N. Noii, A. Khodadadian, J. Ulloa, F. Aldakheel, T. Wick, S. Francois, and P. Wriggers. Bayesian inversion for unified ductile phase-field fracture. *Computational Mechanics*, 68:943–980, 2021.

[133] N. Noii, A. Khodadadian, and T. Wick. Bayesian inversion for anisotropic hydraulic phase-field fracture. *Computer Methods in Applied Mechanics and Engineering*, 386:114118, 2021.

[134] N. Noii, A. Khodadadian, and T. Wick. Bayesian inversion using global-local forward models applied to fracture propagation in porous media. *International Journal for Multiscale Computational Engineering*, 20(3):57–79, 2022.

[135] N. Noii and T. Wick. A phase-field description for pressurized and non-isothermal propagating fractures. *Computer Methods in Applied Mechanics and Engineering*, 351:860 – 890, 2019.

[136] E. Pan. A general boundary element analysis of 2-d linear elastic fracture mechanics. *International Journal of Fracture*, 88:41–59, 1997.

[137] A. Popp, M. W. Gee, and W. A. Wall. A finite deformation mortar contact formulation using a primal–dual active set strategy. *Int. J. Numer. Meth. Engng.*, 79(11):1354–1391, 2009.

[138] N. Provatas and K. Elder. *Phase-field methods in materials science and engineering*. Wiley, 2010.

[139] R. Rannacher. Numerische methoden der Kontinuumsmechanik (Numerische Mathematik 3). Vorlesungsskriptum, 2001.

[140] R. Rannacher. *Probleme der Kontinuumsmechanik und ihre numerische Behandlung*. Heidelberg University Publishing, 2017.

[141] J. Rungamornrat and M. E. Mear. A weakly-singular SGBEM for analysis of cracks in 3D anisotropic media. *Computer Methods in Applied Mechanics and Engineering*, 197(49):4319–4332, 2008.

[142] Y. Saad. *Iterative methods for sparse linear systems*. SIAM, 2003.

[143] Y. Saad and M. H. Schultz. GMRES: A generalized minimal residual algorithm for solving nonsymmetric linear systems. *SIAM J. Sci. Stat. Comput.*, 7(3), 1986.

[144] A. Schafelner. *Space-time finite element methods*. PhD thesis, Johannes Kepler University Linz, 2021.

[145] J. Schröder, T. Wick, S. Reese, P. Wriggers, R. Müller, S. Kollmannsberger, M. Kästner, A. Schwarz, M. Igelbüscher, N. Viebahn, H. R. Bayat, S. Wulfinghoff, K. Mang, E. Rank, T. Bog, D. d'Angella, M. Elhaddad, P. Hennig, A. Düster, W. Garhuom, S. Hubrich, M. Walloth, W. Wollner, C. Kuhn, and T. Heister. A selection of benchmark problems in solid mechanics and applied mathematics. *Arch. Computat. Methods Eng.*, 28:713–751, 2021.

[146] B. Schröder and D. Kuhl. A semi-smooth Newton method for dynamic multifield plasticity. *PAMM*, 16(1):767–768, 2016.

[147] R. Shen, H. Waisman, and L. Guo. Fracture of viscoelastic solids modeled with a modified phase field method. *Computer Methods in Applied Mechanics and Engineering*, 346:862 – 890, 2019.

[148] I. N. Sneddon. The distribution of stress in the neighbourhood of a crack in an elastic solid. *Proc. R Soc London A*, 187:229–260, 1946.

[149] I. N. Sneddon and M. Lowengrub. *Crack problems in the classical theory of elasticity*. SIAM series in Applied Mathematics. John Wiley and Sons, Philadelphia, 1969.

[150] L. Sommer. *An unfitted discontinuous Galerkin scheme for a phase-field approximation of pressurized fractures*. PhD thesis, Westfälische Wilhelms-Universität Münster, 2019.

[151] A. Sonntag, A. Wagner, and W. Ehlers. Dynamic hydraulic fracturing in partially saturated porous media. *Computer Methods in Applied Mechanics and Engineering*, 414:116121, 2023.

[152] C. Steinke and M. Kaliske. A phase-field crack model based on directional stress decomposition. *Computational Mechanics*, 63(5):1019–1046, 2019.

[153] M. A. Sutton, J. J. Orteu, and H. Schreier. *Image correlation for shape, motion and deformation measurements: Basic concepts, theory and applications*. Springer Science & Business Media, 2009.

[154] A. Toselli and O. Widlund. *Domain decomposition methods - algorithms and theory*. Volume 34 of Springer Series in Computational Mathematics. Springer, Berlin, Heidelberg, 2005.

[155] R. Trémolières, J. Lions, and R. Glowinski. *Analyse numérique des inéquations variationnelles*. Dunod, 1976.

[156] R. Trémolières, J. Lions, and R. Glowinski. *Numerical Analysis of Variational Inequalities*. Studies in Mathematics and its Applications. Elsevier Science, 2011.

[157] F. Tröltzsch. Regular Lagrange multipliers for control problems with mixed pointwise control-state constraints. *SIAM J. Optim.*, 15(2):616–634, 2004/05.

[158] F. Tröltzsch. *Optimale Steuerung partieller Differentialgleichungen - Theorie, Verfahren und Anwendungen*. Vieweg und Teubner, Wiesbaden, 2nd edition, 2009.

[159] C. van Duijn, A. Mikelić, M. F. Wheeler, and T. Wick. Thermoporoelasticity via homogenization: Modeling and formal two-scale expansions. *International Journal of Engineering Science*, 138:1 – 25, 2019.

[160] H. von Wahl and T. Wick. A high-accuracy framework for phase-field fracture interface reconstructions with application to stokes fluid-filled fracture surrounded by an elastic medium. *Computer Methods in Applied Mechanics and Engineering*, 415:116202, 2023.

[161] J. Wambacq, J. Ulloa, G. Lombaert, and S. François. Interior-point methods for the phase-field approach to brittle and ductile fracture. *Computer Methods in Applied Mechanics and Engineering*, 375:113612, 2021.

[162] D. Werner. *Funktionalanalysis*. Springer, 2004.

[163] M. F. Wheeler, T. Wick, and S. Lee. IPACS: Integrated Phase-Field Advanced Crack Propagation Simulator. An adaptive, parallel, physics-based-discretization phase-field framework for fracture propagation in porous media. *Computer Methods in Applied Mechanics and Engineering*, 367:113124, 2020.

[164] T. Wick. Coupling fluid-structure interaction with phase-field fracture. *Journal of Computational Physics*, 327:67 – 96, 2016.

[165] T. Wick. Goal functional evaluations for phase-field fracture using PU-based DWR mesh adaptivity. *Computational Mechanics*, 57(6):1017–1035, 2016.

[166] T. Wick. An error-oriented Newton/inexact augmented Lagrangian approach for fully monolithic phase-field fracture propagation. *SIAM Journal on Scientific Computing*, 39(4):B589–B617, 2017.

[167] T. Wick. Modified newton methods for solving fully monolithic phase-field quasi-static brittle fracture propagation. Comp. Meth. Appl. Mech. Engrg., accepted in July 2017, preprint available on my personal webpage, 2017.

[168] T. Wick. Modified Newton methods for solving fully monolithic phase-field quasi-static brittle fracture propagation. *Computer Methods in Applied Mechanics and Engineering*, 325:577 – 611, 2017.

[169] T. Wick. *Multiphysics Phase-Field Fracture: Modeling, Adaptive Discretizations, and Solvers*. De Gruyter, Berlin, Boston, 2020.

[170] T. Wick. Numerical methods for partial differential equations. Hannover : Institutionelles Repositorium der Leibniz Universität Hannover, DOI: https://doi.org/10.15488/11709, January 2022.

[171] T. Wick. Space-time methods: formulations, discretization, solution, goal-oriented error control and adaptivity. `https://thomaswick.org/links/Wi23_st_book_preprint_Aug_8_2023.pdf`, to appear in Springer, Compact Textbooks in Mathematics, 2023.

[172] J. Wloka. *Partial differential equations*. Cambridge University Press, 1987.

[173] J.-Y. Wu, Y. Huang, and V. P. Nguyen. c monolithic algorithm for the unified phase field damage theory. *Comput. Methods Appl. Mech. Engrg.*, 360:112704, 23, 2020.

[174] J.-Y. Wu, V. P. Nguyen, C. Thanh Nguyen, D. Sutula, S. Bordas, and S. Sinaie. Phase field modelling of fracture. *Advances in Applied Mechanics*, 53:1–183, 09 2019.

[175] T. Wu, A. Carpiuc-Prisacari, M. Poncelet, and L. De Lorenzis. Phase-field simulation of interactive mixed-mode fracture tests on cement mortar with full-field displacement boundary conditions. *Engineering Fracture Mechanics*, 182:658–688, 2017.

[176] A. Zehnder. *Fracture mechanics*. Springer-Verlag, 2012.

[177] S. Zhou, X. Zhuang, and T. Rabczuk. Phase-field modeling of fluid-driven dynamic cracking in porous media. *Computer Methods in Applied Mechanics and Engineering*, 350:169 – 198, 2019.

Index